AN ABSOLUTE MEASUREMENT OF THE $^{7}Li(n,n't)^{4}He$ REACTION CROSS-SECTION BETWEEN 5.0 AND 14.0 MeV BY TRITIUM ASSAYING

by

Martyn Thomas SWINHOE B.Sc., M.Sc.

A thesis submitted for the degree of Ph.D. in the Department of Physics (Applied Nuclear Science) at the University of Birmingham.

NOVEMBER, 1978.

UNIVERSITY OF
BIRMINGHAM

University of Birmingham Research Archive

e-theses repository

This unpublished thesis/dissertation is copyright of the author and/or third parties. The intellectual property rights of the author or third parties in respect of this work are as defined by The Copyright Designs and Patents Act 1988 or as modified by any successor legislation.

Any use made of information contained in this thesis/dissertation must be in accordance with that legislation and must be properly acknowledged. Further distribution or reproduction in any format is prohibited without the permission of the copyright holder.

SYNOPSIS

In view of the world's energy situation, it is necessary to investigate all possible means of supply. The principles of controlled thermonuclear fusion are described, together with the role of lithium and the need for nuclear data. Information on ^{7}Li and the $^{7}Li(n,n't)^{4}He$ reaction is given. The conclusion is that the state of the data is inadequate for the CTR development programme.

In the experiment, the tritium is produced in samples of lithium hydroxide, which are then dissolved, leaving the tritium as tritiated water. This is then measured by liquid scintillation counting in the normal way. The counting efficiency is measured as a function of quenching, with standard tritiated water. As a check on this method the $^{6}Li(n,\alpha t)$ cross-section was measured in a reactor irradiation. The result (including a self-shielding correction) was 900 ± 52 barns, in agreement with the accepted value of 940 ± 5 barns.

The neutron dose was measured with an NE213 liquid scintillation detector, the efficiency of which was measured as a function of neutron energy from 1.5 to 25 MeV, using the associated particle technique.

Irradiations were carried out between 4.7 and 14.1 MeV, using the Harwell Tandem Van de Graaff and Cock-croft Walton generator. The cross-section obtained for the $^{7}Li\ (n,n't)^{4}He$ was 28% lower than the ENDF/B-IV evaluation, with standard deviation of 5%. The cross-section of $^{27}AI(\ n,\alpha)^{24}Na$ was measured concurrently and good agreement was obtained with the accepted value.

Other evidence is presented for this result; elastic cross-section measurements from the Triangle Universities (USA), and tritium production measurements in an integral assembly at

karlsruh e (West Germany). The results from the present experiment may also improve the overall fitting of a recent R-matrix analysis to the ^{7}Li nucleus.

Finally, the conclusions are that, at least, a new evaluation is required, and also more measurements are required to resolve the discrepancies especially at 14 MeV.

ACKNOWLEDGEMENTS

I would like to thank Malcolm Scott and Derek Beynon for their comments and suggestions during the progress of the experiment, and John Cookson and Colin Wise for their help during the machine runs. I am also grateful to many people at AERE Harwell: the staff of the Tandem and Cockroft-Walton, Geoff Bradburn (Tritium measurement), Stephen Firkin (Ge(Li) counting) and Les Bint (sample preparation). I would also like to thank Alan Bardell (NPL) for the measurement of the flux is GLEEP and the reactor operators.

I would also like to acknowledge the use of both the Birmingham University computer and the Physics Department film analysis compluter. Also thanks are due to member of the ANS group: Colin Lambert, Neill Taylor, Mike Clark, Dave Wilson and Brian Underwood, largely, but not solely, for their advice on the use of these computers.

The SRC and UKAEA deserve my gratitude for providing financial support for this work.

However, most of all, I would like to thank JOE UTTLEY, whose efforts, advice and encouragement made this experiment not only possible but enjoyable.

CONTENTS.

CHAPTER ONE

INTRODUCTION

1.1. Energy supply and demand.

A substantial part of man's energy needs are met by fossil fuel, and this cannot continue indefinitely.

Estimates of world fuel supplies are shown in Table 1.1 (Roberts, 1975). The present world energy use per year is 0.1 Q., Cotrell, 1975). Assuming for the moment that the world's energy demand does not increase, then the supplies of oil and gas will be seriously depleted in fifty years time, since they make up a large fraction of our current energy consumption. Relatively large reserves of coal are available, but in the absence of oil and gas, these coal supplies would not only be needed for power production but also they would need to replace oil as a raw material in the chemical industry.

The assumption that the world's energy demand will not increase is a poor one. This is for two reasons. Firstly, the developed countries are unable to introduce 'zero-growth' economies, or are unwilling to do so because of the fear of economic competition from other countries who do not take such steps. While it may be possible to expand industrial output without an increase of energy use, it is obviously easier to expand ignoring the energy requirements. Secondly, no developing country will accept limitations on growth as long as its standard of living is far below that of the western world, and the standard of living is inseparably linked to energy use in a country. This increase in demand and the depletion of reserves of energy, means that the subject of energy supply and useage must be seriously considered.

The simplest way of making more energy available is to use the existing supplies more effectively. Energy use needs to be analysed in all respects to find out where energy conservation measures can be usefully introduced. Since the large increase in oil prices by OPEC, people have become much more aware of the whole topic of energy use, and energy conservation has become a subject of serious study. However, even the most drastic conservation measures could not hope to release the energy supplies required for the developing countries to increase their standard of living.

One common power source in which hope is sometimes placed is the thermal nuclear reactor. Many of these have been successfully (and cheaply), operating worldwide for many years. However, a glance at Table 1.1 will show that the available energy is only the same as that from gas. Of course, the time for the exhaustion of thermal reactor fuel is much further off than 50 years at the present useage (a small fraction of total energy use) but energy from this source could not supply a large fraction of the world demand for a significantly greater length of time.

So called 'alternative sources' of energy are also available. These include solar, wind, tidal and wave power. The technology for exploiting these supplies is in its infancy, but even allowing for development, in solar power for example, it is estimated (Long (1975)) that the contribution to U.K. energy consumption could be only 2% within 25 years. Among the problems associated with such sources as tidal and wave power, and geothermal energy, are that sites available for their exploitation are limited, and often not associated with energy needs.

The obvious energy source, from Table 1.1 is the fast

fuel		proved resources (Q)	proved and probable resources (Q)
Coal		7.8	140
Oil		2.2	4
Gas		1.2	3
Uranium	thermal reactors	0.69-1.2	1.7 - 2.6
	fast reactors	42-70	99 - 153

Table 1.1 World energy resources (1Q = 7.6×10^{10} tonnes of coal equivalent. Roberts (1975)

The uranium reserves are given for prices of $15 and $30 per lb.

breeder reactor (FBR), with a huge amount of energy in the reserves. The technology for these is known, and demonstration reactors are running. These reactors do have drawbacks such as the problem of proliferation, and the production of radioactive waste, which have made them unpopular with groups of environmentalists. It is possible, if public opinion was sufficiently affected by this view, that FBR introduction could be prevented.

Another possible means of producing energy, not so far considered, is controlled thermonuclear reactors. These do not have the tarnished image of the FBR, but they represent a long term potential, and could not be introduced in time to provide the expected energy needs. However, if they could be proved economically viable, the introduction of commerical FBR's could be viewed as a temporary expedient, and as such could gain public approval.

In a society as heavily dependent on convenient energy supplies as ours, it is wise to ensure that future supply will meet future demand. The safest way to proceed to that end is to investigate all possible means of energy supply, in order to insure ourselves against the failure of any one. This means that energy conservation, 'alternative' energy, fission and fusion should be considered as fulfilling part of the answer to the problem of energy supply rather than competing with each other to provide the 'best' solution.

The principles of thermonuclear fusion will now be described so that the role of lithium can be understood in terms of the fusion reactor development programme.

1.2. Controlled thermonuclear Fusion

Energy can be obtained from nuclear reactions when the final products are more stable, (having less total mass), than the original interacting particles. This can occur in two principal ways. Firstly when a heavy nucleus splits into two smaller nuclei (fission), and secondly when two light nuclei join to produce a heavier nucleus (fusion). The fact that both processes lead to the liberation of energy is because medium weight nuclei are more stable, (in terms of their binding energy per nucleon), than either heavy or light nuclei. Nuclear fission is already used for power production in reactors utilising thermal and fast neutrons to initiate the process, but fusion has not been demonstrated as a mechanism for producing net useful energy.

The aim of the controlled thermonuclear fusion programme is to demonstrate that this is possible on an economic scale.

There are several reactions involving light nuclei which are candidates for producing power, and several of these are shown in Table 1.2. The reactions produced by deuterium/deuterium fusion would have the immediate advantage that deuterium is abundant in nature (0.018% of sea water) and could be used to produce approximately 10^9 Q of energy (Hubbert (1971)). A comparison with the fuel supplies given in Table 1.1. will show what a vast supply of energy this is. However, the need to fulfil various requirements for an operating reactor, outlined below, means that in the first generation of fusion reactors the reaction used will be deuterium/tritium. The energy available from this reaction is limited by lithium supplies, to 1000Q, excluding lithium supplies in sea-water (US AEC (1973)). (The need for lithium will be explained below.)

Reaction	Energy released (MeV)
$D + D \longrightarrow {}^{3}He + n$	3.27
$\longrightarrow {}^{3}H + {}^{1}H$	4.03
$D + T \longrightarrow {}^{4}He + n$	17.58
$D + {}^{3}He \rightarrow {}^{4}He + {}^{1}H$	18.3

Figure 1.2 Possible fusion reactions.

The cross-section of a nucleus for particular reaction is a measure of the probability of the reaction, and it is normally a function of the relative energy of the reacting particles. The cross-section for the deuterium fusion reaction, rises rapidly from a deuteron energy of 30 KeV, when the deuterons can overcome their mutual Coulomb repulsion. A viable fusion reactor cannot be made by accelerating deuterons to this energy and bombarding a deuterium target with them. This is because deuteron scattering is a much more probable event than fusion, and this scattering often degrades the energy of the incident deuterons, making subsequent fusion reactions impossible. The result is that more energy is needed to accelerate the deuterons than can be recovered from the target. However, if deuterium is heated to a high temperature then those particles in the high energy tail of the Maxwellian distribution have sufficient energy to undergo fusion, and although scattering occurs, no high energy deuterons are lost, since the energy distribution is an equilibrium one. A nuclear reaction which is made to proceed in this way is called a thermonuclear reaction.

At the high temperatures which will be required in controlled thermonuclear reactors (CTRs) the deuterium will be completely ionised. The electrons will move at high velocities and undergo collisions. This acceleration of the electrons will cause the emission of radiation (bremsstrahlung) which is the most important way that the heated nuclear fuel will lose energy. (other energy loss mechanisms exist, such as heat conduction or loss of energetic particles, but these can ideally be made negligible). Fortunately the fusion reaction rate rises more rapidly with temperature than the energy loss by radiation, and there is a critical temperature above which more energy is

produced by fu sion than is radiated or used to provide the conditions for the reaction to proceed. Only above this temperature does power producing fusion become feasible. This temperature for DD fusion is $\sim 40 \times 10^7$K (Glasstone (1960)).

There is another condition for economic power production, and this imposes a condition on the length of time for which the reaction must be kept going in order that the energy used to heat the fuel can be recovered. (This energy is not recovered as the fuel cools down because thermodynamic laws determine the maximum efficiency at which heat can be converted into, say, electricity). The total energy production depends on the density of the fuel and on the time it is reacting; the condition relating these two quantities is (Lawson (1957)), for DD fusion,

$$n\tau \gtrsim 10^{16}$$

where n is the fuel density in nuclei cms^{-3} and τ the reaction time in seconds, and assuming a thermal conversion efficiency of 1/3.

The need to fulfil this criterion has lead to two major approaches to solving the problem of fusion power. One uses relatively low density fuel and long confinement times; the ionised fuel is held in place by various magnetic field configurations. The alternative approach compresses a fuel pellet to very high densities and heats it by incident radiation (light, heavy ions or electrons) so that the confinement time need only be very short; the time, in fact, for the pellet to blow apart. Both these routes may lead to net power production but both are presently limited by technical obstacles. The main effort of CTR research is currently devoted not to DD fusion but to DT fusion. This is because the shape of the DT cross-section and the energy released, mean that the minimum temperature

for fusion (5×10^7K) and the criterion for economic viability ($n\tau \geqslant 10^{14}$) are easier to reach, although the second of these has not yet been attained.

The use of DT fusion as a power source is often looked upon as a stepping stone to DD fusion, or some more exotic reaction whose reaction products are all charged leading to the direct production of electricity. However, DT fusion must be made to work economically if there is to be any fusion power production in the foreseeable future. The DD reaction is a good way to produce energy since there is an abundant supply of deuterium on the earth. The amount of tritium available is very small. It only exists in equilibrium between production by cosmic radiation (and thermonuclear fusion weapons and the water cooled fision reactors) and its natural decay. A viable DT fusion reactor therefore would not only need to fulfill the exacting requirements of the fusion process, but would also need to produce its own tritium fuel supply, as fast as it was consumed. There are two reactions which produce tritium from the available fusion neutrons, with sufficient cross-section to be useful. They are:

$$^6\text{Li} + n \longrightarrow {}^4\text{He} + {}^3\text{H} + 4.5 \text{ MeV}$$

$$^7\text{Li} + n \longrightarrow {}^4\text{He} + {}^3\text{H} + n - 2.47 \text{ MeV}$$

where ^{6}Li is 7.3% of natural lithium and the remainder is ^{7}Li. The need to produce tritium determines the major features of a DT CTR. Both types of reactor (magnetic or inertial confinement) must surround the fusion region with a 'blanket' which absorbs the energy given off by the fusion reactions (mainly, in the form of energetic neutrons) and also produces tritium. The number of tritium atoms produced per triton used in fusion (the tritium

breeding ratio) must be at least unity, and must exceed this in practice, to allow not only for processing losses, but also any increase in a DT fusion reactor programme. Many computer analyses have been carried out on various blanket configurations, to predict reactor parameters including the tritium breeding ratio. The uncertainty on these predicted parameters is due to some extent to the approximations in modelling and calculation, but primarily to the uncertainty on (or non-existence of) data on the cross-sections and other characteristics for the various interaction processes. In order to determine the importance of the deficiencies of the data, it is necessary to establish a criterion for the required accuracy of the parameters.

In the case of the tritium breeding ratio the accuracy which has been suggested (Steiner and Tobias (1974)) is ± 1%. This because a ratio of less than one means the reactor is unfeasible, whereas too large a ratio gives not only an excess of tritium, which being hazardous, must be carefully contained but it means that the blanket need have contained less lithium, making it less expensive. Calculations of the tritium breeding ratio in most blankets (Steiner and Tobias (1974), Crocker et al (1970), Alsmiller et al. (1975)) imply that the tritium production cross-section of ^{7}Li needs to be known to ± 5% in order to give a tritium breeding ratio of ± 1% in lithium metal blankets. In blankets made of lithium compounds, the tritium breeding ratio is less sensitive to the ^{7}Li cross-section and so it may be thought that the uncertainty in the ^{7}Li cross-section could be larger. However, in such blankets the tritium breeding ratio is much closer to unity and therefore is required to a correspondingly greater degree of accuracy.

The present uncertainity in this cross-section is much

greater than ± 5% (section 2.3) and so this experiment was undertaken.

There are two ways in which cross-section information can be accumulated. Firstly, differential measurements can be made where, ideally, monoenergetic neutrons are used and the reaction of interest is directly measured. The experimental arrangement is designed so that the incident neutrons only rarely interact more than once, and to accomplish this requires that most neutrons do not interact at all. This means that the information is only accumulated slowly, making the experiments time consuming and expensive.

Alternatively integral measurements can be made. In this case a neutron source is surrounded by a large amount of material, and the neutrons interact several times in the assembly before they are captured or lost. Information is obtained by the measurement of the neutron energy distribution and reaction rates in various materials. These reaction rates are the integral reaction rate over all neutron energies. These experiments require sophisticated calculational analysis to compare experiment with theory. Discrepancies between the real cross-sections and those used in the calculation, lead to differences between the predicted parameters, (neutron spectrum and reaction rates) which show up deficiencies in the data input to the calculations. It is difficult to unambiguously assign such discrepancies to one reaction or even one nucleus (depending on the composition of the assembly), however, the advantage of such experiments is that they show major discrepancies which need to be investigated in differential measurements, saving time in the investigation of reactions which are less important in the fusion reactor programme.

The $^{7}Li(n,n't)\ ^{4}He$ reaction has already been identified as needing further measurement, and so the present experiment was designed as a differential measurement, with a range of incident neutron energy of 5 - 14 MeV, since in a typical CTR blanket 99% of the tritium production reactions in ^{7}Li occur in this energy range (Steiner and Tobias (1974)).

CHAPTER TWO

LITHIUM AND THE $^{7}Li(n,n't)^{4}He$ REACTION

2.1. Lithium and its neutron induced reactions

Lithium, the lightest of the alkali metals, is a relatively abundant element on the earth, comprising approximately $4x10^{-5}$% of the earth's crust (Hermann (1934)). Naturally occurring lithium contains approximately 93% ^{7}Li and 7% ^{6}Li, although this ratio has been found to vary, depending on the source of supply. (Meadows and Whalen (1970)). The simple composition of the lithium nucleus has resulted in its investigation from a pure nucleur physics point of view, both theorectically and experimentally. The currently accepted energy levels for ^{7}Li, (Ajzenberg-Selove and Lauritsen (1974)) are shown in Fig.2.1. The energy of a ^{4}He-t pair is also shown, and since this is less than the excitation energy of all ^{7}Li excited states except the first, these states are unstable with respect to break-up into a ^{4}He-t pair. Only the first excited state undergoes (n,n'γ) reactions. The possible reactions initiated in ^{7}Li nucleus by neutrons with energy below 14 MeV, are shown in Figure 2.2. Tritium production occurs by the direct 'quasi-elastic' reaction (reaction 4), with ^{5}He as an intermediate nuclei (reaction 5), and by the decay of excited states produced by inelastic neutron scattering (reactions 6,7,9,12 and 14). Reactions other than elastic scattering and those involving tritium production, i.e. reactions (8.10,11,13,15 and 16) have small individual cross-sections amounting to 80 millibarns at 14 MeV. (Conlon (1972)).

2.2. Previous Measurements of the $^{7}Li(n,n't)^{4}He$ Cross-Section

The $^{7}Li(n,n't)^{4}He$ reaction cross-section was first measured by Macklin and Banta (1954), although subsequent authors agree

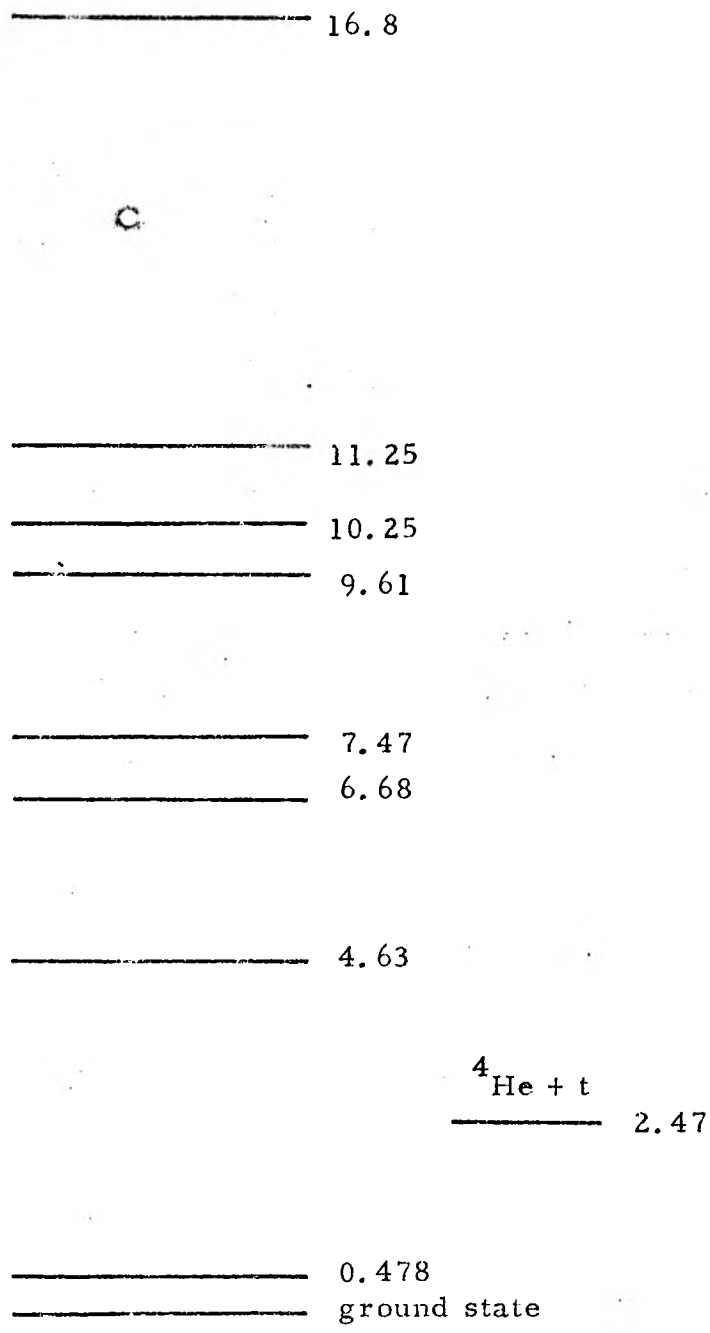

Figure 2.1 Energy levels of Lithium-7 (MeV)

Threshold (MeV)	Reaction	No.	Comments
exothermic	$^{7}Li(n,\gamma)^{8}Li \xrightarrow[.84s]{\beta^-} {}^{8}Be \xrightarrow[3\times10^{-16}s]{} 2\ {}^{4}He$	1	capture
—	$^{7}Li(n,n)^{7}Li$	2	elastic scattering
.547	$^{7}Li(n,n')^{7}Li^{*} \xrightarrow{\gamma} {}^{7}Li$	3	1st level
2.82	$^{7}Li(n,n't)^{4}He$	4	quasi-elastic
3.92	$^{7}Li(n,t)^{5}He \xrightarrow{n} {}^{4}He$	5	
5.29	$^{7}Li(n,n')^{7}Li^{*} \longrightarrow {}^{4}He + {}^{3}H$	6	2nd level
7.63	$^{7}Li(n,n')^{7}Li^{*} \longrightarrow {}^{4}He + {}^{3}H$	7	3rd level
8.30	$^{7}Li(n,2n)^{6}Li$	8	
8.53	$^{7}Li(n,n')^{7}Li^{*} \longrightarrow {}^{4}He + {}^{3}H$	9	4th level
8.88	$^{7}Li(n,d)^{6}He \xrightarrow[.82s]{\beta^-} {}^{6}Li$	10	
9.98	$^{7}Li(n,2nd)^{4}He$	11	
10.98	$^{7}Li(n,n')^{7}Li^{*} \longrightarrow {}^{4}He + {}^{3}H$	12	5th level
11.42	$^{7}Li(n,np)^{6}He \xrightarrow[.82s]{\beta^-} {}^{6}Li$	13	
11.71	$^{7}Li(n,n')^{7}Li^{*} \longrightarrow {}^{4}He + {}^{3}H$	14	6th level
12.62	$^{7}Li(n,3np)^{4}He$	15	
13.62	$^{7}Li(n,2np)^{5}He \xrightarrow{n} {}^{4}He$		

Fig. 2.2 Neutron induced reactions in ^{7}Li (0-14 MeV)

that their results appear to be in error (e.g. see Brown et.al (1963)). Their results are not included here since they used a wide range of incident neutron energy. (A reactor spectrum and an (α,n) source). Four types of experiment have been performed in order to measure this cross-section, and these will be outlined separately in the following section.

2.2.1 Measurement Using Nuclear Emulsions

What was perhaps the most detailed study of this reaction was undertaken by Rosen and Stewart (1961). They irradiated nuclear emulsions which contained lithium, and detected the tracks caused by the charged particles produced in the reactions. After development of the emulsions, the length and orientation of the tracks were measured. From a knowledge of the range of the charged particles in the emulsion, the energy of the individual particles can be calculated. The kinematics of each reaction, either $^{7}Li(n,n't)^{4}He$ or other reactions in ^{7}Li, or with the material of the emulsion, give different sets of particle tracks, and this enables them to be distinguised from one another, Extensive computer processing of the results is required, but the resulting information extends to more than the cross-section, and includes the energy and angular distributions of the neutrons and the charged particles. These results have been used by other experimenters to make corrections to their data (e.g. when a lower neutron energy cut-off was used in time-of-flight experiments (section 2.2.3), the number of events below the cut-off has often been found using the data of Rosen and Stewart . The neutron source in the experiment was a deuteron beam on a 6 cm deuterium gas cell. The flux was measured by counting the number of proton recoils in emulsions without a lithium loading. Natural lithium was used, and it was assumed to be 92.48% ^{7}Li.

energy (Mev)	σ	$\Delta\sigma$	Author	Method	plot. symb.
3.35	6	50	Hopkins et al.(1968)	TOF	X
3.75	8.5	2.2	Brown et al (1963)*	activation	□
4.0	200	200	Batchelor & Towle (1963)*	TOF	0
4.0	109	17	Wyman & Thorpe (1958)	activation	△
4.62	95	8	Brown*	activation	□
4.83	100	22	Hopkins	TOF	X
5.0	104	10	Brown*	activation	□
5.1	208	50	Rosen & Stewart (1961)*	emulsions	+
5.15	220	90	Batchelor*	TOF	0
5.4	330	60	Rosen*	emulsions	+
5.6	350	37	Wyman	activation	△
5.64	328	24	Brown*	activation	□
5.74	330	38	Hopkins	TOF	x
5.8	365	60	Rosen*	emulsions	+
6.36	500	60	Batchelor*	TOF	0
6.5	380	50	Rosen*	emulsions	+
6.96	369	25	Brown*	activation	□
7.0	438	60	Rosen*	emulsions	+
7.5	450	62	Rosen*	emulsions	+
7.5	430	39	Hopkins	TOF	X
7.54	375	41	Batchelor*	TOF	0
8.0	512	62	Rosen*	emulsions	+
8.0	462	64	Wyman	activation	△
8.62	351	25	Brown*	activation	□
9.3	508	70	Rosen*	emulsions	+
9.6	404	41	Wyman	activation	△
10.0	485	71	Cookson et al.(1967)	TOF	▩
10.6	402	60	Rosen*	emulsions	+
12.0	400	60	Rosen*	emulsions	+
13.4	333	20	Wyman	activation	△
13.98	347	9	Benjamin et al.(1962)*	activation	▲
14.0	311	40	Rosen*	emulsions	+
14.0	355	12	Osborn & Wilson (1961)*	activation	0
14.0	325	75	Thomas (1954)*	transmission	▼
14.1	319	17	Wyman	activation	△
14.4	312	24	Antolkovic (1972	emulsions	▽
14.8	316	20	Wyman	activation	△
14.85	352	25	Brown*	activation	□

Table 2.3. Previous measurements of Li(n,n't) He cross-section
*included in Pendlebury's evaluation

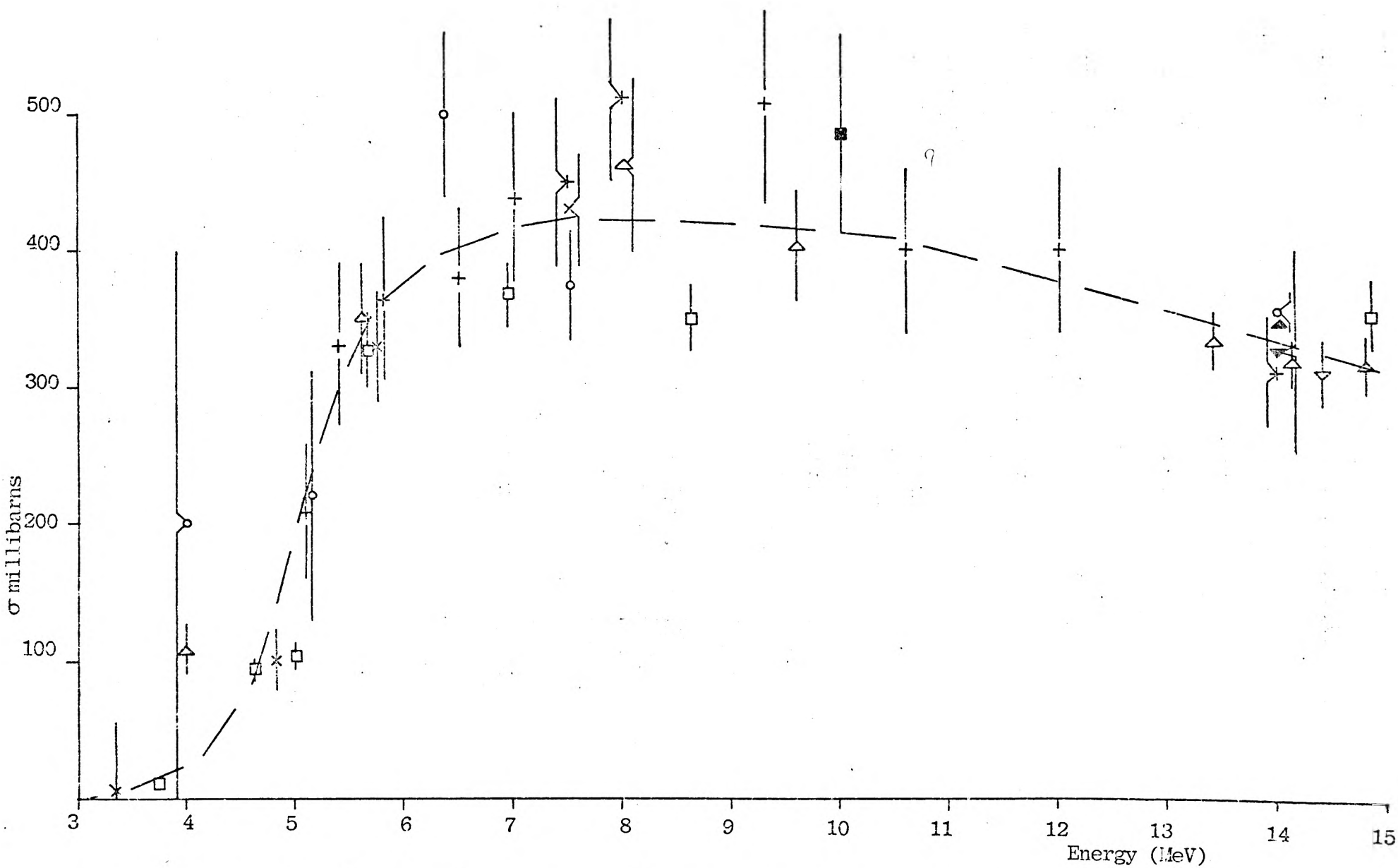

Figure 2.4 Data on the $^{7}Li(n,n't)^{4}He$ reaction cross-section up to 1972. (for key see Table 2.3)

The results obtained are given in Table 2.3. and are plotted in Figure 2.4, as are all the results discussed in section 2.2.

Another experiment using nuclear emulsions was carried out by Antolkovic (1971) at 14.1 MeV.

2.2.2. Measurement using Activiation

The long half-life of the tritium produced in the reaction, enables activation measurements to be performed. An experiment of this type would consist of an irradiation, during which the total neutron flux is measured, followed by a determination of the amount of tritium produced. Internal counting of tritium is necessary because its beta particles are of such low energy ($\bar{E}$ = 7 KeV), and all the activiation experiments performed have used gas proportional counting of the tritrium produced. (Wyman and Thorpe (1958), Osborne and Wilson (1961), Benjamin et al. (1962) and Brown et al. (1963))

Lithium metal samples, suitably canned, (since lithium metal reacts readily with both the oxygen and the nitrogen in the air) were irradiated by various neutron sources. The samples were then placed in a vacuum vessel, where the tritium was released as T_2 or HT, by heating in the presence of hydrogen gas. This radioactive gas was then used as a filling gas of a calibrated gas proportional counter.

Although the tritium measuring system was similar in each case, the flux determinations involved several different types of measurement. Wyman and Thorpe used associated particle measurement of the alpha particle yield when the neutron source was deuterons on tritium for their irradiations around 14 MeV. For lower neutron energies where the source was deuterons on deuterium, the beam current was monitored, and the yield calculated from the dD cross-section. When protons on tritium

were used, a counter telescope flux monitor was employed. Osborn and Wilson, using a 14 MeV dT shource, determined the flux by measurement of the activity induced in an aluminium foil by the $^{27}Al(n,\alpha)^{24}Na$ reaction. Benjamin et al. also used a 14 MeV dT source, but measured the flux with the associated particle method. Finally Brown et al. used pT, dD, and dT sources and measured the flux with a ^{235}U fission chamber which was calibrated at 14 MeV using the associated particle method with a dT source.

2.2.3. Measurement using Time-of-Flight techniques

In this method the neutron spectra at various scattering angles, are found by measuring the flight-time of the neutrons from the sample to the detector. Obviously the lower energy neutrons take longer to reach the detector. Normally a pulsed accelerator is used and the flight-time of the neutrons is measured from the instant when a pulse of charged particles reaches the neutron - producing target, until a neutron causes a pulse in the detector. A typical spectrum obtained from ^{7}Li is shown in Fig. 2.5. A peak is obtained corresponding to the neutron source energy used, which is due to elastic scattering. Other levels in the nucleus give peaks shifted by the energy of the level. In ^{7}Li the peak from the $(n,n'\gamma)$ reaction to the .478 MeV level is not resolved from the elastic scattering peak, at most energies. Reactions which do not occur via a well defined energy level do not produce a peak in the spectrum, but a continuous distribution.

The differential cross-sections for the various processes can be calculated provided that the relative efficiency of the neutron de ector is known over a suitable range of neutron energy. The efficiency need not be known absolutely since the

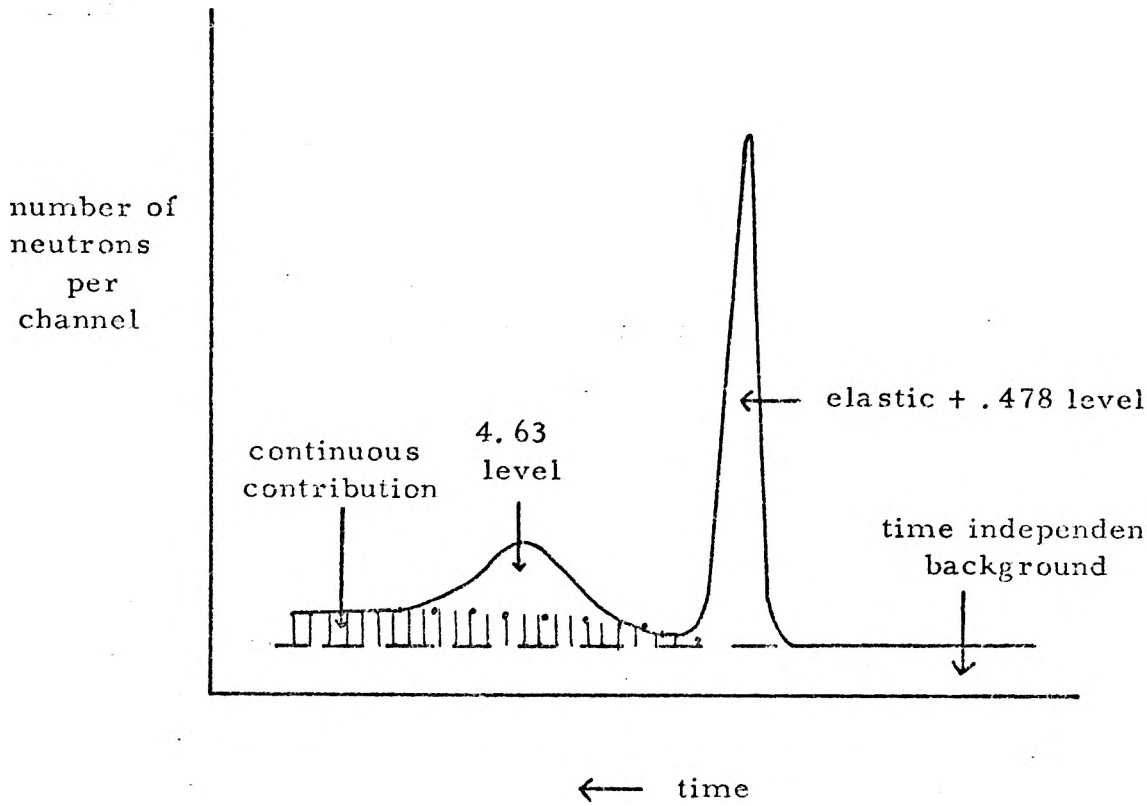

Figure 2.5 Time - of - flight spectrum for scattering from ^{7}Li.

differential cross-section can be normalised by measurement of the incident neutron flux with the detector. The $(n,n't)^4He$ reaction cross-section is calculated from the neutrons in the 4.63 MeV peak, plus those in the continuous distribution. A correction has to be applied for the low energy cut-off of the detector, and this has been done both by interpolation and using the data of Rosen and Stewart. The total cross-section for a particular reaction is obtained by an inte gration of the differential cross-section as a function of angle.

A check on the accuracy of the experiment is given by addition of the (n,n't) and (elastic + .478 level) cross-sections since they should give the total cross-section of ^7Li, which can be measured independently. (Above 10 MeV the contribution of (n,2n) reactions must also be considered). Time-of-flight measurements have been carried out by Batchelor and Towle (1963), Cookson et al.(1967) and Hopkins et al. (1968).

2.2.4. Sphere Transmission Measurements

This type of experiment has been carried out twice, (Ribe, (1953) and Graves (1954)), but only results of the latter have been analysed to provide the $(n,n't)^4He$ cross-section, (Thomas (1954)), as they were considered more accurate.

The method firstly establishes the size of the (n,2n) and (n,3n) cross-sections of ^7Li by measuring the counting rates of a flat response neutron detector with a bare neutron source and with the source covered with a lithium metal sphere. The experiment found that these cross-sections were negligible at 14 MeV. Secondly the spectrum of the transmitted neutrons is measured. The number of events below 12 MeV is corrected for elastic scattering and scattering to the .478 level, and the remaining effect is due to the $(n,n't)^4He$ cross-section, since

other reactions were found to be negligible.

However, in view of the fact that inelastic reactions other than (n,n'γ) and (n,n't) are now considered to have a cross-section of 85 mb at 14 MeV (Conlon (1972)) the result obtained in this experiment must now be considered questionable.

2.3. Existing data and Accuracy

The existing measurements of the $^{7}Li(n,n't)^{4}He$ reaction, given in Table 2.3,. are plotted in Figure 2.4. (Few measurements are available between 8 and 13 MeV incident neutron energy, because low energy particle accelerators are unable to produce reasonably monoenergetic neutrons in this region with any source reaction). Also shown in Figure 2.4. is the recommended cross-section, first suggested by Pendlebury (1964), based on the data available to him. This data is marked with an asterisk in Table 2.3. This recommended curve was not altered in a more recent evaluation by Conlon (1972) and it is used in both the British and American standard data files. (UKNDL and ENDF B III/IV).

Various authors have given estimates of the uncertainty on this recommended cross-section. Crocker et al (1970) suggested an uncertainty of ± 15% at 14 MeV and ± 25% at 8 MeV, and Conlon (1972) suggested ± 10% over the whole energy range. The two most recent estimates have also given a value for the whole energy range, and these are ± 15% by the ENDFB/IV evaluator (Stewart (1974)) and ± 20% by Steiner (1974).

The required uncertainty to produce a ±1% uncertainty in the tritium breeding ratio in a typical fusion reactor blanket is ± 5% (section 1.2.), therefore further $^{7}Li(n,n't)^{4}He$ measurements are needed, and this is why the current experiment was undertaken.

Recently, doubt has been expressed as to the reliability of the recommended tritium production cross-section. (Bachmann et.al (1978)). Also recent measurements of the ^{7}Li elastic cross-section at the Triangle Universities (Purser et al. (1978)) appear to be different from the recommended values, (The

elastic cross-section measurements affect the values for other partial cross-sections in that the total cross-section, which is known to ±5%, must be equal to the sum of the partial cross-sections). These two experiments have created considerable interest in the size of the ^{7}Li tritium production cross-section, and they are discussed, together with the results from this experiment, after the results section of this thesis.

CHAPTER THREE

TRITIUM MEASUREMENT

3.1. Tritium

Tritium, the heaviest isotope of hydrogen, is radioactive, decaying by beta emission, with a half-life of 12.35 years.

$$^{3}H \longrightarrow {}^{3}He + \beta^{-} + \bar{\nu}$$

The spectrum of beta particles from this reaction has been measured (Curran et al. (1949)) and is reproduced in figure 3.1. The range of most of these particles is such that they cannot penetrate even the thinnest of detector windows; the maximum penetration in aluminium being 2 microns, (Evans (1974)). In order to measure the activity, the tritium must therefore be introduced inside the detector. Two possible ways of doing this are available. Firstly, the tritium can be used (in the form of HT or T_2) as part of the gas filling of a gas proportional counter, or secondly, it can be incorporated with a liquid scintillator solution. For the second method, the tritium is normally added in the form of tritiated water, (HTO) or a tritiated organic compound, such as toluene. All previous activation methods have used the gas proportional counter method. For this determination of the $^{7}Li(n,n't)^{4}He$ cross-section, the liquid scintillator method was chosen because no gas handling equipment would be necessary, a liquid scintillation spectrometer was available, (at the Low Level Measurements Laboratory, AERE, Harwell) and it is always advantageous to use as many different approaches as possible to cross-section measurement in order to avoid common systematic errors.

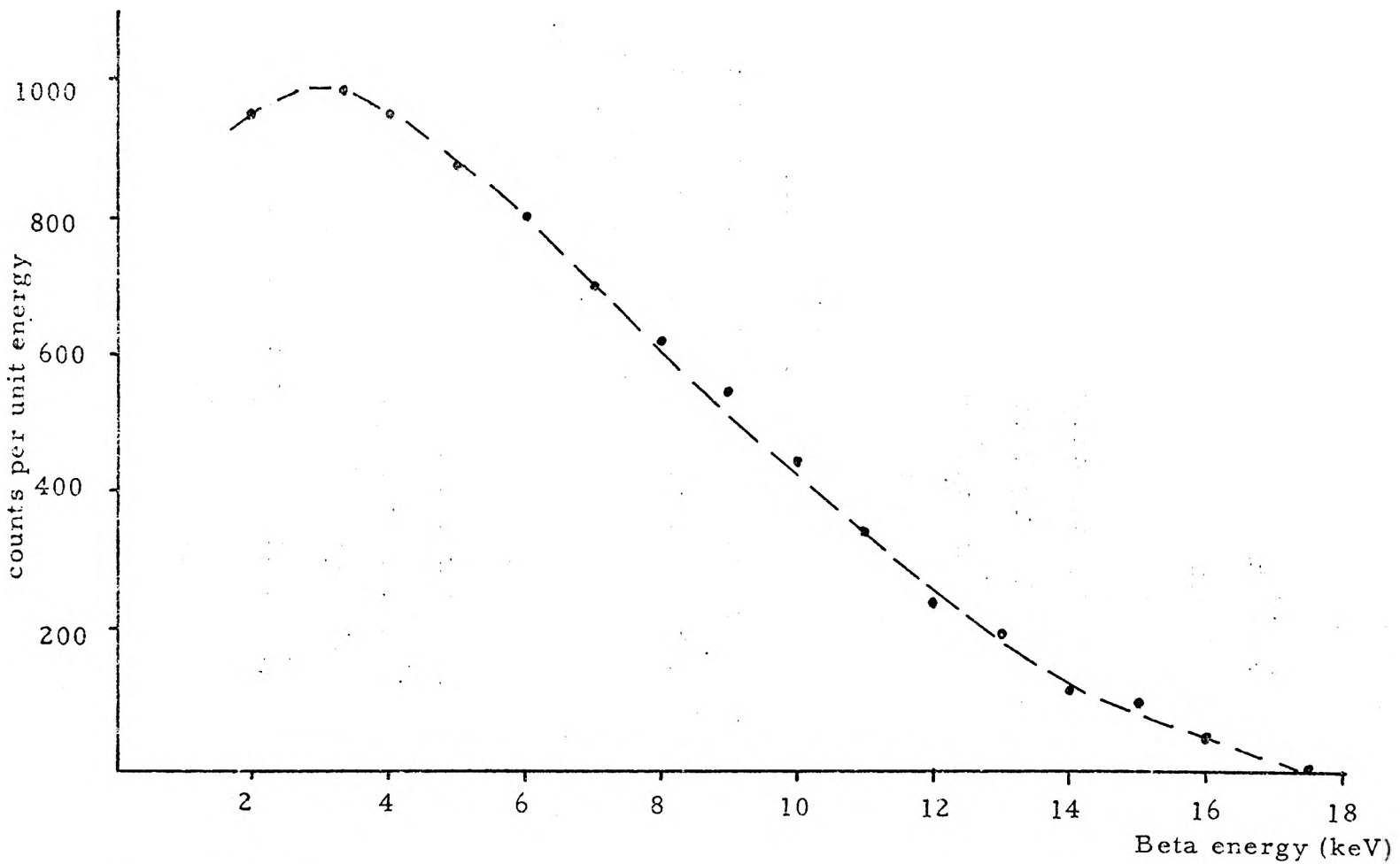

Figure 3.1 The beta particle spectrum of tritium (Curran et al. 1949)

3.2. Internal Liquid Scintillation Counting

Scintillating materials, those which give out light after excitation, have been known for many years. They were discovered by Sir William Crookes in 1903. One of the first, zinc sulphide, was used by Geiger, Rutherford and Marsden in many early experiments for counting alpha particles (e.g. Geiger (1908)). The flashes of light produced by incident charged particles were detected by eye, but this technique was discontinued because it was slow and laborious. Modern scintillation counting developed rapidly after the introduction of the photomultipler tube, which allowed electronic processing of the produced pulses.

Organic and inorganic substances possess the property of fluorescence, and both are currently used in a wide variety of application, as radiation detectors. For internal counting, as is necessary for tritium, only organic scintillators are used, since their luminescence properties remain substantially unaltered in solution, unlike inorganic scintillators which depend on the crystal structure for their action.

3.2.1. Basic Action

A fluor is a molecule which gives out light when it is excited. Organic fluors, either aliphatic or aromatic, are able to do this because they contain π-bonds. That is, some of the electrons are not localised in the neighbourhood of a particular carbon atom, and have energy levels with relatively low excitation energy, which can be excited by charged particles. The energy levels of such a fluor are shown schematically in Figure 3.2.

Tritium counting is done by dissolving a fluor in an organic solvent, with which the sample can be incorporated. A typical liquid scintillation sample would thus consist of a

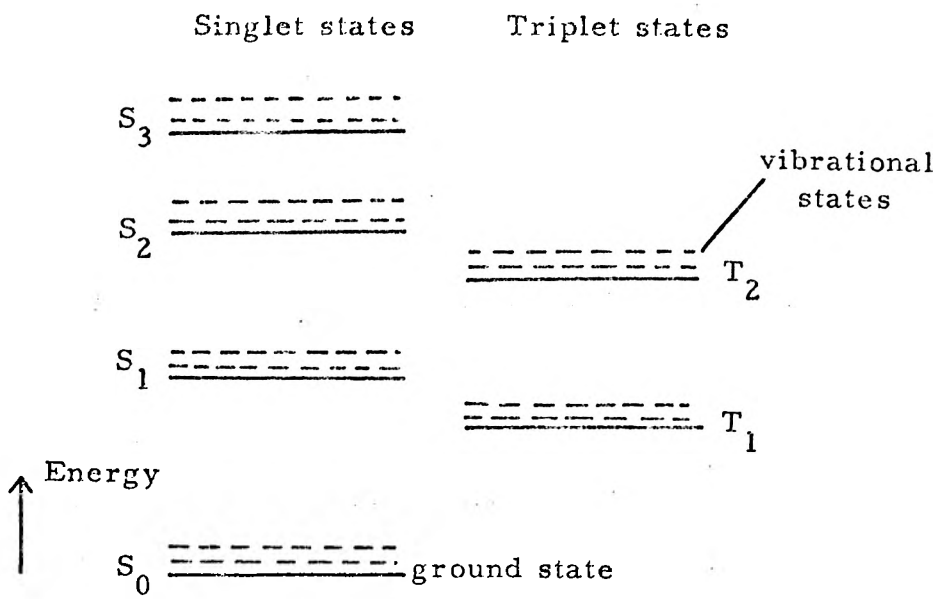

Figure 3.2 Energy levels of a fluor. (Triplet states are not directly excited from the ground state by charged particles).

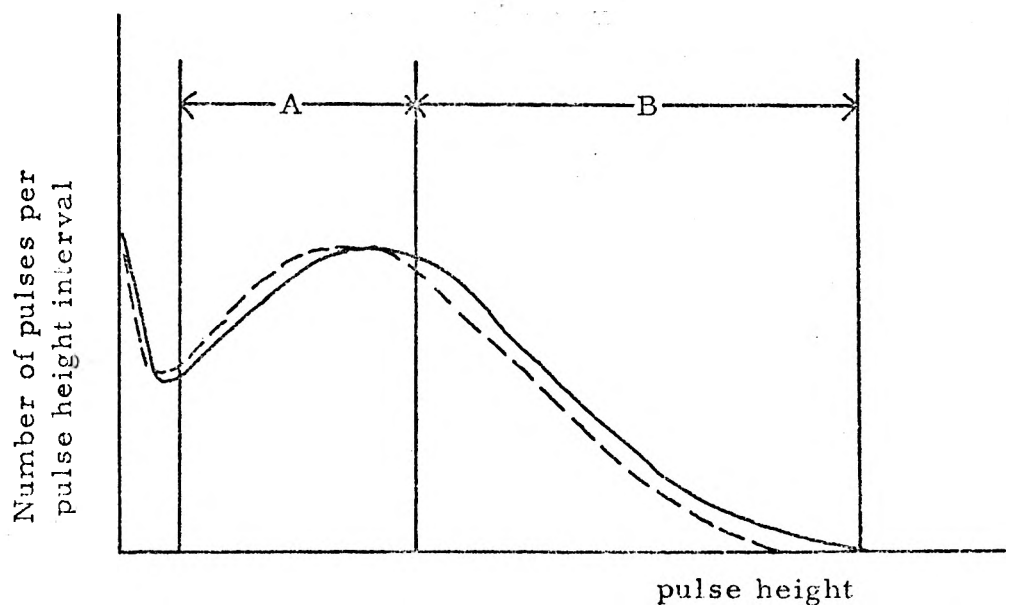

Figure 3.3 Pulse height spectra for two different amounts of quenching.

tritiated compound, (water, benzene etc.), an organic solvent, (dioxane, xylene, etc.) a primary solute, (the fluor), and often a secondary solute, which is also a fluor.

The energetic electrons, produced by the radioactive decay process, move through the sample, exciting the molecules, and also losing energy to the solution in the form of heat. The excited states of the molecules are predominantly singlet states because no spin change is involved in their formation. (For a discussion on the importance of triplet states see section 4.1.(b)). Because the solvent molecules are present in much greater numbers than other molecules, the excited molecules are predominantly solvent molecules. The higher excited states decay to the first excited state by internal conversion, (without the emission of radiation). Then the energy of the excited state is transferred through the solution from solvent molecule to solvent molecule until it is trapped on a solute molecule, which has a lower energy first excited state than the solvent, and so cannot return the energy to a solvent molecule. This first excited state of the solute is responsible for the emission of photons, in a solution with only one solute. In a solution with two solutes, the primary solute transfers energy to the secondary solute which then emits photons. Secondary solutes are used for two reasons. The first is in order to change the wavelength of the photons to provide a larger mean free path through the solution, (since the secondary solute has a smaller concentration than the primary), and the second, is so that the wavelength of the photons more closely matches the sensitivity of the photo-multiplier tube. A fraction of the emitted photons are incident on the photocathode of a photomultiplier tube, where a number of photoelectrons are produced, which give an electronic pulse

after amplification by the tube. The size of the pulse is directly related to the number of photoelectrons, and hence the number of excited molecules, via the number of photons. The shape of the pulse height spectrum depends on the response of the scintillator to different energy particles,and the type of amplification used, (in practice logarithmic amplifiers are normally used, to accomodate pulses of widely different sizes).

The scintillation efficiency of a fluor is defined as the amount of energy liberated as photons, per unit energy deposited by the charged particles. In a typical case this would be 4% (Birks (1964)), so that a 6·7 KeV beta particle (the mean of the tritium beta spectrum) would produce 90 photons, each of 3eV. If these photons were equally split between two photo-multiplier tubes, (to reduce the background, section 3.2.3), each with photocathode conversion efficiency of 25%, (a typical value), then 11 photoelectrons would be produced, (on average), to give rise to the photomultiplier tube pulse.

3.2.2. Quenching and Quench Correction Methods.

The counting efficiency of a particular liquid scintillator sample depends on the exact composition of the solution. All the energy which is dissipated in the solution by the charged particles is not converted into photons. Much of it is lost by radiationless de-excitation of the molecules and appears as heat in the solution. Constituents of a mixed solution, such as used in the present experiment, (which contains water and acetic acid in addition to the scintillator) provide extra paths for this de-excitation. This process is called chemical quenching.

In addition to this loss, photons which have been produced can be absorbed by solution constituents. Because such absorption occurs in coloured materials this effect is known as

colour quenching. This did not occur in the solution used in the present experiment.

These two processes cause the production of pulses with reduced size, which therefore can fall below the lower pulse acceptance level of the electronics, (set to remove noise), and hence reduce the counting efficiency. As the proportion of chemical constituents in the solution will vary slightly from sample to sample, some method must be used to determine the efficiency for each sample individually. The methods which can be used will now be described.

a) Internal Standard

In this technique, the unknown sample is counted to determine its counting rate. Then a known amount of the same radionuclide is added. When the sample is counted again, the increase in the counting rate gives the counting efficiency of the solution.

The problems with this method are that the sample is destroyed after it has been counted once, and the addition of more radionuclide could alter the efficiency of the solution. High specific activity additions must be used to give small additive volumes, and hence small perturbations to the solution, and this causes problems in determining the added activity accurately.

b) Sample Channels Ratio

This method (Baillie (1960), Bush (1963)) uses the change in shape of the pulse height spectrum, which occurs when the amount of quench changes. Two spectra with different amounts of quench are shown in Fig. 3.3. The spectral shift occurs because of the reduction in pulse height, and is directly related to the amount of quench, which in turn determines the efficiency. The spectral shift is quantified in terms of the ratio of the counts

in channel A to the counts in channel B. In this way a calibration curve can be made by using solutions containing known amounts of radioactivity but different, (and unknown), amounts of quench. This is often done by adding drops of acetone to the solution. The efficiency of any sample is then determined by reference to the point on the calibration curve corresponding to the measured channels ratio of the sample.

The advantages of this method are that the sample is not destroyed and so can be recounted. However, as the spectrum is split into two parts in order to determine the channels ratio, the statistical accuracy is reduced and so counting times have to be increased to compensate. This is particularly relevant for low activity samples where the statistics may be poor in any case.

c) External Standard count rate

In this method on external gamma source is placed near the sample. The gammas penetrate into the solution and produce pulses, via recoil electrons, and the number of counts above a certain discrimination level is recorded. The quenching in the sample reduces the mean height of the gamma ray pulses, (and hence the number of pulses above the discriminator), and so the count rate is a measure of the quenching. The efficiency is calibrated, using standard samples, as a function of gamma count rate, and so the counting efficiency for any sample can be found.

The disadvantages of this method are that it requires the source strength to remain constant, and to be accurately positioned; it is very sensitive to electronic gain changes, and the volume of scintillator must be the same in every sample. The main advantage is that the external source can be active

enough to give a statistically good number of counts in a short measuring time.

d) External Standard Channels Ratio

As the name suggests, this method is a combination of b and c above, and incorporates their best features, namely reproducibility, short measuring times, and ease of use. The procedure is almost identical to that of the samples channels ratio, except that the spectrum of an external gamma source is used. A calibration curve of efficiency versus channels ratio is produced in the same way. Facilities for using the External Standards Channels Ratio method are available on most modern commercial liquid scintillation spectrometers, and this is the method used for quench correction in the present experiment, on the Packard 3255 used.

3.2.3. Sources of Background.

For low-level counting, the background is very important since it determines the minimum activity which must be produced in the activation experiment. Also the uncertainty on the cross-section must include the uncertainty on the background. In order to minimise both the activity which must be produced, and the uncertainity on the result, the background must be minimised. The sources of background and how they can be minimised, will now be discussed.

a) Photomultiplier noise.

Thermal excitation of the photocathode of a photomultiplier tube can cause electrons to be released, which give rise to pulses in the tubes. This effect is reduced by cooling the photo-multiplier tubes, and in the spectrometer used in the present experiment the counting takes place at about 8^{o}C. Further cooling leads to difficulties with the liquid scintillator

solution separating from the aqueous fraction.

More importantly, this effect, together with others, is greatly reduced by using two photomultiplier tubes to view the liquid scintillator cell, and demanding coincidences between the two. As the noise from the two tubes is uncorrelated, the noise pulses in the final spectrum are reduced to just the randon coincidence rate of the two tubes. In the present instrument, the coincidence resolving time is 100 nS.

b) Background in the vial

The glass of the vial contains a certain amount of ^{40}K, which emits 11 KeV beta particles and these cause light pulses in the scintillator. The vials in the present experiment are made from low potassium glass in order to reduce this contribution.

There are two background producing processes which occur in the scintillator solution itself, the first being phosphorescence. Most of the photons, which are produced by a radioactive event, are produced in a very short period, (c.1nS), from the decay of the singlet excited states of the solute. However, the triplet excited states can decay to the singlet ground state, but have very long lifetimes. These states can give photons, during the counting of the sample, when they have been excited by exposure to daylight before counting. This effect is reduced by allowing the samples to "cool" in the dark for several hours before counting. Also since they are single photon events they are greatly reduced by coincidence counting (as for photomultiplier tube noise).

The second effect in the solution is chemiluminescence. Photons are produced by chemical reactions which leave molecules in excited states. This effect is reduced by avoiding chemicals which are known to undergo such reactions, and by allowing time

for these reactions to go to completion, before the samples are counted. These events again, are single photon events, and so the same remarks apply as for phototube noise and phosphorescence.

Background counts also arise from cosmic rays and environmental gamma activity near the counter. These events are usually few in number, and give large pulses which fall outside the range of the tritium counting window.

Finally, another background contribution is due to any tritium in the unirradiated pellet, or in any or the chemicals used. This was reduced by obtaining as pure samples as chemicals as possible, together with low tritium activity water, (section 3.6.).

The background contribution from all of these processes was determined by including unirradiated pellets in the chemical processing. Measurements were made in this way, with and without accompanying irradiated samples, to gauge the effect of tritium intercontamination. No effect was found.

Background counts from the photomultiplier tube are not affected by quenching in the sample. All other background is affected, and so the number of background counts should be corrected for the counting efficiency of the background sample, since the phototube contributes a negligible fraction of the back-ground in this case.

3.3. Conversion of produced tritium to be tritiated water.

Dierckx (1976) suggested a method for the measurement of tritium production from lithium, for use in foil spectroscopy. The method uses lithium carbonate as a sample, which is irradiated in a neutron flux to produce tritium. After the irradiation, the sample is dissolved in acetic acid, as follows:

$$Li_2CO_3 + 2CH_3COOH \longrightarrow 2(CH_3COOLi) + H_2O + CO_2$$

Dierckx states that at this stage the tritium is bound as HTO. The lithium acetate which is produced, is immiscible with liquid scintillator solutions, and so the second stage, is to precipitate the lithium as the fluoride, using hydrofluoric acid:

$$CH_3COOLi + HF \longrightarrow LiF + CH_3COOH$$

This removes the lithium acetate and replaces it with acetic acid, which is miscible with liquid scintillators, but does act as a quench. Liquid scintillator is now added to the resulting solution which is then ready for counting.

The major question concerning the above technique, is whether all the produced tritium does go into solution as tritiated water. Work has been carried out on the behaviour of tritium in lithium compounds by Lindner and Van Urk at the IKO Institute (Amsterdam). They irradiated various lithium salts containing ^6Li, in a reactor, and then analysed the forms of tritium which were produced when the compounds were dissolved.

There are various ways that a tritium atom can exist in a material. Firstly, a tritide ion. This reacts with water to give hydrogen tritide in the following way :

$$T^- + H_2O \longrightarrow HT\uparrow + OH^-$$

The hydrogen tritide behaves similarly to normal hydrogen, and may dissolve in the water, or escape as the gas. Secondly,

the opposite charge state to the tritide ion can exist. This is called labile tritium (T^+) and the significant feature of its behaviour, is that it exchanges with hydrogen ions. For example, in water:

$$T^+ + H_2O \longrightarrow HTO + H^+$$

Any tritium existing in the labile form in the sample is therefore bound into tritiated water on dissolution. Other forms of tritium can exist. In compounds containing hydrogen, molecular HT can be produced and is stable in the lattice of the sample, and behaves as the tritide on contact with water. When oxygen is present, the hydroxyl group can be formed (OT^-) which reacts in the same way as labile tritium atoms. Subsequently the term labile will be used to designate those tritium atoms which go into solution, as tritiated water, since the labile fraction was determined by measurement of the tritiated water produced on dissolution. (Van Urk 1970). Pellets of different materials were irradiated and dissolved in water in a gas tight enclosure. The labile fraction could then be found by separately measuring the activity in the water and the activity in the gas. The results for the compounds with high labile fractions, are shown in Table 3.4. Lithium carbonate was not measured in this experiment 'because of the potential complication that T-C bonds are formed on recoil (of the tritium nucleus)' (Lindner 1977).

This was the information available at the beginning of the present experiment and therefore the material chosen for the sample, was lithium hydroxide since it has the highest labile fraction (Tritium is not produced by (n,t) reactions in oxygen below 15 MeV neutron energy).

In order to convert the tritium in lithium hydroxide into tritiated water, a procedure based on that of Dierckx was used.

Compound	Labile fraction %
LiOH	99.7 ± 0.1
$LiOH \cdot H_2O$	99.3
$LiCRO_4 \cdot H_2O$	98.9
$Li_2SO_4 \cdot H_2O$	97.6
LiH_2PO_4	97.0
Li_3PO_4	95.8
Li_2O	93.4

Table 3.4 Labile fractions for some lithium compounds (Van Urk (1970))

This is described in detail in 3.6.

A recent experiment (Kudo et al. (1978)) has been carried out on the behaviour of tritium in lithium oxide, lithium hydroxide and lithium carbonate. The tritium was formed as in the experiment by Van Urk, by a reactor irradiation of compounds containing ^{6}Li.

Tritium, (in various forms), was released by heating the samples in a gas tight system, without the addition of water. Even under these conditions almost all the tritium produced in the samples ($>$ 96%) was released in the form of tritiated water. Mass spectrographic analysis of the products of heating indicated that the tritiated water was released at temperatures between 200-400^{o}C, which is greater than the temperature at which absorbed water, and water of crystallisation is evolved (100^{o}C). The conclusion to be drawn from this evidence, is that in all the compounds (Li_2O, LiOH, Li_2CO_3), the tritium is stored as LiOT and is released according to the equation

$$LiOT + LiOH \longrightarrow Li_2O + HTO$$

which is known to occur in the correct temperature range. The results of these experiments indicate that the stability of the tritium in the irradiated compounds should be high, with little chance of escape before dissolution, and that the tritium should readily go into solution as tritiated water on reaction with acetic acid. This agrees with the measurements of Herzing et al. (1976) who measured the tritium production in a fusion reactor blanket mock-up, using Dierckx's technique. They found that samples which were given the same irradiation, gave the same measured amount of tritium even when the time of chemical processing differed by several months.

3.4. Pellet design and manufacture

A sample was required which would subtend a known solid angle during irradiation, and which could be easily handled during the chemical processing at the end of the experiment. For these reasons a compressed pellet was chosen. The material chosen (section 3.3.) was lithium hydroxide, obtained from the Chemistry Division of AERE, Harwell. The isotopic composition of the samples was 99.99% ^{7}Li, so that any contribution to tritium production from the $^{6}Li(n,\alpha)$ reaction, (which has a very high cross-section at thermal neutron energy), would be minimised.

The chemical composition of the sample was measure by the Environmental and Medical Sciences Division, AERE, Harwell who found a lithium content of 27.96± 0.05%, corresponding to $LiOH\cdot\frac{1}{17}H_2O$. The water in the pellet could be due to atmospheric absorption. However, when a pellet was weighed as a function of time, no significant weight change occurred, and so the assumed formula was taken as constant.

The tritium produced in the pellets is stored as LiOT, and in this form it will not escape from the pellet after it is formed, (section 3.3.). However, there is a period between the formation of a triton and its capture by an oxygen atom, when it may have considerable energy. If the tritons are produced near the surface of the pellet then they could escape. The factor which determines the fraction escaping, is the range of the tritons in the material of the pellet.

If we consider uniformly produced tritons, emitted isotropically in the pellet, then the fraction of tritons escaping can be calculated. Consider a triton produced at depth x into the sample, with a range R (as in Figure 3.5). All

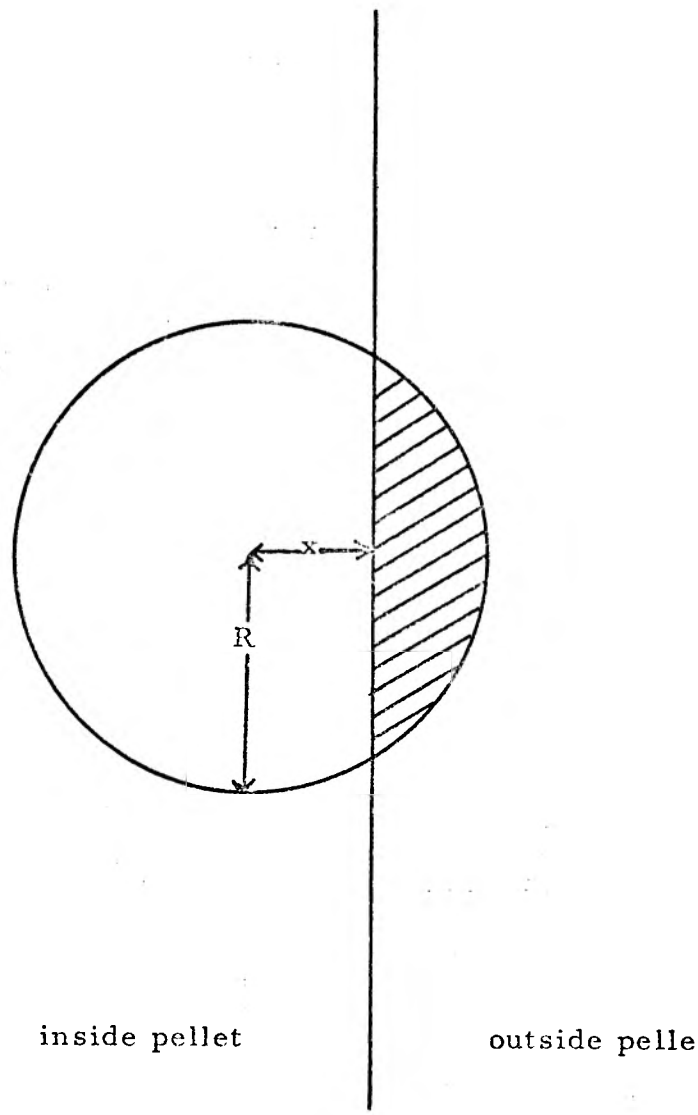

Figure 3.5 Geometry for calculation of triton escape

the tritons whose paths end on the shaded portion of the sphere will have escaped. As tritons formed further into the pellet than the range cannot escape, the total fraction escaping, F, is given by

$$F = \frac{S}{V} \int_0^R \frac{2\pi R(R-X)\,dx}{4\pi R^2}$$

where S is the surface area of the pellet, and V is the volume. On integration, this gives

$$F = (S/_{4V}) \times R$$

The range of the tritons depends on their energy, and because the $^{7}Li(n,n't)^{4}He$ reaction has three products, the triton spectrum is not easily calculated. The effect of triton escape will be worst at 14 MeV incident neutron energy, where most energy is available for the products, and at this energy the produced triton spectrum has been measured. (Valkovic et al. (1967)). It was found that a large fraction of the tritons produced, at an angle of 4^{o} to the incident neutrons, had an energy of 10.5 MeV. If we make the crude approximation that the tritons are emitted isotropically in the centre of mass frame, with a uniform energy distribution such that they give 10.5 MeV at 0^{o} in the laboratory frame, then this corresponds to a centre of mass energy for the triton of 6.6 MeV. The energy of the tritons emitted at 90^{o} to the incident neutron direction would be 7 MeV, and at 180^{o} would be 3.5 MeV. The corresponding ranges for tritons at 0^{o}, 90^{o} and 180^{o} would then be 0.3, 0.2 and 0.1 mm for lithium hydroxide, of density 1.5 $g.cm^{-3}$.

The expression previously derived for the fraction of tritons escaping, can now be evaluated. For a cylindrical pellet, the expression must be divided into three parts, with different ranges. The neutrons are incident on one flat face;

for escape from this face the appropriate triton range corresponds to 180^{o} emission, from the opposite flat face the range corresponds to 0^{o} emission, and the tritons escaping from the curved surface, have a range corresponding to 90^{o} emission. Combining these, the fraction escaping from a 1.5 cm diameter, 0.4 cm thick pellet of $1.5 g.cm^{-3}$ lithium hydroxide would then be 3%. Although this is only an approximate estimate, the calculation shows that the effect of triton escape is not negligible for an absolute cross-section determination.

In order to overcome this problem, the pellets were irradiated in a case made of the same material (lithium hydroxide). These are illustrated in Figure 3.6. The thickness of the case (c.1mm) was chosen so as to be greater than the maximum range of a triton. They were made, together with the pellets, by compressing lithium hydroxide in a die, to several hundred tonnes. The resulting pieces were quite robust, and no binder was found necessary.

The size of the triton loss, is very much reduced in this way. No net loss is experienced on the curved surface of the pellet where the number of tritons lost is equal to the number gained. The flat faces do experience a net loss due to the attenuation of the neutron flux through the pellet, together will the greater forward range of the tritons. The size of this effect is estimated to be 0.08%.

The final mechanism for tritium loss which should be mentioned, is the possibility of tritons reacting with the nuclei of the pellet. By considering the probability involved, even for a large absorption cross-section, this effect is found to be negligible.

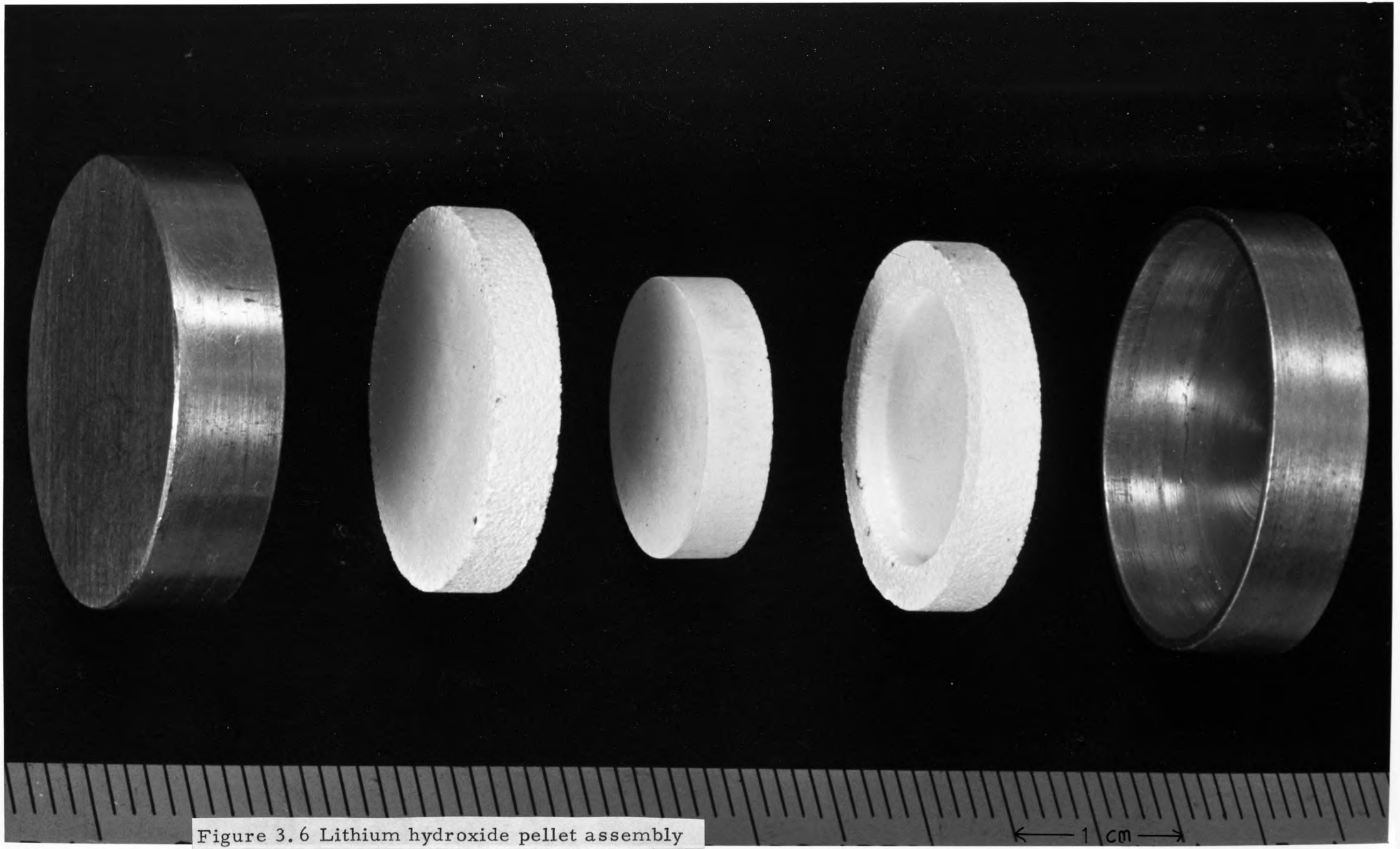

Figure 3.6 Lithium hydroxide pellet assembly

3.5. Experimental Procedure

The irradiated lithium hydroxide pellets were removed from the lithium hydroxide case, and placed into a weighed glass scintillation vial, which was then reweighed. This gave the weight of the pellet. (Glass vials were used because a better seal was achieved than with polyethylene vials. Because the rate of scintillator loss was negligible, this allowed the samples to be recounted after an interval of some weeks, in order to check the quench curve, and some of the measurements.)

Then 1.5 cm^3 of water was added from a pipette. This water had a lower tritium content than normal distilled water, in order to reduce the number of background counts.(This water was obtained from the Low Level Measurements Laboratory AERE, Harwell, and was kept in a container such that, as water was taken, it was replaced with dry air, so that atmospheric water could not enter the 'dead' water). Then 4 cm^3 of glacial acetic acid was added, and the vial was closed. The reaction

$$LiOH + CH_3COOH \longrightarrow CH_3COOLi + H_2O$$

forming lithium acetate, was allowed to go to completion, which took approximately 10 days. After this period, when the solution was clear, 1 cm^3 of 40% hydrofluoric acid was added to precipitate lithium fluoride, and so remove lithium acetate from solution:

$$CH_3COOLi + HF \longrightarrow LiF + CH_3COOH$$

The amount of HF added was less than was needed to remove all the lithium acetate. This was necessary since any excess HF would attack the liquid scintillator and the glass vial.

The scintillant chosen for this experiment was Dimilume. (Packard Instrument Co.). This consists of a primary solute of

phenylenebisphenyloxazole, (POPOP)in a solvent of xylene. It also contains a detergent, to increase its ability to mix with aqueous solutions, and a chemiluminescence inhibitor. This scintillator cocktail is specifically recommended for use with acid solutions. 15 cm^3 of this scintillant was added to the vial and the resultant solution was shaken to ensure complete mixing. The sample was then complete.

The scintillation counting was done by the Low Level Measurements Laboratory at AERE, Harwell, with a Packard 3255 automatic liquid scintillation spectrometer. This gives the counting rate of the sample in a standard tritium counting window, and also the external standard channels ratio. (3.2.2(d)). Before the samples were counted they were allowed to stand in the dark for at least 12 hours to allow any phosphorescence to decay, and to allow the lithium fluoride precipitate to completely settle.

The counting efficiency of each of the samples was found from an external standard channels ratio quench curve, which was determined in the following way. Unirradiated lithium hydroxide pellets were dissolved as above, and hydrofluoric acid was added. A standard solution of tritiated water was obtained from the Radiochemical Centre at Amersham, and this contained 1.2 microcuries of tritium per gram of water, and was known to an accuracy of $\pm$1% (1 standard deviation). Approximately 0.1g of this solution was added to each of the quench samples. The added weight was found by weighing the vials before and after the addition of the tritiated water. A correction was applied for evaporation of acetic acid while the tritiated water was being added. The evaporation rate, (measured on separate solutions) was 0.2 mg per min and this lead to a correction of 2%

to the mass of the tritiated water. The error on this correction was about 25%. The total error on the activity introduced into the solution is, therefore, made up of 0.5% (evaporation correction), 1% (standard solution) and 1% (weighing) which gives an overall error (1 standard deviation) of 1.5%.

The scintillator was then added to these standard samples in the same way as above, and they were counted. A total of 8 million counts was accumulated, and so the statistical error on the results is negligible, as is the contribution due to the background. The resulting quench curve, i.e. efficiency versus external channels ratio, is shown in Figure 3.7. A straight line fit was made to the data (also shown) by the method of least squares, and this was used to find the efficiency of the samples from the measured external standard channels ratio. The uncertainty on the straight line fit was deduced from the value of chi-squared, and this was found to be 2.2%. (A second order polynomial fitted to the same data gave no significant improvement in the fit to the points and so was not used).

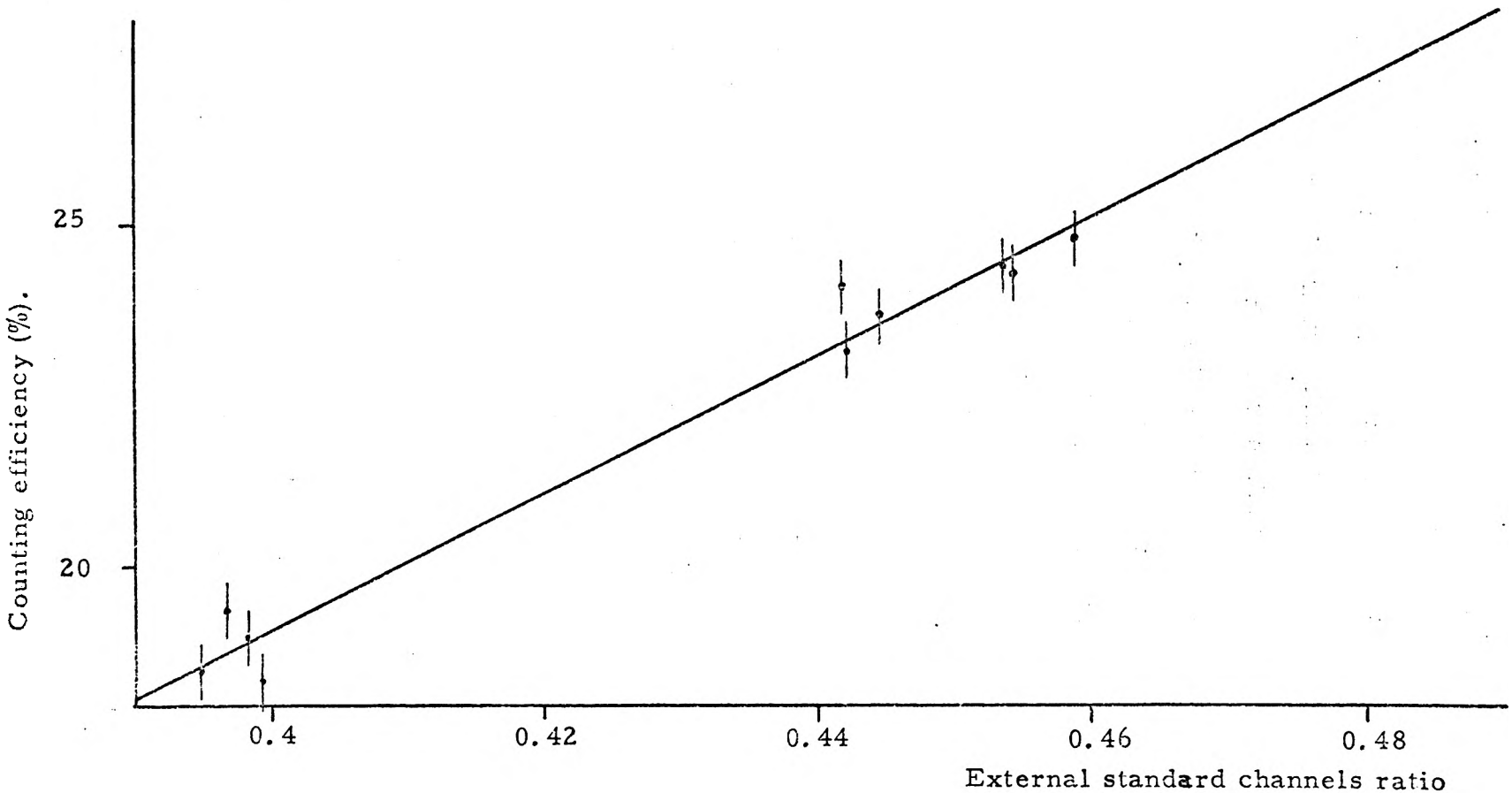

Figure 3.7 Quench curve. (Note suppressed zero)

3.6. Multiple Scattering.

When a beam of neutrons is incident on a block of material, the reactions which occur can be divided into two classes. Firstly there are those reactions which involve previously unreacted neutrons from the beam (The 'uncollided flux'). The rest of the reactions are initiated by neutrons which have undergone a reaction of some sort, such as elastic scattering, or by a neutron produced by a previous reaction such as an (n,2n) reaction.

When the total reaction rate is measured as in this experiment, it is important to determine the fraction of reactions which were caused by the uncollided flux. This enables a correction to be made to the total tritium production, and hence the cross-section can be calculated.

The way in which the amount of multiple scattering was calculated, used a Monte Carlo program, SPECIFIC II (Holborough and Lipscombe (1971)) which uses the UKNDL data library. Monte Carlo programs were also used in section 4.2.3, and the way in which they work will be briefly outlined.

The cross-section data for the necessary nuclides would be input, together with the geometrical arrangement of the experiment. A neutron source position would be chosen. This could either be a point, or distributed over a volume. In the latter case random numbers would be used to choose one particular starting place in the volume but in both cases, random numbers would give the direction of travel of the source neutron.

The probability that a neutron of energy E travels a distance X without interacting, in a direction with total cross-section $\Sigma(E)$, is $e^{-\Sigma x}$. A random number is chosen from this distribution, after the total cross-section along the neutron

path has been calculated, and the resulting value is the position for the next reaction of the neutron. The reaction type occuring at this position is then chosen from the available possibilities, according to their relative probabilities. If the neutron survives the event, then the new neutron parameters (direction and energy), are calculated from the kinematical model of the reaction, and the tracking is continued in the same way until the neutron reaches a position or energy when it is no longer of interest. Any secondary neutrons from reactions such as (n,2n) are also tracked.

The computer can record any parameter of interest during the experiment. For the modelling of liquid scintillation detector (section 4.2.3), the light output from each reaction caused by one neutron, would be added to give the size of the light pulse. The pulses from all tracked neutrons would then give the pulse height spectrum for a particular detector. (The light output relationship for particular product particles, would be fed in together with the cross-section data). In the multiple scattering correction, the important quantity is the neutron flux or reaction rate (flux times reaction cross-section times number of nuclei) in particular regions. The flux can be determined, after all the neutrons have been tracked, (usually tens of thousands) either by the number of collisions in a particular region, or from the total path length traced out by neutrons in the region. In regions of low cross-section, like the pellet and case assembly, where 90% of incident neutrons do not interact at all, the track length method of flux determination gives results with less statistical uncertainty.

The multiple scattering correction is worked out by calculating the tritium production reaction rate in the real

assembly, (lithium hydroxide), and then working it out again with all secondary neutrons 'switched off'. The switching is done by using a fictitious material, ABSORBIUM, which only undergoes absorption reactions. The reaction rate is worked out with the assembly made of ABSORBIUM of such a density that the total macroscopic cross-section is the same as the lithium hydroxide. The flux in this case is just the uncollided flux, since any neutrons which have reacted have disappeared.

The ratio of the total reaction rate to the uncollided flux reaction rate gives the fraction of tritium produced by multiply scattered neutrons. The results obtained are shown as a function of incident neutron energy in figure 3.8. The shape of the curve broadly follows the shape of the $^{7}Li(n,n't)^{4}He$ reaction cross-section. The dip at 5 MeV neutron energy corresponds to a dip in the total cross-section, and hence a reduction in the number of reacted neutrons.

The errors shown on the figure are statistical errors only. Any other uncertainity will be due to errors in the cross-section data set, and this has been assigned a value of 15%, giving a total error of 20% for the correction. Since the correction is small, this only corresponds to 0.8% uncertainty in the measured tritium production cross-section, when the correction is greatest.

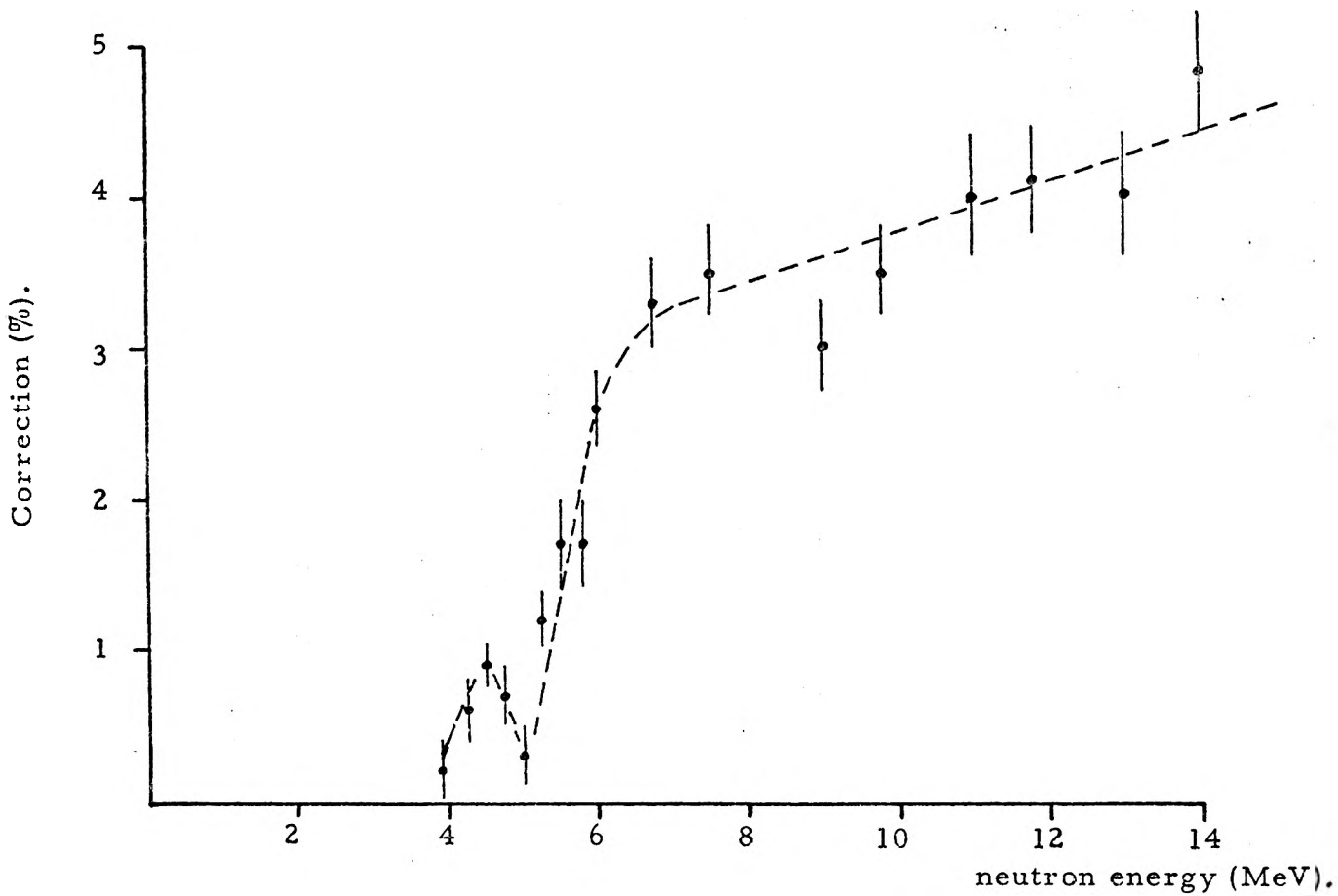

Figure 3.8 Multiple scattering correction.

3.7. Measurement of the $^{6}Li(n,t)^{4}He$ reaction cross-section

Lithium-6, the less common isotope, undergoes a tritium production reaction with thermal neutrons:

$$^{6}Li + n \longrightarrow {}^{4}He + t$$

The cross-section for this reaction is known very accurately (±0.5% Stewart (1974)) in the thermal neutron energy region. This makes the $^{6}Li(n,t)$ reaction an ideal test of the tritium measurement system used in this experiment.

A source of thermal neutrons of known intensity was available in GLEEP, a graphite moderated thermal reactor at AERE Harwell. This reactor has an irradiation facility enabling the rapid positioning of a sample inside the core of the reactor. The neutron flux at this position has been calibrated relative to an ionisation chamber monitor, using activation measurements of gold and manganese-nickel foils (Axton 1963).

There are two effects which complicate a measurement of this sort. Firstly the cross-section of ^{6}Li should be measured in a Maxwellian neutron distribution, whereas the flux in the reactor will have non-Maxwellian components. This is overcome by a cadmium ratio measurement (part (a) below). Secondly the neutron flux at the irradiation position will not be the same when an absorbing sample is placed there. This effect requires a flux perturbation calculation outlined in (part (b) below).

a) Cadmium Ratio method

The reaction rate in a sample can be calculated using the Westcott (1960) flux convention. The Westcott flux is defined as the reaction rate of a material with a pure $\frac{1}{v}$ cross-section, and unit cross-section at a neutron velocity of 2200 m/sec. If the normal scalar neutron flux is $\phi(E)$ at neutron energy E, then the Wescott flux is given by:

$$\phi_w = \int_0^\infty \left(\frac{E_o}{E}\right)^{\frac{1}{2}} \phi(E)\,dE$$

The integrated reaction rate in a thin sample with cross-section $\sigma(E)$ and N nuclei can thus be written

$$\int_0^\infty \sigma(E)\phi(E)\ N\ dE = \phi_w N \sigma_o (g+rs)$$

where g and s are measures of the departure of the cross-section from $\frac{1}{V}$ behaviour, and r is a measure of the departure of a particular spectrum from Maxwellian. The reaction rate for a real sample, D_o, is given by

$$Do = \int_0^\infty Z(E)\ \sigma(E)\ \phi(E)\ N\ dE$$

where Z(E) is the self shielding factor at energy E. We can divide this integral into parts by considering the cross-section to be a sum of a $\frac{1}{V}$ part ($\sigma_1(E)$) and a non-$\frac{1}{V}$ part. ($\sigma_2(E)$):

$$Do = \int_0^{0.1eV} Z(E)\ \sigma_1(E)\ \phi(E)NdE + \int_{0.1}^\infty Z(E)\ \sigma_1(E)\ \phi(E)NdE$$

$$+ \int_0^{0.1} Z(E)\ \sigma_2(E)\ \phi(E)NdE + \int_{0.1}^\infty Z(E)\ \sigma_2(E)\ \phi(E)N\ dE$$

where the cadmium cut-off energy is 0.1eV. The third term represents the contribution of the non-$\frac{1}{V}$ part of the cross-section below 0.1eV. It is a good approximation for most materials to assume this term is zero. The reaction rate, D_{cd}, when the sample is covered with a layer of cadmium to absorb all neutrons below 0.1eV, can be written similarly

$$\frac{D_{cd}}{t} = \int_{0.1}^{\infty} Z(E)\ \sigma_1(E)\ \phi(E)N\ dE + \int_{0.1}^{\infty} Z(E)\ \sigma_2(E)\ \phi(E)N\ dE$$

where t is the mean transmission of neutrons above 0.1eV through the cadmium layer. By subtracting these two expressions we obtain

$$Do - \frac{D_{cd}}{t} = \int_{0}^{0.1eV} Z(E)\ \sigma_1(E)\ \phi(E)N\ dE \qquad 3.2$$

This integral is over a largely thermal energy range, and we can define a thermal self-shielding factor $\bar{Z}$ such that

$$\int_{o}^{0.1} Z(E)\ \sigma_1(E)\ \phi(E)N\ dD = \bar{Z} \int_{0}^{0.1} \sigma_1(E)\ \phi\ (E)N\ dE \qquad 3.3$$

($\bar{Z}$ will be calculated in the next section (b))

The cadmium ratio of an ideal $\frac{1}{V}$ absorber can be calculated from

$$R = \frac{\int_{o}^{\infty} \sigma_o(\frac{E_o}{E})^{\frac{1}{2}} \phi(E)\ dE}{\int_{o.i}^{\infty} \sigma_o(\frac{E_o}{E})^{\frac{1}{2}} \phi(E)\ dE}$$

This factor enables the integral on the R.H.S. of equation 3.3. to be corrected to include the reaction rate of σ_1 above the cadmium cut-off:

$$\int_{o}^{\infty} \sigma_1(E)\ \phi(E)\ N\ dE = \frac{R}{R-1} \int_{0}^{0.1} \sigma_1(E)\ \phi(E)N\ dE \qquad 3.4$$

The factor R/R-1 is near unity since a $\frac{1}{V}$ cross-section has fallen to a relatively low value at 0.1eV. From equation 3.1 we have:

$$\int_{o}^{\infty} \sigma\ (E)\ \phi(E)N\ dE = \phi_w\ \sigma_o N$$

for a purely $\frac{1}{V}$ cross section. Using this expression for the σ_1

reaction rate, together with equations 3.3 and 3.4 we obtain

$$\sigma_o = \frac{1}{\bar{Z}} \cdot \frac{1}{\phi_w N} \cdot \frac{R}{R-1} \left(Do - \frac{D_{cd}}{E}\right)$$

N is known from the material used, D_o and D_{cd} have been measured, and ϕ_w, R and t have been determined for GLEEP when 1mm thick cadmium cases are used (Axton (1963)). The values found were $\phi_w = 1.663 \times 10^8$ n/cm^2/s/μA of ionisation chamber monitor current, R 42.64, giving $\frac{R}{R-1} = 1.024$ and t was 1.00. It now remains to calculate $\bar{Z}$.

b) Flux Peturbation Calculation

An expression for the reaction rate in a pellet embedded in a moderator will now be considered. The reaction rate is proportional to the average flux over the volume of the pellet, $\bar{\phi}_v$. (Spatially averaged, not energy averaged - only one, thermal group is considered here). It is conventional to calculate this flux in two stages. Firstly the flux depression factor is defined as the ratio of the mean flux over the surface of the pellet, $\bar{\phi}_s$, to the unperturbed flux, ϕ_o :

$$F(\gamma, \tau) = \bar{\phi}_s/\phi_o$$

where τ is the optical thickness of the pellet, and γ is the ratio of the scattering cross-section to the total cross-section of the moderator. This function is normally written

$$F(\gamma, \tau) = \left[1 + \left[\tfrac{1}{2} - E_3(\tau)\right] g(\gamma, \tau)\right]^{-1}$$

where $E_3(\tau)$ is the normal third exponential integral, and the function $g(\gamma, \tau)$ depends on the scattering cross-section of the moderator, the radius of the pellet, and the author of the particular paper. However, for all $g(\gamma, \tau)$ functions considered (Bothe (1943), Tittle (1951), Meister (1956 and Ritchie and Eldridge (1960)) the function $F(\gamma, \tau)$ turns out to be approximately

1.0, for the pellet used. For 0.5% ^{6}Li the maximum deviation of $f(\gamma, \tau)$ from 1.0 for any author was 0.3%

The second factor relates the mean flux over the surface to the mean flux over the volume of the sample. This is the self-shield function $G(\tau)$.

$$G(\tau) = \bar{\phi}_v / \bar{\phi}_s$$

The normal expression for this (Williams (1965)) is given as

$$G(\tau) = \frac{1}{\tau}\left[\tfrac{1}{2} - E_3(\tau)\right] \qquad 3.5$$

however this relates to the whole of the irradiated sample, and in the present experiment only the reaction rate in the centre pellet (without the case) is of interest.

If the situation is as shown in Fig. 3.9 then the reaction rate can be determined in two parts. Firstly due to the flux from side A and secondly from side B. The flux is expanded in Legendre polynomials:

$$\bar{\phi}_s = \sum_l \frac{2l+1}{2} K_l P_l(\cos\theta)$$

Then the reaction rate in the section t_1 to t_2 due to the flux A is then (ignoring scattering)

$$\int_1^0 \sum \frac{2\,1+1}{2} K_1 P_1(\cos\theta) \int_{t_1}^{t_2} \exp\left(-\frac{\Sigma_a x}{\cos\theta}\right) dx \Sigma_a d\cos\theta \qquad 3.6$$

where Σ_a is the macroscopic absorption cross-section. Similarly the flux due to side B

$$\int_0^1 \sum \frac{2l+1}{2} K_1 P_1(\cos\theta) \int_{t_1}^{t_2} \exp\left(-\frac{\Sigma_a (t-x)}{\cos\theta}\right) dx \, \Sigma_a d\cos\theta \qquad 3.7$$

If we only consider the first term in the Legendre expansion of expression 3.6 we obtain

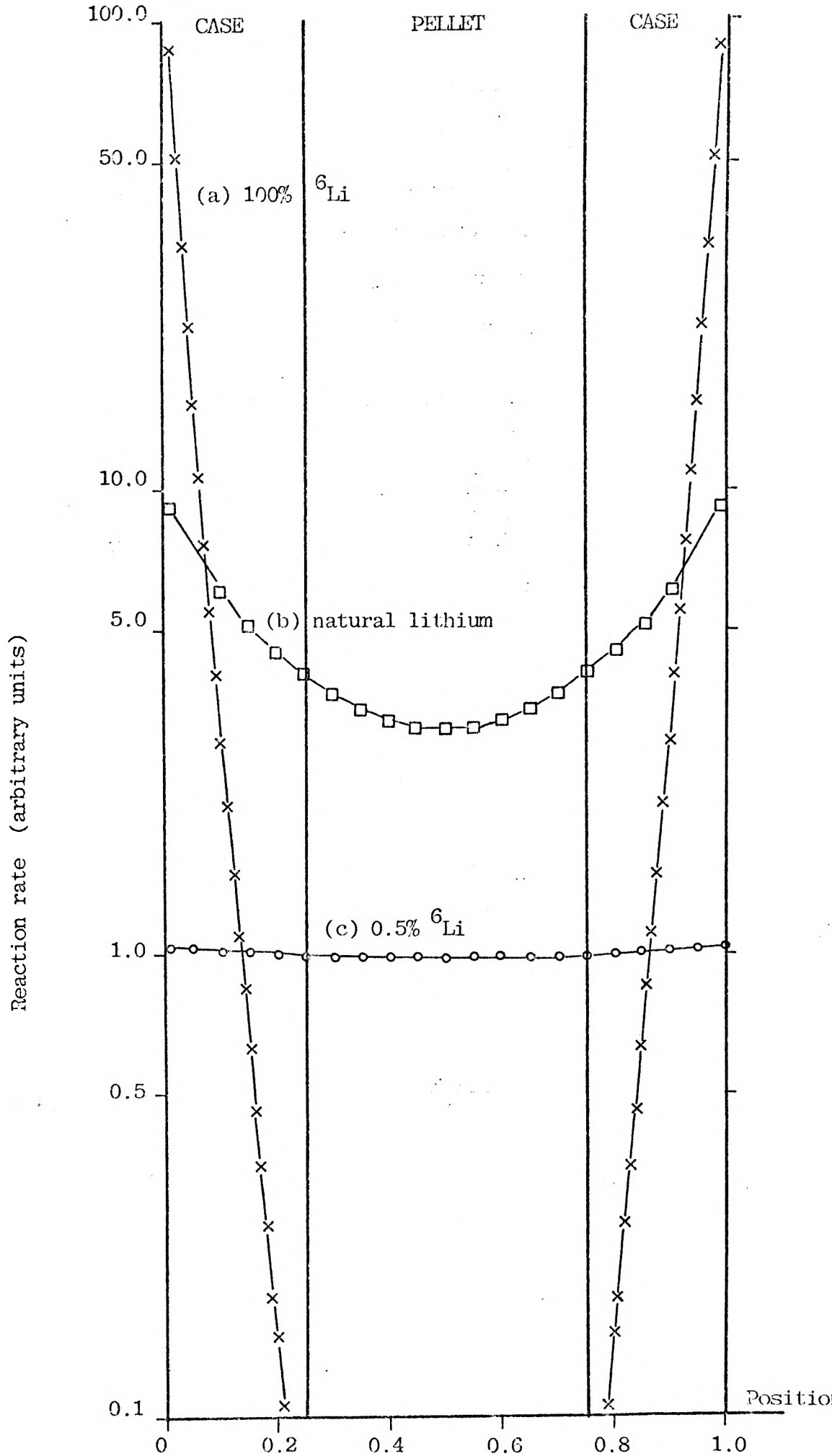

Figure 3.9 Reaction rate in a lithium hydroxide assembly as a function of position, for various ^{6}Li concentrations.

$$\Sigma_a \frac{Ko}{2} \int_0^{\pi/2} \sin\theta \int_{t_1}^{t_2} \exp\left(-\frac{\Sigma_a X}{\cos\theta}\right) dx$$

which can be written

$$\frac{\Sigma_a Ko}{2} \; E_3(t_1 \Sigma a) - E_3(t_2 \Sigma a)$$

since

$$\int_0^{\pi/2} \sin\theta \cos\theta \exp\left(-\frac{t\Sigma a}{\cos\theta}\right) d\theta = \int_1^{\infty} \frac{\exp(-t\Sigma a X)}{x^2} ds = E_3(t\Sigma a)$$

similarly expression 3.7 becomes

$$\frac{\Sigma a Ko}{2} \left[E_3((t-t_2)\Sigma a) - E_3((t-t_1)\Sigma a) \right]$$

Then the total reaction rate between t_1 and t_2 is then

$$\frac{\Sigma a Ko}{2} \; E_3(t_1 \Sigma a) - E_3(t_2 \Sigma a) + E_3((t-t_2)\Sigma a) - E_3((t-t_1)\Sigma a)$$

which corresponds to expression 3.5 for $t_1 = 0$ and $5_2 = t$. The fractional reaction rate in the interval t_1 to t_2 is then

$$F(t_1, t_2) = \frac{E_3(\tau_1) - E_3(\tau_2) + E_3(\tau - \tau_2) - E_3(\tau - \tau_1)}{1 - 2E_3(\tau)}$$

and this has been calculated in 100 intervals across the pellet using different ^6Li isotopic abundances. The results for 100% ^6Li, 7% ^6Li (natural) and 0.5% ^6Li concentrations are shown in Fig. 3.9 (a), (b), and (c) respectively.

These results show that a low $^6Li/^7Li$ ratio is necessary if a large correction is to be avoided.

The expression derived for the self-shielding above assumes that the sample is part of an infinite plane sheet of material. However, when a finite sample is used, neutrons can enter the sides of the disc, without traversing any absorbing material. Thus the average flux is increased and the self-shielding effect is reduced. A correction for this effect has been calculated by

Hanna (1963). By considering the trajectory of a neutron entering through the curved side of the disc, and integrating over all possible trajectories, the normal self-shielding function (equation 3.5) is modified to:

$$G(\tau) = \frac{1}{\tau}\left[\tfrac{1}{2} - E_e(\tau)\right](1+\epsilon) \qquad 3.6$$

where ϵ is given by

$$\epsilon = \frac{2\,(I_1 - I_2)}{\left[\tfrac{1}{2} - E_3(\tau)\right]\pi R}$$

where R is the radius of the disc, and I_1 is given by:

$$I_1 = t\left[\frac{\pi}{4} - \frac{2}{3\tau} + \int_0^{\pi/2} e^{-\tau \sec\theta}\left[1-\cos^2\theta + \frac{2}{\tau}\cos\theta - \frac{2}{\tau}\cos^3\theta\right]d\theta\right]$$

and I_2 is given by

$$I_2 = \frac{\tau^2}{2\Sigma}\left[\int_0^1 E_2(2\Sigma R \sin\theta)\,d(\cos\theta)\right]$$

The way in which is expression was applied to the irradiated pellets will be described below.

Reactor Irradiation

The irradiations were carried out on GLEEP, which was running at 3 kW. The relative flux is measured using an ionisation chamber, the current from which is recorded by the voltage required to equal the voltage across a 10 MΩ resistor. (the "backing-off voltage", b.o.v).

On the day of the irradiations, a calibration of the flux was made by A.Bardell (National Physical Laboratory, Teddington) using cadmium ratio measurements on gold foils of various

thicknesses. Different irradiation times were used to produce approximately the same activity in each foil.

A suitable concentration of ^{6}Li in the lithium hydroxide pellets was made by mixing 96% $^{6}LiOH$ and 99.99% $^{7}LiOH$. The $^{6}Li/^{7}Li$ ratio was measured by mass-spectrometry at AWRE (Aldermaston), and found to be 0.0056 $\pm$ 0.0002. The pellets were irradiated in a case of the same material, inside a thin aluminium can (Figure 3.6). The bare irradiation lasted 20 minutes with a b.o.v. of 60.02. The cadmium covered sample was placed inside a cadmium box of 1 mm wall thickness and irradiated for 20 minutes with a b.o.v of 59.97.

Finally a measurement was made of the perturbed flux inside an empty lithium hydroxide case, both with and without the cadmium can, for three different thicknesses of gold foil. This was done in order to check the flux perturbation calculation for lithium.

The activities of all the gold foils (measured at NPL), were corrected for gamma self-absorption, the cadmium covered activity and neutron self-shielding. (For the latter, edge effects are not important). These corrections are shown to be valid by the agreementbetween the values of the flux given by different thicknesses of foils. The value obtained for the unperturbed flux was 1.59 x 10^{8} $n/cm^{2}/s/uA$ of ionisation chamber current. The value of the flux inside the lithium hydroxide case was 1.52 x $10^{8} n/cm^{2}/S/$ A which is5% less than the unperturbed flux. The uncertainty on these fluxes due to systematic and statistical errors is $\pm$2%.

The flux perturbation calculation which includes edge effects was used for the pellet. In order to check its validity a calculation was carried out for the flux inside the lithium

hydroxide case. The analytical expression cannot deal with the precise geometry involved, and so the approximation was made that the material of the case was uniformly distributed over the volume of the case. The calculated self-shielding factor was 0.935 compared with the measured value of 0.95. This gives a certain amount of confidence in the calculation, but a 3% error has been assumed in order to allow for the discrepancy.

The calculation of the cross-section was carried out using the self-shielding factor for the pellet alone, together with the measured value of theflux inside the empty case. The self-shielding factor for the pellet was 0.945. (If the edge effects are ignored, the corresponding self-shielding factor is 0.88).

The cross-section is calculated from

$$\sigma = \frac{(T_{bare} - T_{covered})}{N_{Li} \times \text{mean flux} \times \text{irradiation time}} \times \frac{\text{cadmium ratio}}{\text{labile faction}}$$

where T_{bare} and $T_{covered}$ are the number of tritium atoms produced in the bare and covered irradiations respectively and N_{Li} is the number of ^{6}Li atoms in thepellet. The latter is calculated from the $^{6}Li/^{7}Li$ ratio and the lithium content of the pellet. This was measured in the Applied Chemistry Division at AERE, Harwell, and found to be (27.5 $\pm$ 0.1)%. The number of tritium atoms produced was measured by processing the irradiated pellets in the way described in section 3.5, and the results of these measurements are shown in Table 3.10. The background on these measurements is not included since it will be the same for both pellets which were made from the same batch of material. The labile fraction (section 3.3) was taken to be 0.997. The value obtained for the 2200m/s cross-section of the $^{6}Li(n, \alpha t)$ reaction was 900 barns.

The undertainty on this result is due to uncertainities on the $^{6}Li/^{7}Li$ ratio ($\pm$4%), flux measurement ($\pm$2%), tritium measurement ($\pm$2.2%) and on the flux perturbation calculation ($\pm$ 3%). The overall error obtained (by adding these in quadrature) is $\pm$ 5.8%.

Thus the final value obtained for the thermal $^{6}Li(n,\alpha t)$ cross-section is 900 $\pm$ 52 barns. The accepted value (Stewart (1974)) is 940 $\pm$ 5 barns. The present result, although not a precise measurement of the ^{6}Li cross-section, does give a good indication that the tritium measurement method does not have a large systematic error.

irradiation	pellet mass g	counts per minute	external channels ratio	counting efficiency (%)	distintegations per second	No. of tritium atoms	No. of lithium 6 atoms
bare	1.010	3128	.4444	23.5	221.8	1.25×10^{11}	1.32×10^{20}
cadmium covered	1.010	136.6	.4421	23.3	9.78	5.48×10^{9}	1.32×10^{20}

Figure 3.10. Tritium counting results from reactor irradiation.

CHAPTER FOUR

NEUTRON DETECTION

This chapter describes the way in which the neutron flux was measured during the cross-section measurements.

Some irradiations were carried out using the D(d,n) neutron source reaction, with a deuteron beam from the Tandem Van de Graaff at AERE, Harwell. The neutron flux in these irradiations was measured with an NE213 liquid scintillation detector, which was calibrated in an absolute efficiency experiment, described in section 4.2.

The remainder of the irradiations were carried out using the T(d,n) neutron sources with a 500 KeV Cockcroft-Walton accelerator, (also at AERE, Harwell). For these, it was not possible to use the calibrated detector, because the high beam current caused count rate problems even at the largest available distance from the source. The neutron flux was, therefore, determined from the yield of alpha particles from the source reaction. A comparison of the two methods of flux measurement was made at low beam currents, and this is described in Section 4.3.

The first section of the chapter deals with the basic behaviour of neutrons and liquid scintillators, and explains the principle of the method used for pulse shape discrimination (between neutrons and gamma rays) in this experiment.

4.1. Neutrons and Liquid Scintillators

4.1.1. The Pulse Height Spectrum

When neutrons are incident on a liquid scintillator, they react predominantly with protons, because of the size of the cross-section and the large concentration of hydrogen in organic compounds. The interaction is n-p scattering, which produces

a recoil proton and a scattered neutron. The distribution of these protons is almost isotropic in the centre of mass frame, over the energy range 0 - 14 MeV. (The anisotropy involved amounts to about 6% at 14 MeV and so does not significantly affect the shape of the energy distribution of protons, although this is taken into account in the calculations of efficiency later in this section.) The energy distribution of protons in the laboratory frame of reference is therefore rectangular and is shown in Fig. 4.1. The pulse height spectrum from the detector is also shown. There are several processes which give the distribution its characteristic shape. Firstly the relationship between light output from the scintillator and the energy of a proton is non-linear, (as shown in Fig. 4.2), and this leads to a relative increase in the number of small pulses. The resolution of the detector has the effect of smearing the distribution; the size of this effect depends on the size of the detector and the efficiency of the photocathode. Neutrons which interact more than once in the scintillator can give peaks in the distribution, this again is due to the non-linearity of the light output relationship. The number of multiple interactions will be determined by the neutron primary energy and the scintillator volume. Protons whose tracks pass through the walls of the active region of the detector, give smaller pulses then they should, and so this too, increases the number of small pulses. A small contribution to the pulse amplitude spectrum, at least up to 14 MeV comes from the (n,α) and (n,p) reactions in carbon.

A discriminator level, (bias), is set on some part of the pulse height spectrum, in every experiment, to cut out unwanted pulses. For example, room returned background neutrons,

BIRMINGHAM UNIVERSITY LIBRARY

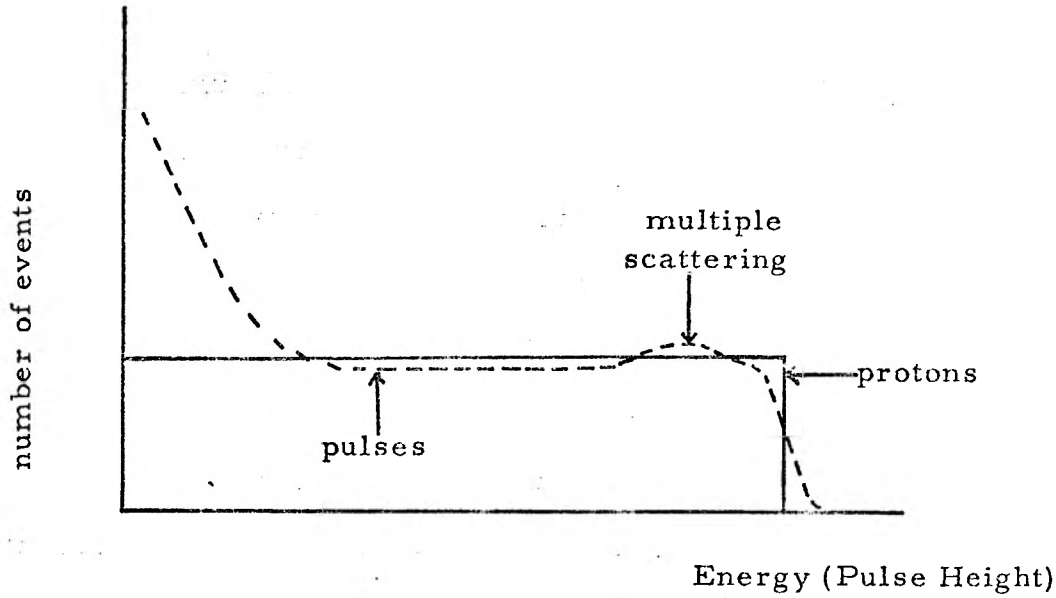

Figure 4.1 Proton energy distribution and resulting pulse height distribution.

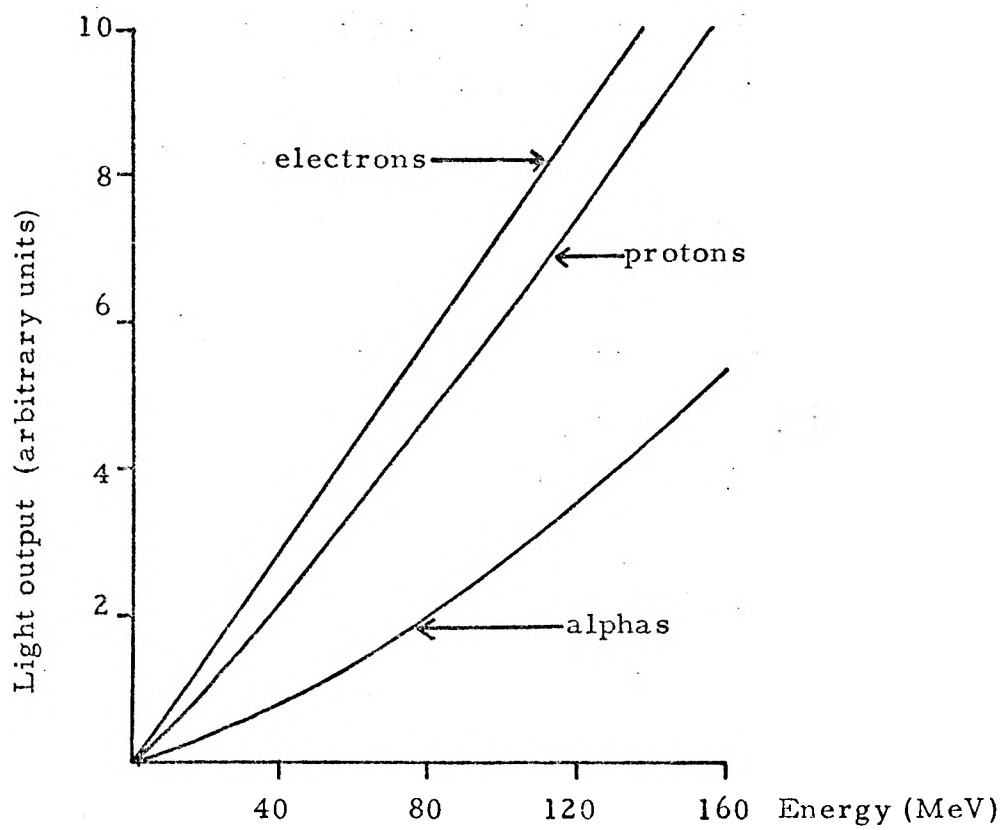

Figure 4.2 Light Output Relationships.
(Nuclear Enterprises scintillator catalogue 1973)

secondaries from reactions in the sample, or neutrons from deuteron break-up when using the D(d,n) source reaction. The higher the bias it is possible to use, the lower is the percentage background, which comes mainly from lower energy neutrons. This bias obviously affects the detection efficiency of the counter, and so the efficiency must be determined for all neutron energies and biases required in the experiment. The ability to select the bias can be useful in an experiment. For any incident neutron energy, a bias can be chosen which will give an efficiency curve reasonably flat in the region of the incident neutron energy, which obviously reduces any error in flux measurement, when a spread of neutron energies is present from the source.

4.2.1. Pulse Shape Discrimination

Accelerator produced neutrons are always accompanied by gamma rays, and as both neutrons and gammas give pulses in a liquid scintillator, it is necessary to distinguish the two, in order to measure the true neutron flux.

Gamma rays between a few hundred KeV and a few MeV interact in liquid scintillators, causing recoil electrons and lower energy scattered gamma rays. The electrons move through the scintillator giving their energy to other electrons, causing excited molecules, and a small amount of ionisation. The protons produced by neutrons also move through the scintillator, giving some of their energy to electrons, causing excited molecules, but also, due to their much higher specific energy loss (because of their much greater mass), causing a much greater fraction of ionised molecules than do electrons. It is this difference which enables the two types of radiation to be distinguished.

The excited states of the liquid scintillator solvent (and solute), are of two types. There are the singlet states, in which the electron spins are anti-parallel, (as in the ground state), and triplet states where the electron spins are parallel. Transitions from singlet to triplet states (or vice versa), are very unlikely because it is necessary to change the spin direction of the electron. Thus the excitation caused directly by electrons or protons, leads to singlet excited states. However, ionisation and recombination leads to the production of both singlet and triplet excited states. (As no spin change is necessary). The excited states in the solvent lead to corresponding states in the solvent, for the same considerations.

The light output from the scintillator comes predominantly from the de-excitation of the first singlet excited state (S_1). These states have a lifetime of between 1 and 30 nS. The lifetime for radiation emission from the first triplet excited state (T_1), decaying to the ground state (S_o), is of the order of 1μS. In practice, the triplet excited states lose their energy by combination:

$$T_1 + T_1 \rightleftharpoons S_1 + S_o$$

The S_1 molecule can subsequently radiate a photon. The light output in this way obviously has the same spectrum as the main light output, but a different time constant, since it depends on molecular collisions. The time constant of this slow component is of the order of 100nS since it depends on the diffusion rate in the solution.

The integrated light output from a proton and an electron, with the same total light output, is shown in Fig. 4.3. This

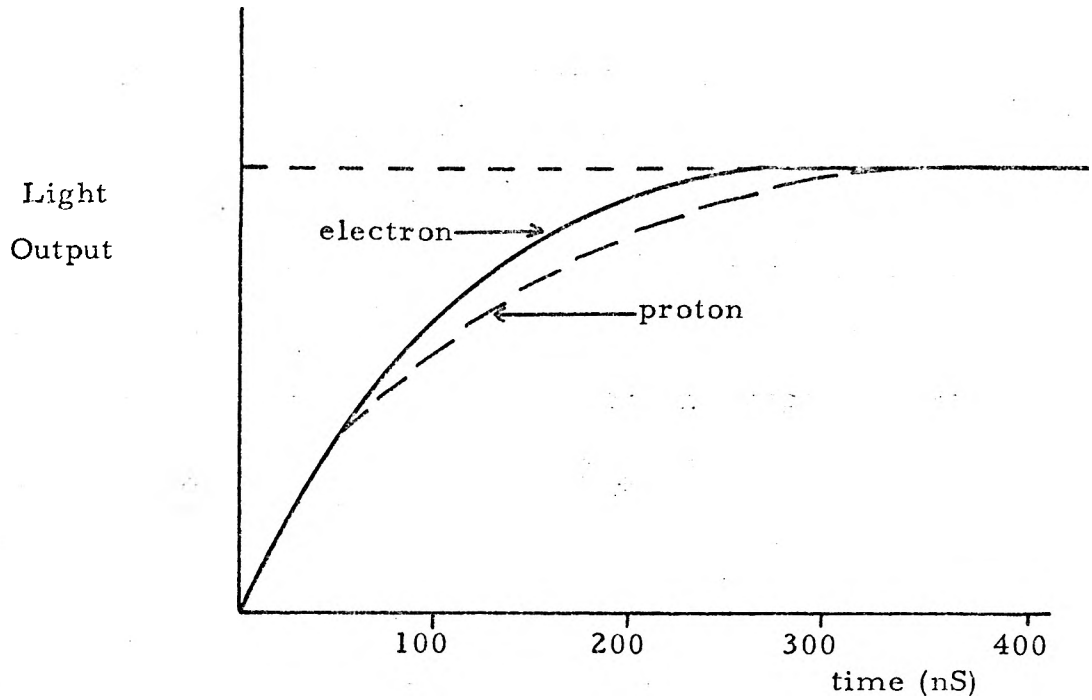

Figure 4.3 Integrated light output from an electron and a proton as a function of time.

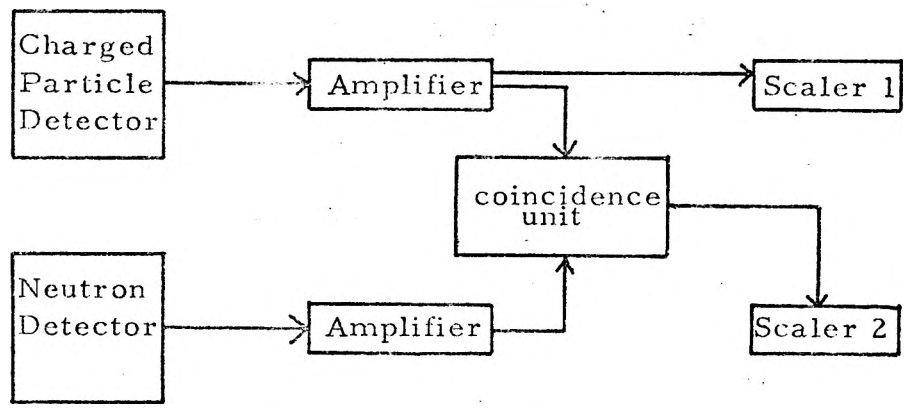

Figure 4.4 Circuit for ideal associated particle measurement.

shows that in the case of a proton, a larger fraction of light output is contributed by energy stored in the triplet states, originating from the larger amount of original ionisation.

The pulse shape discrimination (P.S.D) unit used in this experiment was designed in AERE, Harwell (Adams and White 1977) and is manufactured by Link Systems Ltd. The principle of operation is as follows. Two integrals are taken of each pulse, one for 25nS, and the other for 400nS, starting concurrently, triggered by a threshold discriminator. These integrals are weighted with respect to one another by a certain factor, (controlled by the user), and then are compared. If the first weighted integral is greater than the second then the pulse is from a gamma ray and if not it is from a neutron. The weighting factor is set up using a pure gamma source.

4.2. NE213 Efficiency Measurement

The detector was calibrated using the associated particle method. The principle of the method will be outlined for an ideal experiment, before the actual measurement is described.

4.2.1. The Principle of the Method

The efficiency of a neutron detector is simply the ratio of the number of neutron pulses detected to neutrons incident on the detector. In many neutron producing reactions, a charged particle is produced at the same time as the neutron. The associated particle method takes advantage of this, and determines the number of neutrons, from the number of charged particles, since detectors can be used which have 100% detection efficiency for an incident charged particle.

The experiment would consist of a charged particle detector (e.g. surface barrier silicon detector), defining a certain solid angle for the charged particles at the neutron source. The solid angle would define a direction and spread of the emitted neutrons (from the reaction kinematics), which would be incident on the neutron detector, placed at the appropriate position.

Neutrons which were not associated with detected charged particles would also be incident on the neutron detector, and so to remove pulses from these, coincidences would be demanded between the charged particle and neutron detectors. The necessary circuit would be as shown in Fig. 4.4. The neutron detector efficiency is given simply by the ratio of scaler 2 to scaler 1 in the figure.

4.2.2. Experimental Procedure

The neutron detector used in this experiment was a cylindrical cell of NE213* liquid scintillator, 5.08 cm in

*(Nuclear Enterprised, Edinburgh)

diameter and 3.81 cm deep. This was connected to a 5.08 cm. diameter low noise RCA 8850 pholotmultiplier tube, operated at 1200V. Before any measurement was made, the detector and electronics were kept switched on for several days, to allow the gain to stablise. The gain of the detector was checked using the edge positions of the Compton distribution of electrons from various gamma ray sources. The discriminator level was set, for most of the runs, on the half-height position of the ^{22}Na 0.511 MeV anihilation gamma distribution, which corresponds approximately to the maximum energy of the recoil electrons of .34 MeV. Some measurements were also made with the discriminator level set on the total energy peak of the gamma from ^{241}Am (0.06 MeV). The efficiency for higher biases could be determined subsequently, since the scintillator pulse, together with the corresponding time of flight information, was stored for every event, on a DDP516 computer. This information could be sorted subsequently, using any pulse height limits on the scintillator pulse spectrum.

In order to cover the required neutron energy range (1.5-25 MeV), three neutron producing reactions were used. ($D(d,n)^3He$, $T(p,n)^3He$ and $T(d,n)^4He$). The energy of the incident particle beam (from the Tandem Van de Graaff at AERE, Harwell), could be varied from 2-13 MeV, and this, together with the use of three different angles for the charged particle detector, enabled a neutron energy range of 1.5 to 25 MeV to be covered. The energy range available from each reaction is given in Table 4.5.

Two target chambers were used, one for charged particle angles of 43^o and 65^o and another for 25^o. The former is shown in Fig. 4.6. The incident beam (protons or deuterons) passes through a 0.00005" nickel foil into the gas cell, and the unreacted portion

Reaction	Incident beam energy (MeV)	Helium angle (°)	neutron energy (MeV)	energy spread ±(MeV)
$T(p,n)^3He$	12	43	6.8	0.3
	5	25	1.6	0.1
$D(d,n)^3H$	12	43	11	0.8
	6	43	6.0	0.3
$T(d,n)^4He$	12	65	25	0.4
	3.6	65	16	0.2

Table 4.5 Energy ranges and energy spread for the source reactions used in the efficiency measurement.

Figure 4.6 Target chamber used for NE213 efficiency measurements.

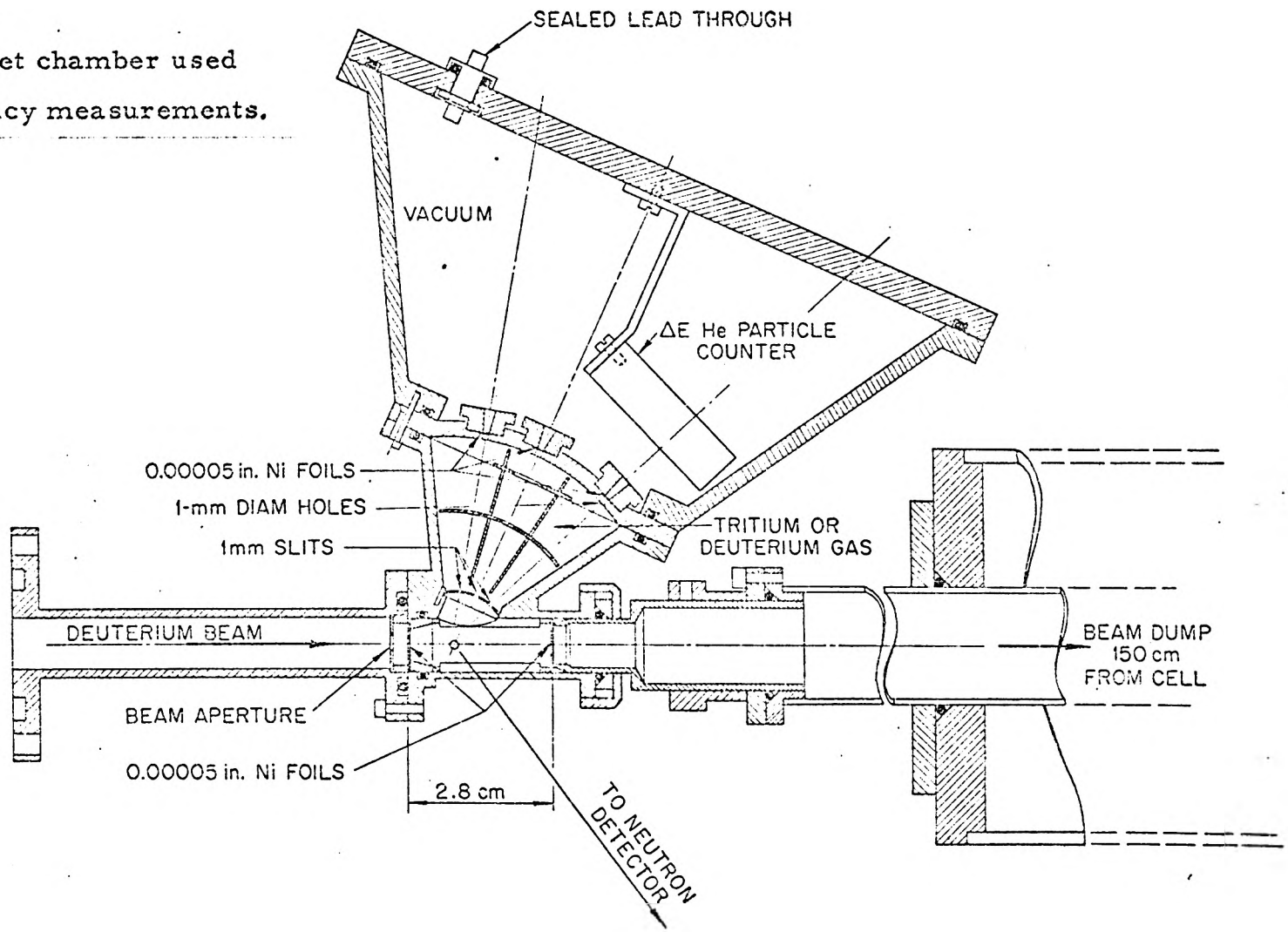

passes through an identical exit window, and then travels 1.5m before being stopped. This was done to reduce the neturon, and particularly the gamma background.

The charged particles are defined into a cone by a 1 mm vertical slit, and a 1.5 mm diameter hole. The hole is covered with a 0.00002" thick nickel foil, through which the charged helium particles pass. This separates the target gas (⅓ atmosphere) from the detector chamber, which is evacuated. The characteristics of the neutron cone can be determined from the published data. The kinematics of the reactions determine the mean energy of the neutrons and their energy spread, and also the size and shape of the cone. The energy spreads involved are shown in Table 4.5. The detector was scanned across the neutron cone before any measurement, to ensure that the detector intercepted the whole of the cone.

There are several effects not mentioned in the ideal experiment which must be considered in the real case, and the necessary data must be recorded in order to allow for them. The circuit used in the experiment (illustrated in Fig.4.7), is therefore significantly more complex than that shown for the ideal experiment.

The pulses from the silicon detector are divided into fast and slow pulses, by using two amplifiers. The slow pulse is used to obtain a spectrum, and the fast is used to start the time-to-amplitude converter (TAC), to record the neutron time of flight.

The pulses from the NE213 are also split into a fast and slow. The slow pulse comes from the part-way down the photo-multipler dynode chain, and is used to set the main neutron bias of the experiment and to give pulse height information.

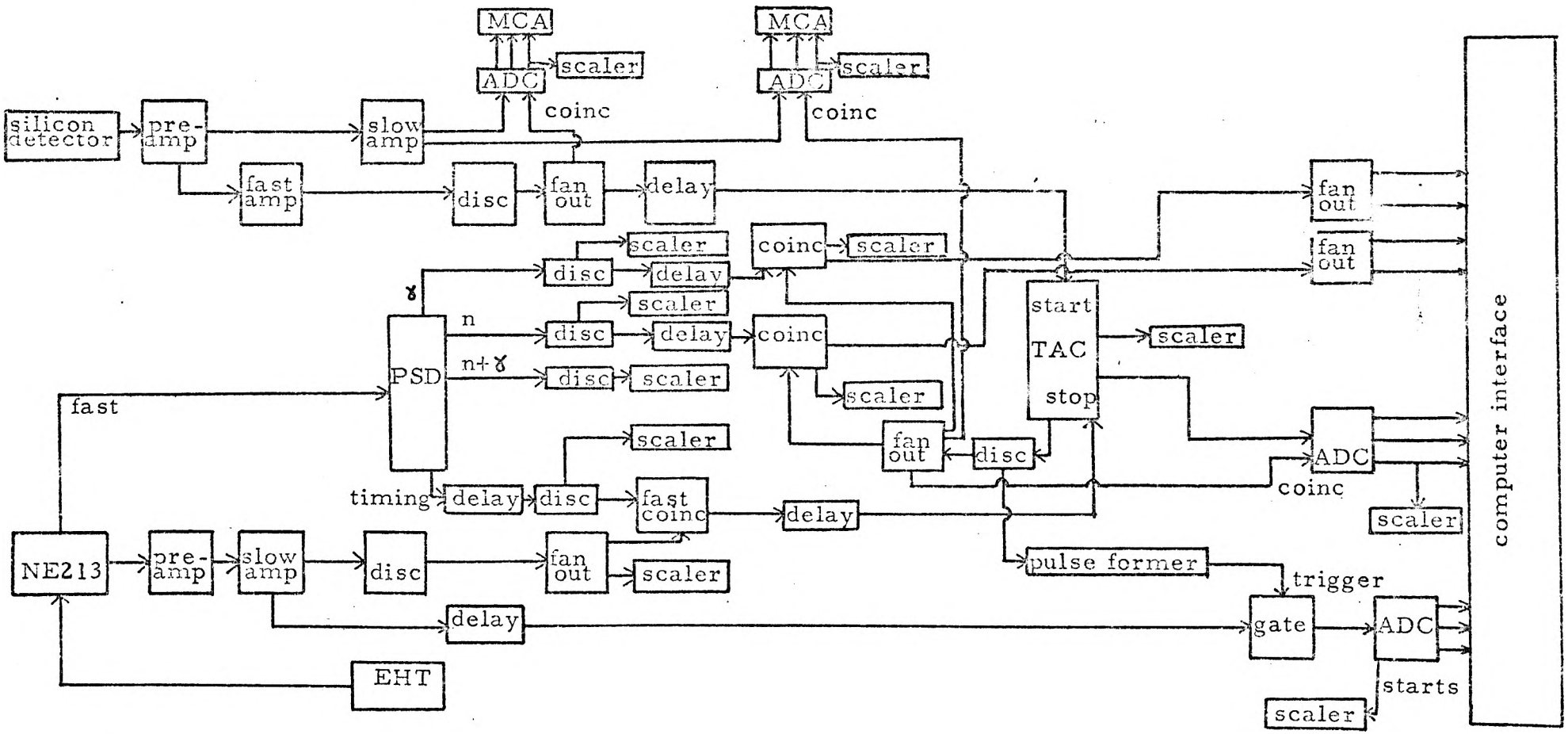

Figure 4.7 Circuit used for associated particle efficiency measurements.

The fast signal, from the photo-multiplier tube anode, was used as the input to the P.S.D. unit. This unit operates with two discriminator levels. The first ('threshold'), determines the minimum size of pulses to be processed. One fast pulse is output for each input pulse above the threshold level. These fast output pulses are referred to as 'timing' pulses. The second discriminator ('lower output level') determines another level for the remaining outputs from the unit; one for neutrons one for gammas and one for neutrons plus gammas. Both these discriminators were set so that they were below the slow pulse discriminator level, (by checking the counting rates), so that they did not affect the efficiency of the counter.

The timing output was input to a fast coincidence unit, together with the NE213 slow signal (above the bias), so that a fast pulse was obtained for every event above the bias. This signal was used to stop the neutron time of flight TAC. The neutron plus gamma output was scaled to enable the setting of the lower output level.

The neutron output and the gamma output were input to two coincidence units, where in each case the other input was a NE213 slow/silicon fast coincidence (actually the TAC output). (For all coincidence units and TAC inputs, delays were used to allow for differences of cable length and speed of processing units). The outputs from these two coincidence units were produced by neutrons above the main bias, and gammas above the main bias respectively. These outputs were counted to use in calculation of the deadtime (section 4.2.2.(c)), and also used to provide a flag to the computer telling whether the event was a neutron or a gamma. This signal was used in preference to the P.S.D. neutron or gamma output, simply because the count

rate was smaller, and so fewer unnecessary pulses were presented to the computer. The output of the TAC was also stored on the computer (via an ADC) so that for every event, the computer has a record of pulse height, time of flight, and a flag for a neutron or a gamma. Some of the incident neutrons give a pulse in the detector by means of $(n,n'\gamma)$ reactions in the material of the counter. This means the corresponding flag for these events is for a gamma. The time of flight information however, corresponds to that of a neutron, and so these events form a peak in the gamma time of flight spectrum. The efficiency can be calculated including or excluding these events giving either total or neutron efficiency. In use, it is the neutron efficiency which is important for flux measurement.

The helium particles detected by the silicon counter, are recorded by a multichannel analyser. The detector also counts singly charged particles, protons or deuterons, scattered from the incident accelerator beam, by the gas in the cell. For some beam energies, the scattered particle spectrum can interfere with the lower edge of the helium particle peak. The correction for this intereference (section 4.2.2.(a)), requires the spectrum of charged particles which are in coincidence with a neutron. This is done, using a second multichannel analyser, by gating the ADC with coincidence (TAC) pulses. This reduces the true charged particle count rate, by an amount corresponding to the neutron detection efficiency, but the non-associated particles are reduced to a much greater degree, since they are only counted if a random NE213 detector pulse happens to coincide. This spectrum is used in the first of three corrections which have to be applied, and which will now be described.

a) Scattered Incident Particles

Charged particles produced in the neutron source reaction are not the only ones which can give pulses in the silicon detector. Incident beam particles can be scattered, by the target gas in the cell, into the defined helium particle cone and cause a pulse. These particles can interfere with the helium particle spectrum, and therefore a correction to the spectrum has to be made. This correction is kept to a minimum by choosing the detector, and its voltage, to give a depletion layer just thick enough to stop the helium particles. The singly charged scattered particles (protons or deuterons) have a much greater range in silicon, for the same energy, and therefore deposit less energy. A typical pulse height spectrum, illustrated in Fig. 4.8 (a), shows the peak due to the He particles and pulses due to the scattered beam particles (p,d).

The spectrum of silicon pulses was recorded both normally and also gated by TAC coincident pulses. The gated spectrum corresponding to Fig.4.8(a) is shown in Fig. 4.8(b). The number of events is lower than the ungated spectrum, but the scattered events are preferentially removed, to leave the helium particle spectrum shape, which is then used to correct, when necessary, for the scattered events in the total spectrum. The correction is done by fitting the gated spectrum (GS), to the ungated spectrum (UG), by minimising the quantity X^2 given by

$$X^2 = \sum_{I=n}^{N} \left(UG(I) - A \times GS\,(G \times I) \right)^2$$

where A is a factor to allow for the different number of events, and G a factor to allow for different ADC gain. n is the channel at which the peak reaches ¾ of its maximum height, and N is the

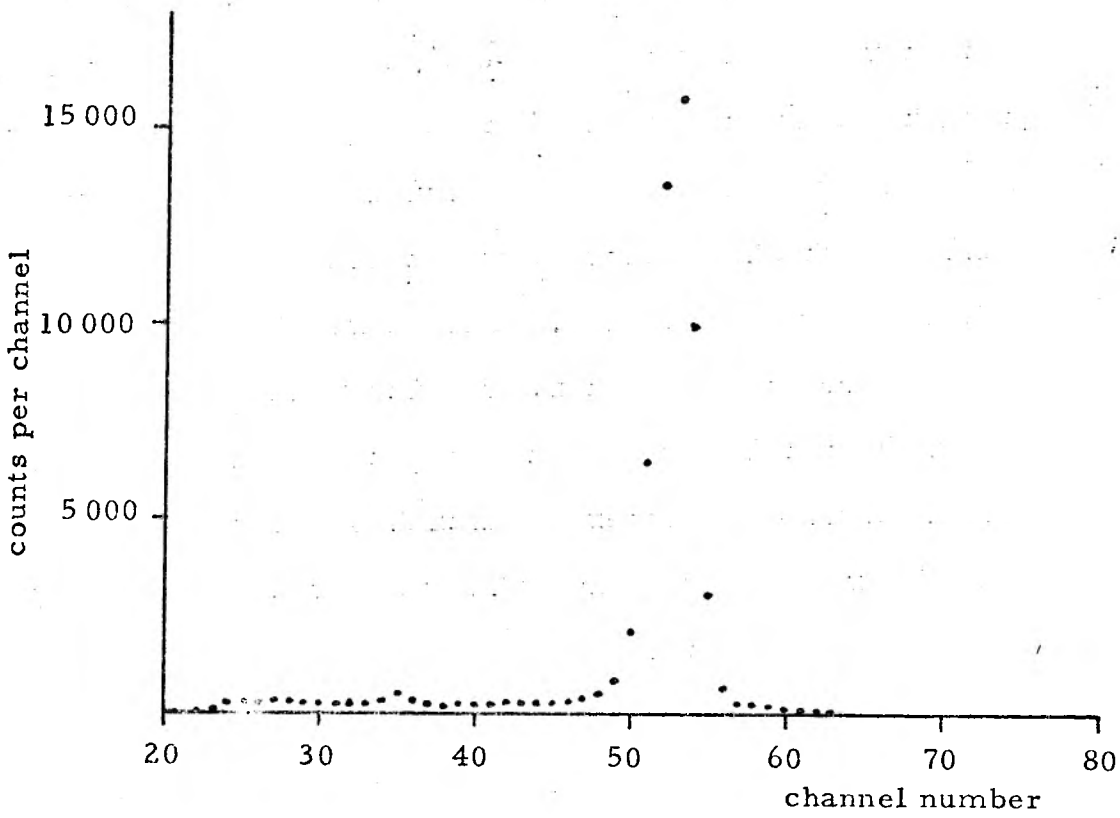

Figure 4. 8(a) Ungated charged particle spectrum

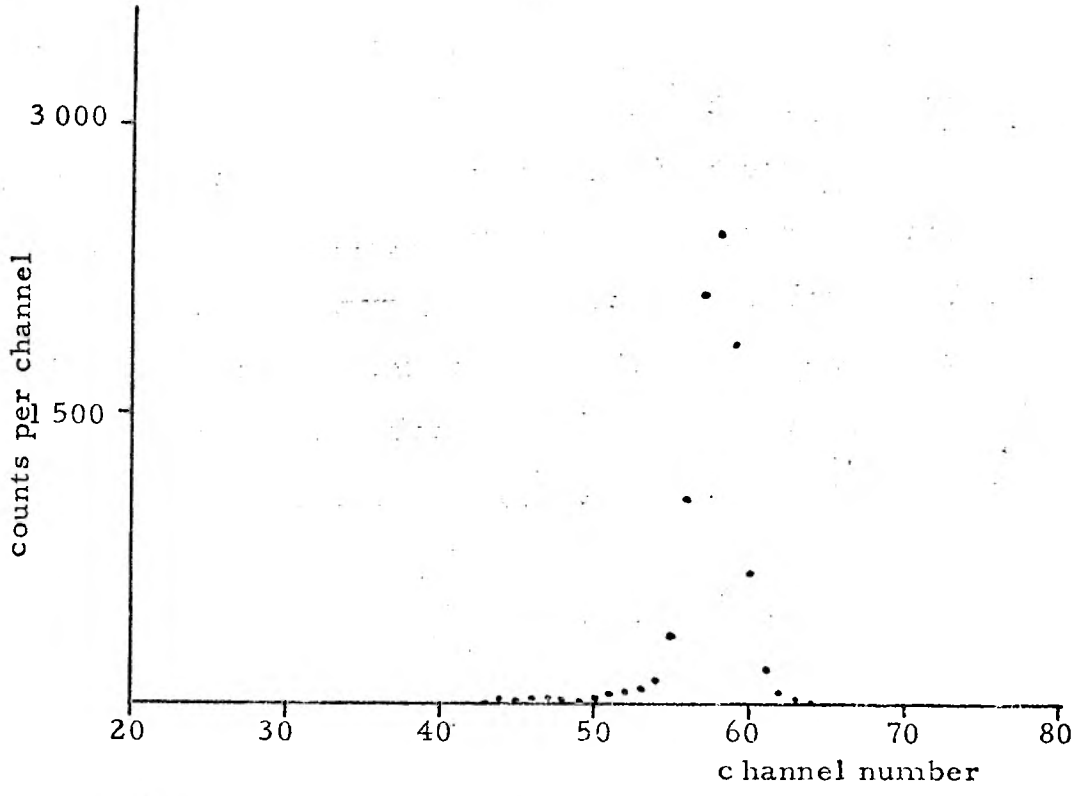

Figure 4. 8(b) Gated charged particle spectrum.
(Note change in scale)

maximum channel number.

The procedure used was to change the gain of the gated spectrum by various factors, G_i, such that

$$GS_i(I) = GS\ (I \times G_i)$$

(interpolation here was necessary since $I \times G_i$ was not normally an integer). Then the gain shifted spectrum was normalised according to

$$A \sum_{I=n}^{N} GS_i(I) = \sum_{I=n}^{N} UG(I)$$

Then X^2 was evaluated for each of these gain factors, and the value of G, (G_o), corresponding to minimum X^2, was found by interpolation. (Forward difference interpolation was found to be satisfactory for both interpolation steps).

Finally, the gated spectrum was gain shifted by the factor G_o, and normalised as above. This resultant spectrum is shown together with the ungated spectrum for a number of cases, in Fig. 4.9. (a), (b), (c) and (d). The fitted curve enables the low energy side of the ungated He peak to be "cleaned-up" by replacing the sum over the spectrum, $\sum_{I=1}^{N} UG(I)$ with

$$\sum_{1}^{n} A_o \times GS(G_o \times I) + \sum_{n+1}^{n} UG(I)$$

where n is the channel number above which the fitted curve and the ungated spectrum are the same, within statistics. (In many cases the correction was very small or zero, especially for neutrons produced by $T(p,n)^3He$)

b) Random neutron pulses

If the electronics had been as in Fig.4.4, then some of the coincidences would have been random events, i.e. from

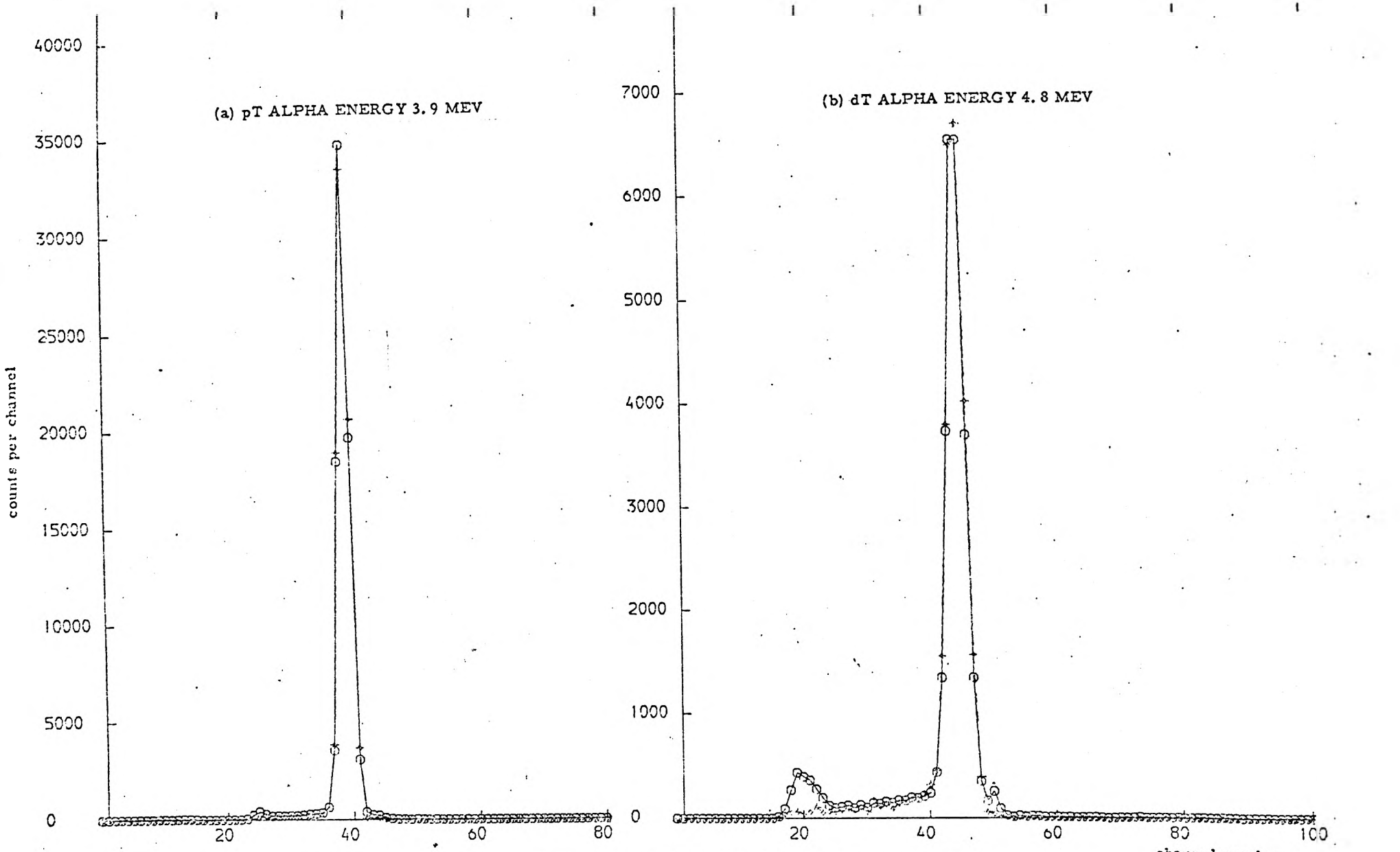

FIGURE 4.9 UNGATED (0) AND FITTED GATED (+) CHARGED PARTICLE SPECTRA

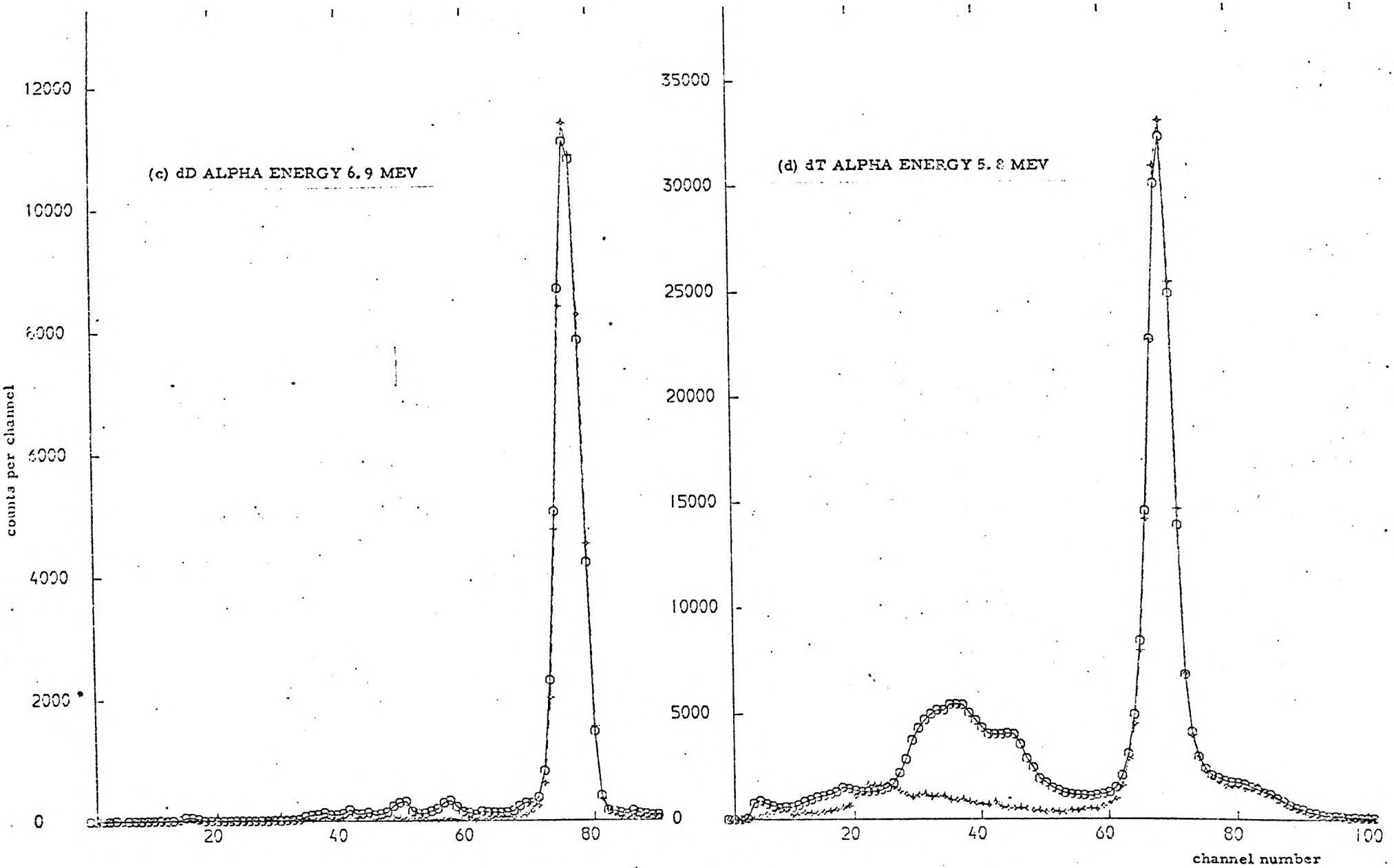

FIGURE 4.9 UNGATED (0) AND FITTED GATED (+) CHARGED PARTICLE SPECTRA

neutrons which were not in the cone, causing pulses in the detector. This would have increased the efficiency above its true value. To overcome this problem, the time of flight distribution between a silicon detection pulse and a scintillator pulse, is recorded over a 100nS time interval, using a TAC. The resulting spectrum is shown in Fig.4.10. The peak is due to real (associated) events, and the flight time independent events are the random background.

The number of neutrons detected in the cone, is found by subtracting the time independent background from beneath the peak.

c) Deadtime correction

When any device, such as a discriminator, is dealing with one pulse, it is insensitive, for a certain period, and so any pulse which arrives in this time is ignored. This period is referred to as the deadtime of the device. In a system of many devices, the overall deadtime is determined by the device with the greatest deadtime. In this experiment the limiting device is the Pulse Shape Discrimination Unit, with a measured deadtime of 1.3μs. This can be checked in the present system, since the number of neutrons above the bias, plus the number of gammas above the bias, should give the total number of slow pulses above the bias. The difference is due to the deadtime. The result obtained is slightly less than 1.3μs, but this can be explained by events in which the long slow pulse in the coincidence unit, overlaps two fast pulses and two outputs are given. This compensates for the effect of the PSD deadtime to some extent. The deadtime correction used to treat the data was the 1.3μs of the PSD. The maximum count rate in the NE213 detector during the efficiency measurement was 20 Kc/S, and the corresponding

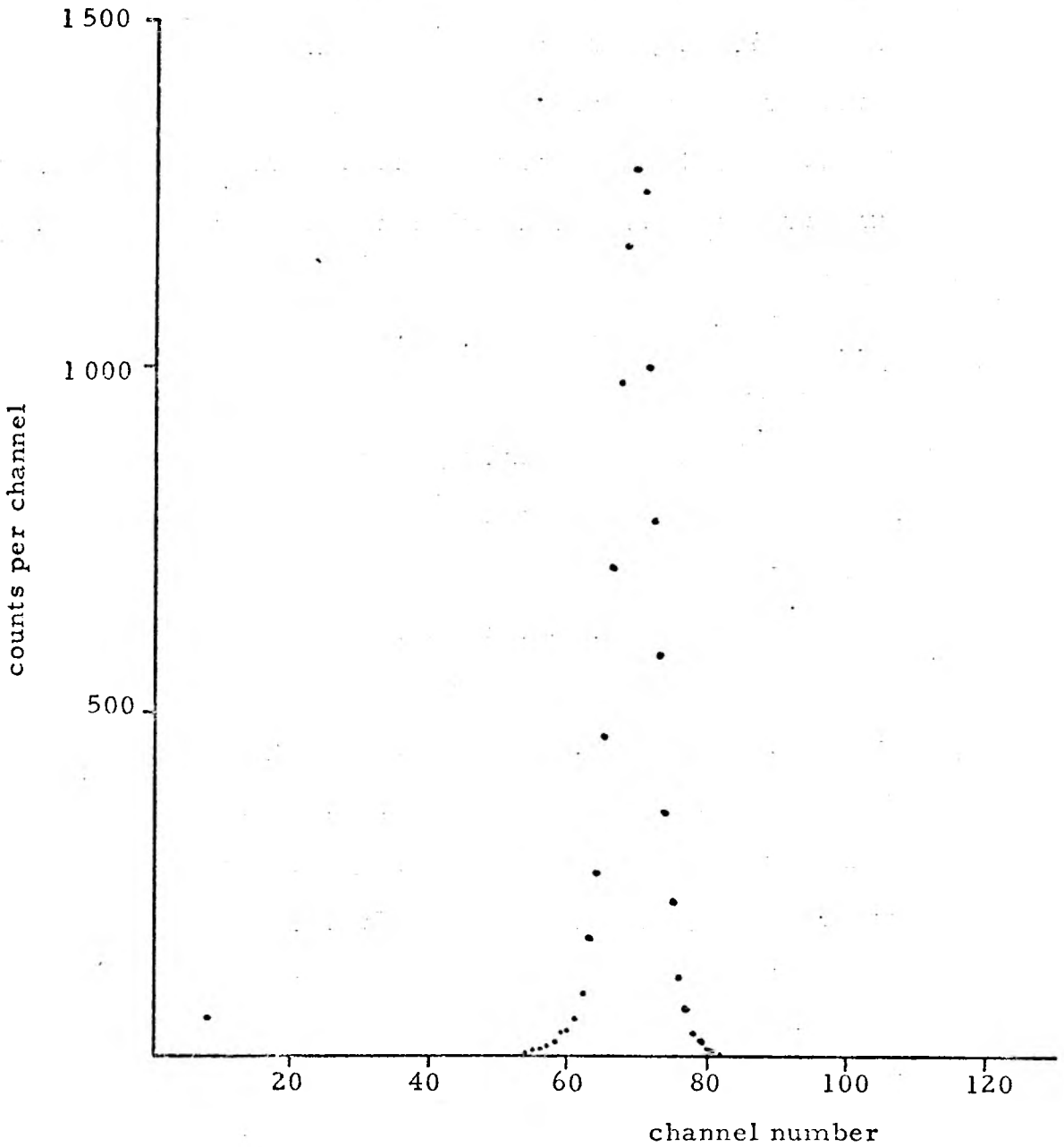

Figure 4.10 Time-of-flight distribution for 3.0 MeV neutrons. (128 channels = 100nS)

maximum correction was 3%.

The results for the central total efficiency are shown in Fig. 4.11 after corrections (a), (b) and (c) above were applied.

4.2.3. Average efficiency and comparison with computer predictions

The efficiency plotted in figure 4.11 is the central, total (neutron plus gamma), efficiency, ϵ_T. This is for neutrons incident on the centre of the detector, interacting via charged particle reactions (including n-p scattering), and gamma production reactions. In a neutron flux measurement, (using pulse shape discrimination), neutrons are incident on the whole of the detector, and only charged particle reactions are counted, since $(n,n'\gamma)$ reactions cannot be distinguished from gamma background without time of flight information. The efficiency which needs to be used to calculate the flux, the average neutron efficiency, $\bar{\epsilon}_n$, is less than the central total, not only because the gamma contribution is not included, but also because events which occur near the edge of the detector do not have the same probability of being detected as central events. This is because the charged particles have more chance of escaping through the walls of the active region, and the light collection efficiency, (the fraction of light produced that is incident on the photocathode) is less at the edges of the detector than in the centre.

A value for the average neutron efficiency can be found experimentally by scanning the associated particle neutron cone across the detector. This was done at a neutron energy of 16.3 MeV and the result is shown in Figure 4.12. The plotted points are the measured neutron efficiency for the detector position, without allowing for the fact that not all of the neutron cone is incident on the detector. The shape is therefore explained in

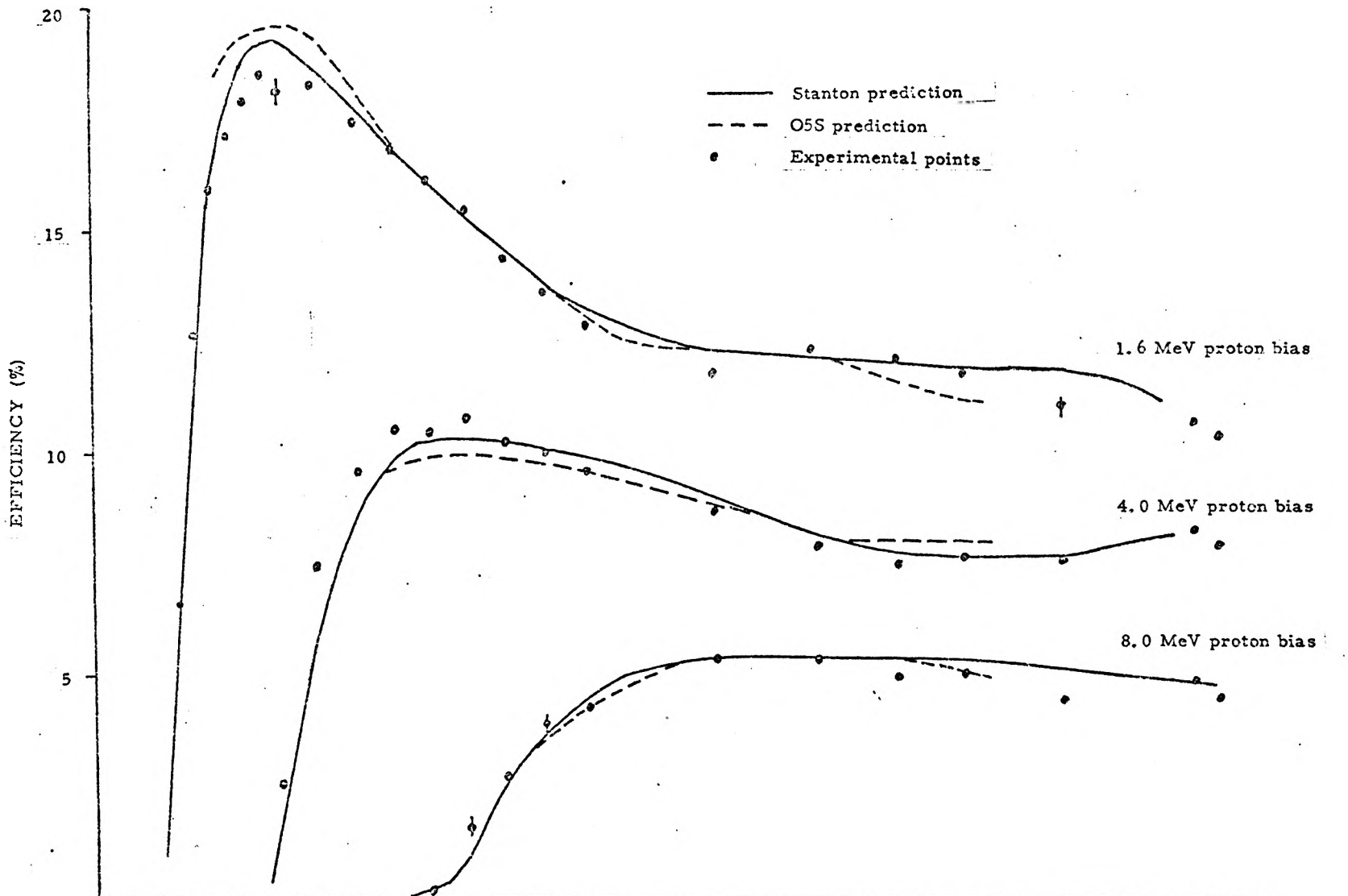

FIGURE 4.11 NE213 CENTRAL TOTAL DETECTION EFFICIENCY

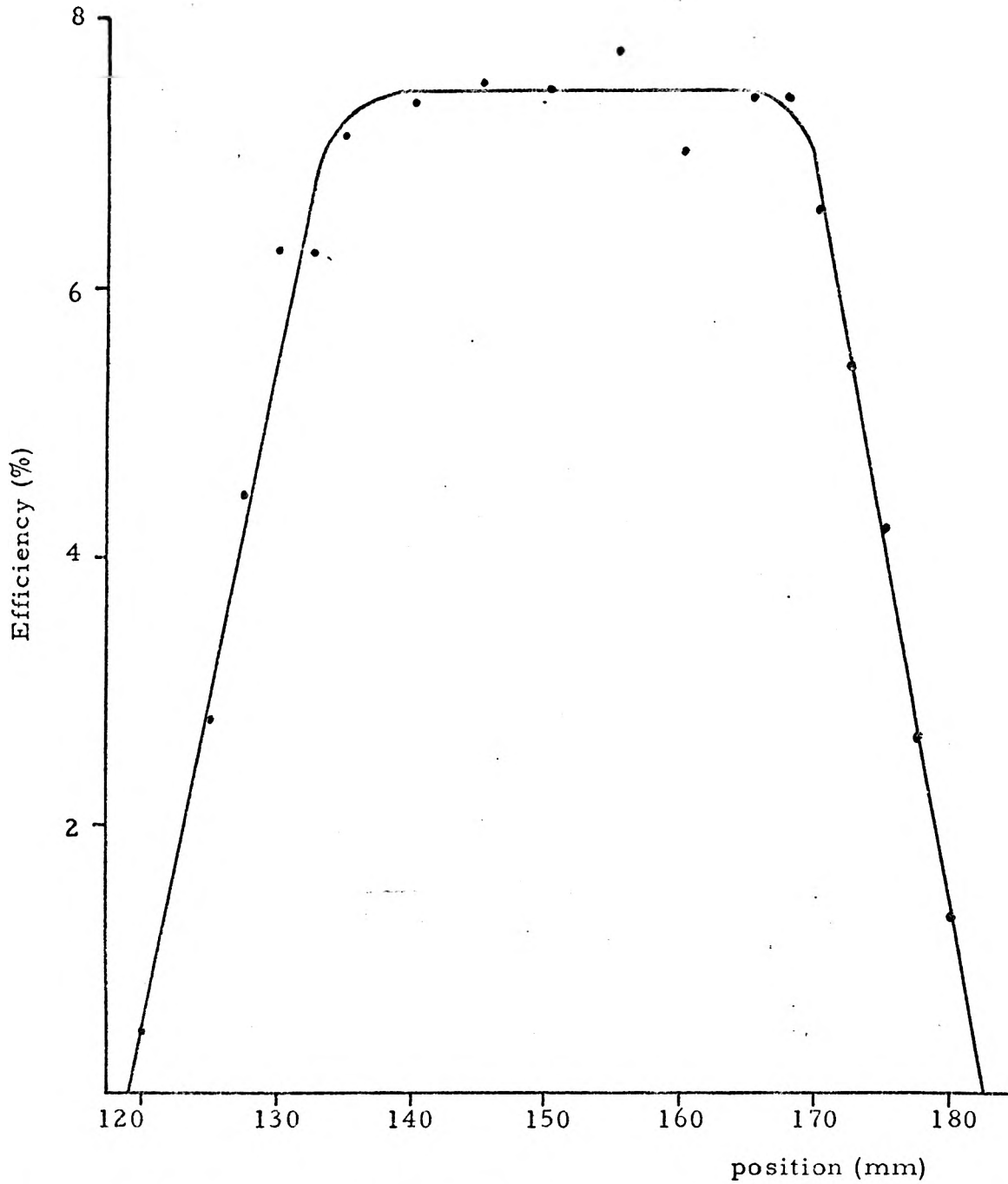

Figure 4.12 Observed neutron efficiency as a function of detector position.

the following way. The central part of the scan is flat, indicating that the detector efficiency is constant over the central area. Then the observed efficiency starts to fall slowly as the real efficiency near the edge of the detector falls, then the observed efficiency falls rapidly as the neutron cone starts to miss the detector. The average efficiency can be deduced from this scan as follows:

Consider the real detector efficiency to be made up of discs of uniform efficiency ϵ_i and area A_i as in figure 4.13. This can be done as long as the efficiency is cylindrically symmetric. Similarly the neutron cone (containing a total number of neutrons per second, N) can be subdivided into cones, each with radius r_j at the detector, and constant neutron density n_j. The observed counting efficiency is given by:

$$E_o(D) = \sum_i \sum_j \frac{\epsilon_i A_{ij}(D) n_j}{\pi r_j^2 N} \qquad 4.1$$

where D is the separation of the detector centre and the cone centre, and $A_{ij}(D)$ is the overlapping area of the i^{th} disc with j^{th} cone.

We can evaluate the following integral from the data

$$Y = 2\pi \int_0^{R_1+R_2} E_o(D)\, D\, dD \qquad 4.2.$$

where R_1 is the radius of the detector and R_2 is the maximum radius of the neutron cone at the detector. This integral was evaluated numerically using Simpson's rule. From equation 4.1, 4.2 can be rewritten:

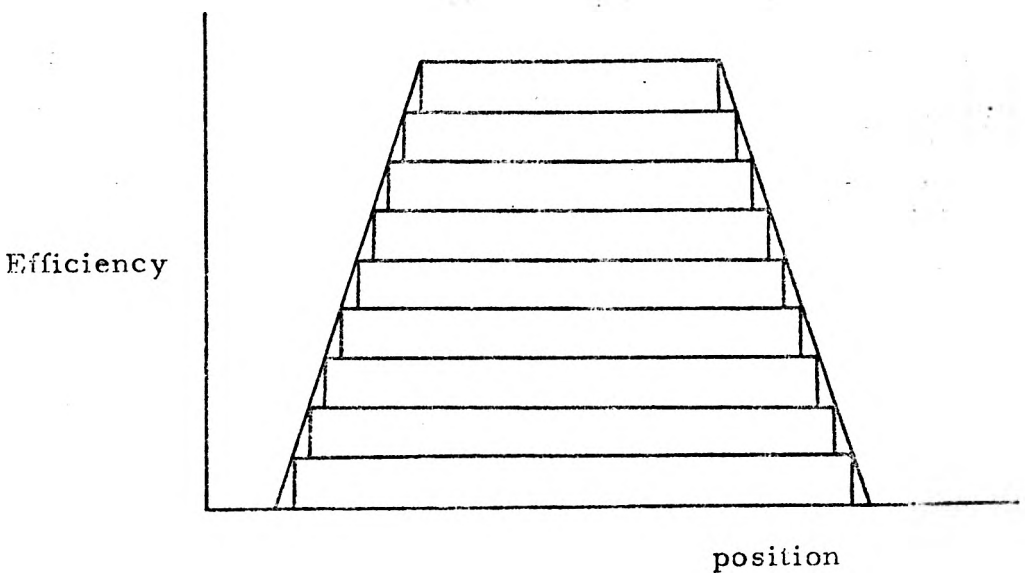

Figure 4.13 Cylindrically symmetric detector efficiency composed of discs.

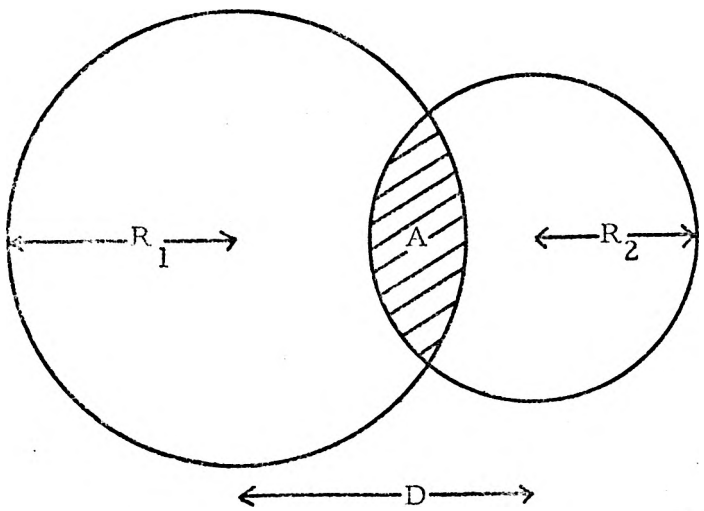

Figure 4.14 Geometry for average efficiency determination

$$Y = \sum_i \sum_j \frac{\epsilon_i N_j}{N} \left[2\pi \int_0^{R_i+R_2} \frac{A_{ij}(D)\, D\, dD}{\pi r_j^2} \right]$$

The term in brackets can be simplified by use of a geometrical theorem (Cookson et al. 1975) which relates the overlapping area of two circles (Figure 4.14) in the following way

$$2 \int_0^{R_1+R_2} \frac{A(D)DdD}{R_2^2} = \pi R_1^2$$

This gives the expression Y

$$Y = \sum_i \sum_j \frac{\epsilon_i N_j A_i}{N}$$

which simplifies to

$$Y = \sum_i \epsilon_i A_i$$

This is simply the definition of average efficiency multiplied by the total area of the detector. The average neutron efficiency was found in this way for an incident neutron energy of 16.3 MeV. The mean neutron efficiency was less than the central total efficiency by 6.9%, 8.1% and 7.5% for proton biases of 1.6, 4.0 and 8.0 MeV respectively.

The central efficiency has been determined for a wide range of neutron energies, (1.5 - 25 MeV), and so if the variation of $\bar{\epsilon}_n/\epsilon_T$ was known as a function of energy then the average neutron efficiency could be determined.

In order to investigate this effect, two computer programs were used. These were Stanton (1971) modified by McNaughton (1975) and 05S (Textor and Verbinski (1968)). These programs work on the Monte Carlo principle, (see section 3.6). The basic neutron interaction in a liquid scintillator is n-p

scattering and for this process the program needs to know the total cross-section, (which is well-known in the neutron energy range considered, and the angular distribution of the recoil protons. Stanton's code initially considered isotropic centre of mass scattering for neutrons below 30 MeV, but this was modified to take into account non-isotropic behaviour between 5 and 30 MeV. The data used for this was taken from the differential, centre mass ^{1}H (n,n)^{1}H cross-section, determined from Yale phase-shifts, given in Hopkins and Breit (1971). Carbon reactions ((n,p),(n,α), etc.) are modelled by both the programs, and the necessary cross-sections for these are input.

All the interactions in the scintillator which give out light, have the light output calculated from given relationships. 05S uses light units related to the maximum light output from a cobalt gamma ray, ("cobalts") and Stanton records a given light output as the energy of an electron which would give that light output. (The relationship between electron energy and light output is linear above c. 200 KeV).

Other input requirements are the size and shape of the detector and its resolution. The original form of Stanton's program, as modified by McNaughton, did not allow for proton loss from the active region, but this was added by Cookson (1978).

The efficiency is output by both programs for various discriminator settings, (biases), given in the light output units used by the program. (Cobalts for 05S and electron energy for Stanton). In order to compare the experimental and predicted efficiencies, the correct bias must be chosen. For a particular bias setting in the experiment, (in a given ADC channel), the corresponding proton energy is found in the following way. The

pulse height spectrum from the neutrons appears as Figure 4.1. The half-height position of the edge corresponds to the case where the neutron has transferred all its energy to the proton. The channel number of this position, for each neutron and energy used in the efficiency measurement, was recorded. Any bias setting can, from its channel number, be converted into proton energy from the relationship obtained. Then to find the correct bias to use with the computer output, the number of light units corresponding to this proton energy, was determined from the light output relationship used in the program. In this way any small variation in the light output relationship of the program relative to that of the detector is irrelevant. It is still important that the relative light output for protons, electrons and alphas should be correct relative to each other.

The results for the central total efficiency obtained are shown in Figure 4.11 together with the measured points. The overall agreement between the program output and the measurements is very good. The maximum discrepancy is 6% (Stanton) and 8% (05S). Some of this discrepancy could be explained by errors in the light output relationships, and the modelling of the charged particle reactions. Also there could be some error in converting the channel number of the detector bias into proton energy. (This would not affect the accuracy of any flux measurement, but would affect the agreement between the programs and the data).

The main interest in the program, so far as this experiment is concerned, is in the prediction of the average efficiency. This is determined by making the neutrons randomly incident over the front face of the detector. Neither of the programs allows for the variation of light collection efficiency with position

in the scintillant, and so absolute agreement between the average efficiency determination (at 16.3 MeV) and the programs' prediction would not be expected. However both programs indicate that except on the steeply rising part of the efficiency curve (near the bias) the ratio $\overline{\epsilon}_T/\epsilon_T$ is constant. This result has been used in order to work out the average neutron efficiency for all neutron energies, since the detector is never used on this steeply rising portion of the efficiency curve. This mean neutron efficiency, illustrated in Figure 4.15, is used when calculating all the fluxes in the irradiation experiments.

4.2.4. Accuracy

The error bars on the efficiency results come from two sources. Firstly there is the statistical error on the number of pulses accumulated. Secondly the bias setting on the computer sorted data was varied by ±1 channel on the pulse height spectrum. This was to allow for any error in setting the bias and for any gain change during the experiment which could affect the result. The maximum uncertainty on any individual point is approximately ±2%.

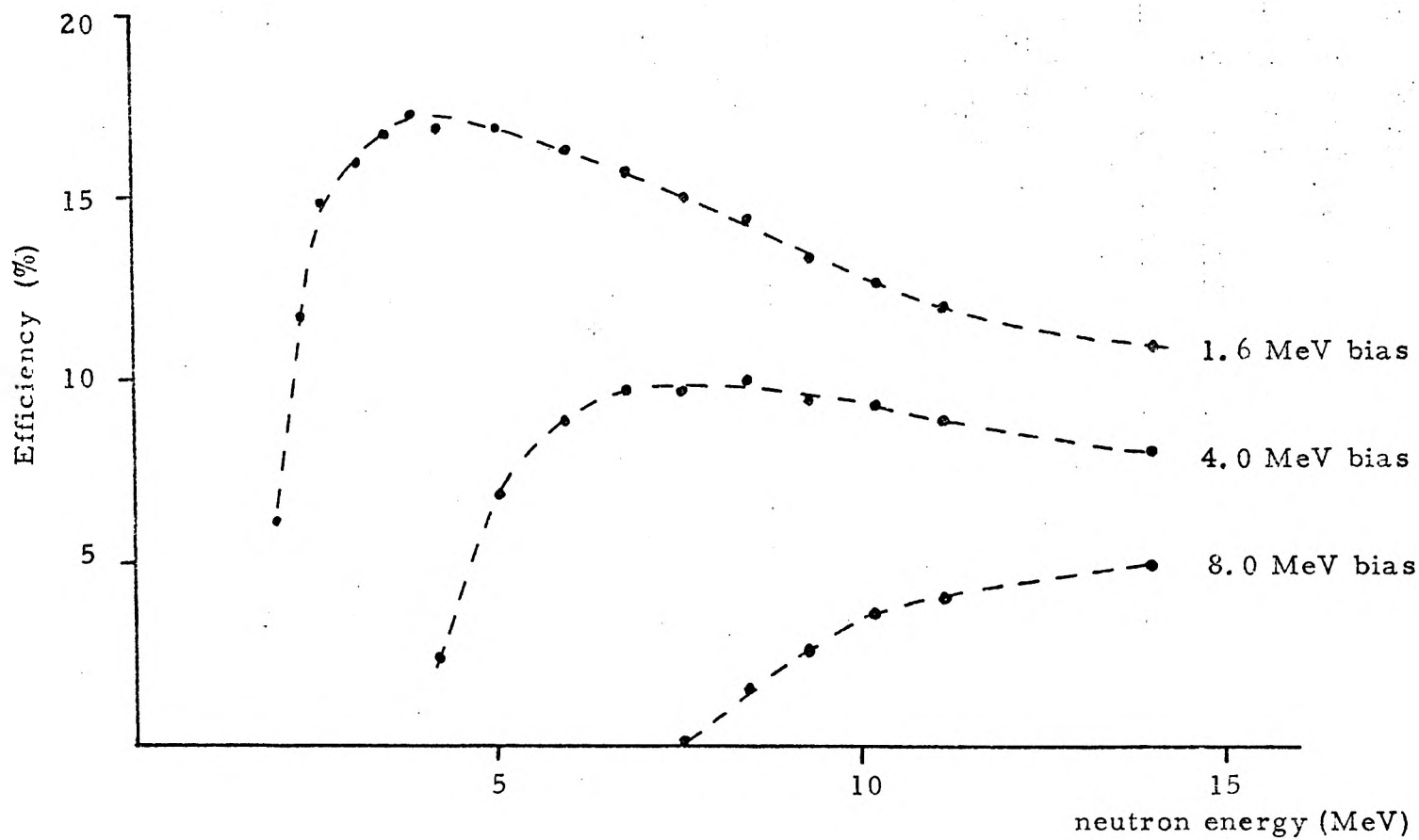

Figure 4.15 Average neutron detection efficiency. (visual fit).

4.3. Comparison of the calibrated detector with the alpha particle yield from a solid tritiated target at 14 MeV.

A comparison was made between the NE213 scintillation detector and a surface barrier silicon alpha particle detector on a Cockcroft-Walton accelerator, so that the 14 MeV neutron flux could be measured with a high beam current, when the count-rate in the NE213 detector became unacceptably large.

This experiment involved the charged particles emitted from a titanium tritide solid target, with a low energy (400 KeV) incident deuteron beam. Only the number of charged particles and neutrons per steradian were measured, rather than the timing of each event as in the previous section.

The target and silicon detector arrangement is shown in Fig.4.16. A collimator was placed in the beam line to confine the beam to the tritiated area. Collimators were also used in the side arm of the assembly to prevent alpha particles which had been scattered from the walls, reaching the detector. The area of the detector was defined by a 1.47 mm diameter aperture. The circuit used for the measurement is shown in Fig. 4.17.

Good agreement was found between the number of alpha particles per steradian and the number of neutrons per steradian, calculated using the measured average neutron efficiency of the NE213 detector. The difference was less than 2%.

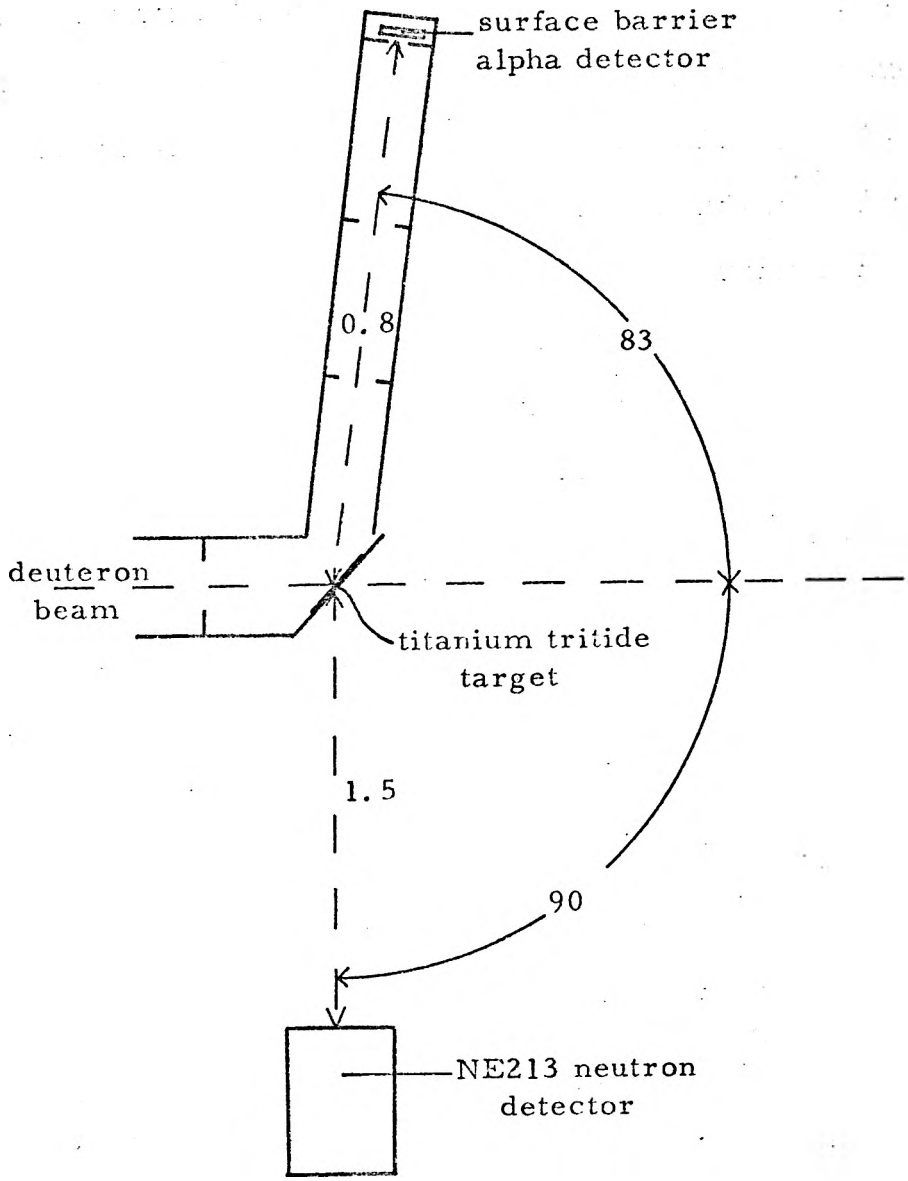

Figure 4.16 Cockcroft-Walton target assembly

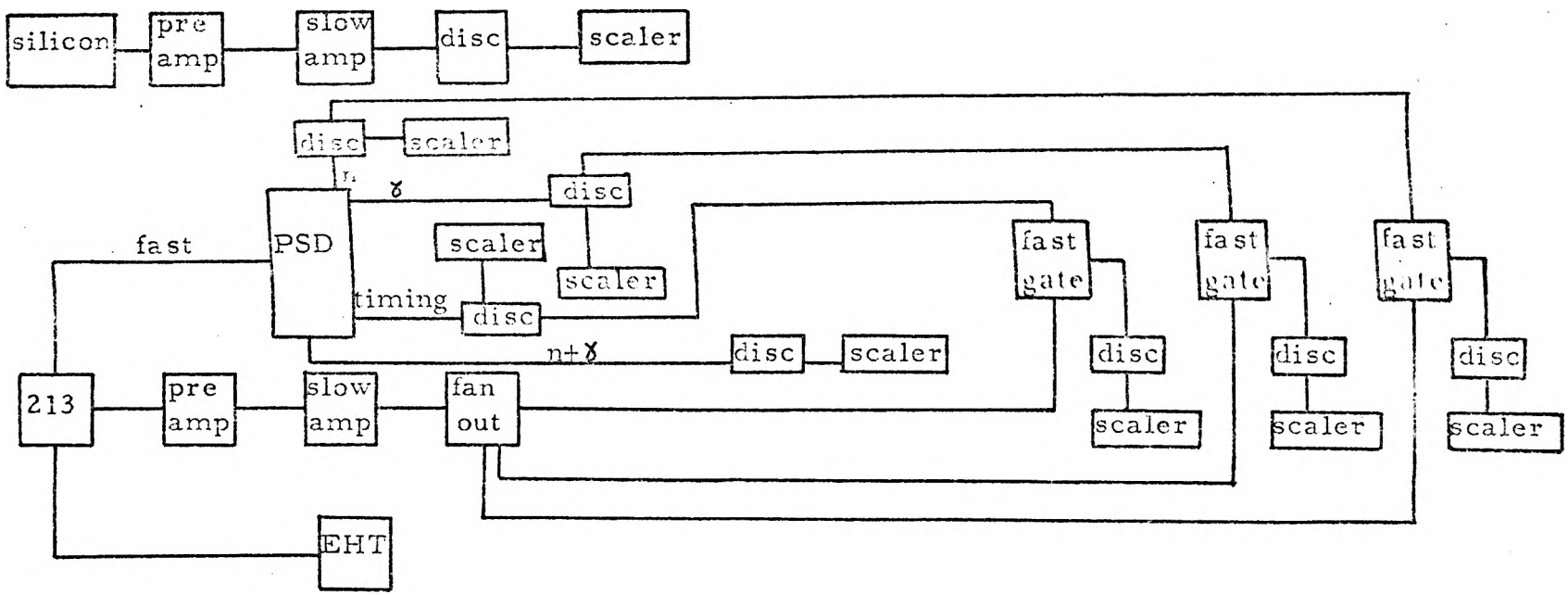

Figure 4.17 Circuit used for the comparison of the NE213 neutron detector and the associated particle method at 14 MeV.

CHAPTER FIVE

IRRADIATIONS AND RESULTS

Irradiations were carried out using two charged particle accelerators at AERE, Harwell. These were a Tandem Van de Graaff, and a Cockcroft-Walton accelerator. The irradiations on the Tandem gave absolute measurements of the $^{7}Li(n,n't)^{4}He$ reaction cross-section, whereas those using the Cockcroft-Walton gave the lithium cross-section relative to that of the $^{27}Al(n,\alpha)^{24}Na$ reaction cross-section. The measurements on the two different machines are described separately in the following sections, and the use of activation foil monitors is also explained.

5.1. Irradiations on the Tandem

In these experiments, the neutron flux was measured using the calibrated NE213 detector. The neutron source reaction chosen was $D(d,n)^{3}He$ since this has a larger 0^{o} differential cross-section for neutron production than $T(p,n)^{3}He$ for neutrons with energies between 5 and 12 MeV. (The $T(d,n)^{4}He$ reaction is unsuitable since it only gives neutrons of higher energy). The use of the dD reaction does necessitate a correction for the effect of 'break-up' neutrons. These neutrons are produced from the reaction D(d,np)d, which, being a three body reaction, produces a continuous spectrum of predominantly low energy neutrons. The amount of tritium produced by these break-up neutrons is small or zero in all the irradiations except in the case of 11.8 MeV incident neutrons, and the correction for this effect is discussed in section 5.1.3.

A calculation of the effective soid angle of the pellet is needed since not only is the neutron source extended, but also the differential neutron production cross-section is not constant

over the range of angles incident on the pellet. This calculation is presented in section 5.1.2. The foil monitor cross-sections are calculated in section 5.1.4 and those of lithium in section 5.1.5. The following section deals with the pertinent features of the neutron source.

5.1.1. The Neutron Source

The source of neutrons for the experiment was chosen to be dD for the reasons given above. The target was deuterium gas at 2 atmospheres pressure, contained in a 10 cm long gas cell. The deuterons entered the cell through a 0.0002" thick nickel window (4.5 mg/cm^2), and those which passed through the gas were stopped in a 0.02" platinum beam stop. The neutron flux produced by this cell was limited by the deuteron current which could be passed through the entrance foil without puncturing it. This current varied from 0.5 μ amp for 3 MeV deuterons to 2 μ amps for 9 MeV deuterons. This flux limitation meant that 24 hour irradiations were needed to produce accurately measurable amounts of tritium without introducing unreasonably large energy spreads on the neutron beam.

The geometry of the irradiations is shown in Figure 5.1; all the irradiations were carried out with the sample at 0^o to the incident beam. The lithium hydroxide pellet and case were held together inside a firmly fitting aluminium box, and the monitor foils used were fixed on its outside. This assembly was then placed inside a 1 mm thick cadmium case to absorb thermal neutrons.

The mean energy of the neutrons incident on the sample depends on the energy loss of the deuterons in the gas cell and also on the position of the sample. This is because neutrons produced near the end of the gas cell have an increased chance

of passing through the sample. The energy of neutrons produced at position x in the gas cell (Figure 5.1.), E (x), is given by

$$E(x) = E_o - ex \qquad 5.1$$

where E_o is the energy of neutrons produced by the deutrons immediately after they have passed through the entrace window and e is the deuteron energy loss per cm. (The difference in energy of neutrons produced by different energy deuterons is equal to the difference of the deuteron energy in this energy range). The mean energy of neutrons incident on the centre of the sample isgiven by:

$$\bar{E} = \int_o^L \frac{E(x)}{(d+L-x)^2}\,dx \Big/ \int_o^L \frac{dx}{(d+L-x)^2}$$

since the relative probability that a neutron formed at x passes through the sample is $\frac{1}{(d+L-x)^2}$. Using expression 5.1. we obtain

$$\bar{E} = E_o - e\left[d + L + \frac{d(d+L)}{L}\ln\frac{d}{d+L}\right]$$

This mean energy has been calculated for all the irradiations using the specific energy loss data of Northcliffe and Schilling (1970). (The energy loss in deuterium at 2 atmospheres was taken to be the same as hydrogen at 2 atmospheres since almost all of the energy loss of the deuterons is due to the interactions with electrons, the number density of which is the same for hydrogen and deuterium). The values obtained for the mean neutron energy are virtually the same as the neutron energy from those deuterons in the centre of the gas cell, except for the case of low energy deuterons (with large energy loss per centimetre), when the sample is close to the end of the gas cell. For the neutron detector the mean energy is always the same as that from the centre of the gas cell.

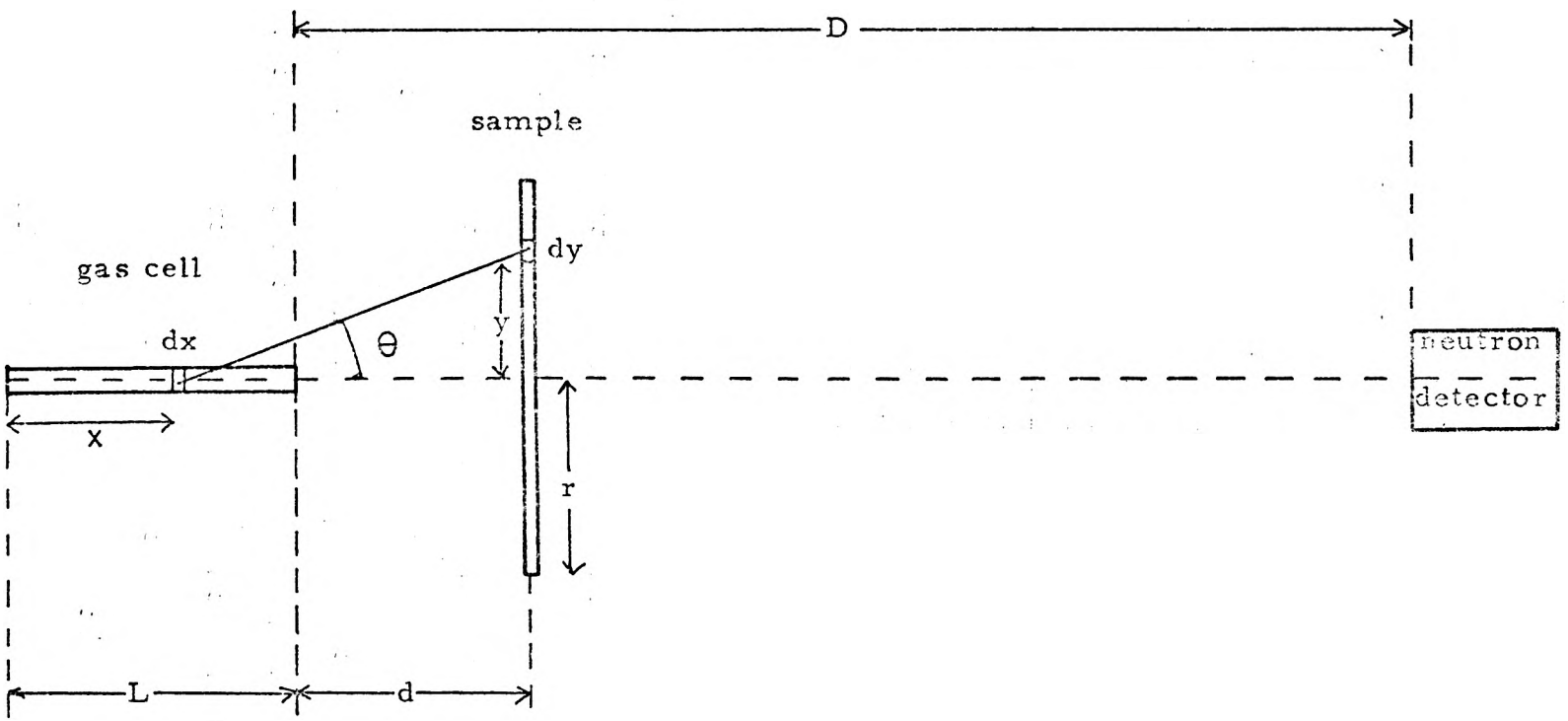

Figure 5.1 Geometry of tandem irradiations. (not to scale)

The mean energy over the whole pellet is slightly different from the mean energy incident on its centre, due to the variation of neutron energy with angle. This energy spread was calculated using the data of Liskien and Paulsen (1973). This effect is smaller than that from the deuteron energy spread.

The mean energy and energy spread for each case is given in Table 5.2. Column 1 gives the energy of deuterons incident on the gas cell. Columns 2 and 3 give the energy loss of the deuterons in the entrance window, and in 1 cm. of gas respectively. Column 4 gives the distance from the sample to the end of the gas cell, which is used in the calculation of the mean energy, given in column 5. Column 6 gives the angle subtended by the pellet at the end of the gas cell and column 7 gives the resulting energy spread. Column 8 gives the neutron energy spread due to deuteron energy loss in the gas, and Column 9 gives the total neutron energy spread.

Incident deuteron energy	energy loss in (i) window (ii) 1cm gas (MeV)		distance to sample (cm)	mean neutron energy (MeV)	angular spread (deg)	energy spread from (i) angle (ii) gas (MeV)		Neutron energy spread (MeV)
2.9	.43	.13	3.50	4.70	12	.05	.68	.73
3.4	.41	.10	6.67	5.64	6.4	.02	.53	.55
4.9	.35	.06	10.67	7.47	4.0	.02	.31	.33
7.1	.26	.05	10.67	9.77	4.0	.02	.24	.26
7.1	.26	.05	3.50	9.72	12.0	.14	.25	.39
9.1	.22	.04	11.67	11.76	4.0	.03	.19	.22

Table 5.2. Mean neutron energy and energy spread for the Tandem irradiations.

5.1.2 Neutron Flux Determination

The neutron flux was measured with an NE213 liquid scintillation detector which had previously been calibrated as in Chapter four. The circuit used was the same as for the comparison of the 14 MeV associated particle detector and the NE213, and is shown in Figure 4.1.7.

If the solid angle subtended by the detector at the neutron source is $\Delta\Omega$ and the average neutron efficiency is $\bar{\epsilon}_n$, then the total number of neutrons per steradian at 0^o, N(0) is given by

$$N(o) = \frac{n_T}{\Delta\Omega\bar{\epsilon}_n} \cdot f_d \cdot f_b \cdot f_{tr}$$

where n_T is the number of neutron pulses above the detector bias, and f_d, f_b, and f_{tr} are correction factors for dead time, background and transmission of the sample respectively. The way in which these factors were determined is outlined below, and the relevant values for each irradiation are shown in Table 5.3.

The average neutron efficiency was taken from the previous calibration (section 4.2.3) and the correction for deadtime was made in the same way as for the efficiency measurement, (section 4.2.2.(c)). The correction for background is necessary since room returned neutrons will be incident on the detector. These neutrons must be excluded from the flux measurement since their number will be proportionately much greater at the detector than at the sample position, where the primary flux is much stronger. The size of the background is generally small ($\sim$2%) at the detector and so will be negligible at the sample. The single case where the background is higher, (4.7 MeV neutrons with 7.4% background) is due to the low bias (1.6 MeV protons) used in that case, and the background will be predominantly low energy neutrons

which will not affect the sample as they will be below the reaction threshold.

The background was measured separately at each energy by interposing a shadow cone between the source and the detector. The cone was made of steel and was 30 cms long, with a calculated transmission of 0.43% at 14 MeV, and less at lower energies. In the background measurements the beam current integrator was used as a monitor for normalising the runs with and without the cone. These measurements gave the background for the particular bias used in the irradiations. Measurements were also made of the pulse height spectrum at each energy with a reduced detector bias (2 MeV), and low beam current, for the open beam, the cone in, and with the gas cell empty. These showed that the neutron spectrum was essentially 'clean', since the pulse height spectrum for the open beam was the same shape as the spectra from the efficiency calibration in which only monoenergetic neutrons were recorded. Also, with the cone in, the spectrum was predominantly low energy neutrons falling below the threshold of the $^{7}Li(n,n't)^{4}He$ reaction. The neutron output from the empty gas cell has a broad energy spectrum extending to the primary neutron energy but at a level much less than the neutron background as measured above. The activity induced in the sample due to these neutrons is negligible, and in any case is partly included in the neutron dose measurement.

When the sample pack was in place, neutrons were scattered and absorbed from the primary beam. This means that the flux measured by the detector was not that incident on the sample. The size of this effect was measured by transmission in a similar way to the background, with and without a pellet in place, for each primary neutron energy. Again the current integrator was

used as a monitor.

The air between the source and the detector (at 2.8m) behaves in a similar way to the sample, by scattering and absorbing neutrons in the beam. All neutrons undergoing a non-elastic event with the light nuclei of the air will be lost since they will fall below the detector bias. The size of this effect can be calculated and is approximately 0.8% over 2.8m. The size of the effect due to scattering was checked by measuring the flux at 1.2m, using the current integrator as a monitor. The result is consistent, within statistics, with a 1% loss of neutrons over the flight path, and an appropriate correction was made to the flux. The error contribution will be negligible.

Calculation of Solid Angle.

The calculation of solid angle is not straightforward for two reasons: the neutron source is extended, and the differential cross-section for neutron production from the dD reaction varies with angle. The way in which the solid angle is calculated will now be outlined, using that of the sample as an example, and referring to thequantities defined in Figure 5.1.

The number of neutrons produced in the element of the gas cell dx in direction θ is:

$$\frac{n(o)}{\sigma(o)} \cdot \sigma(\theta) \frac{dx}{L}$$

where $n(\theta)$ is the number of neutrons per steradian at θ^{o}, $\sigma(\theta)$ is the diffential cross section for neutron product at θ^{o}, $n(o)$ and $\sigma(o)$ the corresponding quantities at 0^{o} and L is the length of the gas cell. The number of neutrons passing through the annulus of the sample defined by y and dy from element dx is

$$n(x,y) = \frac{2\pi\ y \cos\theta}{(d+L-x)^2 + y^2} \frac{n(o)}{\sigma(o)} \sigma(\theta) \frac{dx}{L} \qquad 5.2.$$

Using data from Liskien and Paulsen (1973) fits were made to $\sigma(\theta)$ of the form

$$\sigma(\theta) = \sigma(0)\ (1-A \sin^2\theta)$$

where the coefficient A depended on the deuteron energy. This expression represents the differential cross-section adequately over the range 0^o-15^o necessary for the solid angle calculations. Using this fitted expression in equation 5.2 we obtain an expression for the total number of neutrons incident on the sample

$$n = \int_{x=o}^{L} \int_{y=o}^{r} \frac{2\pi y dy \cos\theta\ n(o)\ (1-A \sin^2\theta)dx}{L\ (\ (d+L-x)^2 + y^2)}$$

which can be integrated to yield

$$n = \frac{2\pi n(o)}{L}\left[(d^2 + r^2)^{\frac{1}{2}} - (\ (d+L)^2 + r^2)^{\frac{1}{2}} + L\right]$$

$$+ \frac{2\pi n(o)A}{3L}\left[(\ (d+L)^2 + r^2)^{\frac{1}{2}} + \frac{(d+L)^2}{(\ (d+L)^2 + r^2)^{\frac{1}{2}}} - 2(d+L)\right]$$

$$- \frac{2\pi n(o)A}{3L}\left[(d^2 + r^2)^{\frac{1}{2}} + \frac{d^2}{(d^2 + r^2)^{\frac{1}{2}}} - 2d\right]$$

This expression was used to determine the solid angle of the sample and the detector. If the angular variation of the differential cross-section had been ignored, the expression for the number of neutrons incident on the disc of radius r at distance d would be

$$n = n(o)\frac{\pi r^2}{d(d+L)}$$

For the detector the two expressions give virtually the same results, but for the sample the two differ considerably in some cases and the percentage difference is given in Table 5.3 The neutron flux incident on the sample for each irradiation is also given.

$\bar{E}_n$ (MeV)	detector distance (m)	detector efficiency (%)	trans-mission	back ground (%)	dead time (%)	neutrons per steradian	angular distribution correction (%)	neutrons through sample
4.70	2.80	17.0	0.87	7.4	1.0	1.38×10^{13}	3.5	5.14x10"
5.64	2.75	9.0	0.868	2.3	1.0	1.15×10^{13}	1.3	1.90x10"
7.47	2.75	9.9	0.866	2.3	1.5	2.44×10^{13}	0.7	1.95x10"
9.77	2.75	9.25	0.874	2.3	3.0	3.93×10^{13}	1.2	3.06x10"
9.72	2.80	9.25	0.874	1.9	2.0	5.48×10^{13}	8.4	1.78×10^{12}
11.76	2.75	4.3	0.869	1.6	1.6	6.51×10^{13}	1.7	5.19x10"

Table 5.3 Number of neutrons per steradian, and through the sample, for each irradiation, showing the factors involved in the calculation.

The error on the number of neutrons incident on the sample comes from two sources; the error on the number of neutrons per steradian at 0^{o} and the error on the expression for the solid angle of the sample.

The error on the first of these is ± 2.5% made up from ±2% on the detector efficiency, ± 1% on the detector solid angle, ± 0.5% on the background and ± 1% on the transmission.

The error on the sample solid angle was calculated assuming a ± 1mm uncertainty in its positioning, and including a 10% error on the correction made for the angular distribution of neutrons. The positional uncertaining gives ± 1.5% for d=10 cm, ± 2.3%for d = 6 cm and ± 4.4 % for d = 3.5 cm.

The overall error on the neutron dose was obtained by adding the error on the number of neutrons per steradian, the positional uncertain ty and the error due to the angular distribution in quadrature.

5.1.3. Deuteron break-up Correction

When the $D(d,n)^{3}He$ reaction is used as a neutron source with incident deuteron energy greater than 4.45 MeV, then a competing reaction becomes possible

$$D + D \longrightarrow D + n + p$$

in which one of the deuterons breaks up into a neutron and a proton. The produced neutrons are not monoenergetic because the reaction has three products. These neutrons can interfere with the tritium production from the overlap of n(E) with $\sigma(E)$ in the present experiment, and their contribution must be calculated in order to determine the $^{7}Li(n,n't)^{4}He$ cross-section precisely.

This correction was carried out using data on the spectrum of the break-up neutrons from two sources, Lefevre (1962) and

Smith and Meadows (1974). The calculation was carried out in the following way. The contribution from deuteron break-up, to tritium production is given by:

$$\frac{\int_0^{\infty} \sigma_{Li}(E)\, n_{bu}(E)\, dE}{\int_0^{\infty} \sigma_{Li}(E) n_o(E)\, dE}$$

where $n_{bu}(E)$ is the number of neutrons from breakup with energy E, and n_o is the number of neutrons from the main reaction. This can be evaluated approximately as

$$\sum_{i=1}^{N} (\sigma_{Li})_i\, (n_{bu})_i\, \Delta E \Big/ \sigma_{Li}(E_o)\, n_o(E_o)$$

where the breakup integral has been replaced by a scan over N groups, with group cross-section and number of neutrons $(\sigma_{Li})_i$ and $(n_{bu})_i$ respectively. The tritium production from the main reaction has been evaluated assuming a delta function at the principle energy E_o. In evaluating the correction using the data of Lefevre, $(n_{bu})_i$ was replaced with $(\sigma_{bu}(o))_i$, the differential cross-section for neutron production in the 1^{th} group, and $n_o(E_o)$ with $\sigma_o(o)$ the differential cross section for neutron production at 0^o from the main reaction. The data of Smith and Meadows gives the yield of breakup neutrons relative to the yield of the main reaction. The corrections obtained, using 0.1 MeV energy intervals, were zero below 9 MeV neutron energy, 4×10^{-2}% for 9.75 MeV neutrons and 8% for 11.8 MeV neutrons. The final correction was only done with the data of Lefevre since that of Smith and Meadows does not extend to high enough energy. To allow for uncertainty in the low energy part of the lithium tritium production cross-section, and in the measurement of the neutron spectrum an error of $\pm$15% has been

assigned to the correction, which gives a 1.4% contribution to the uncertainty on the measured cross-section at 11.8 MeV.

5.1.4 Foil Monitors

Foil monitors were used to check the measurements of the $^{7}Li(n,n't)^{4}He$ reaction cross-section by providing a check on the flux and solid angle measurement, and also to provide a back-up relative measurement if the electronics of the NE213 detector failed. (The latter provision was not required, except at the lowest energy where normalisation to the foil cross-section was necessary).

The foils used in the experiment were aluminium and nickel. Aluminium (27) undergoes an (n,α) reaction to produce ^{24}Na which decays via gamma emission with a 15 hour half-life. Nickel (58) undergoes an (n,p) reaction to produce ^{58}Co which has a 71 day half-life.

The induced activity in each foil was measured (in the Applied Chemistry Division AERE Harwell) with a Ge(Li) detector. These detectors have a very high resolution because large numbers of electrons are promoted to the conduction band by each gamma ray interaction. This high resolution means that peaks from different energy gamma rays are in general well separated, and can be measured individually. The spectrum produced from an irradiated sample can be quite complex, containing many peaks. The activity caused by the above mentioned reactions was measured using the 1369 KeV gamma from ^{24}Na and the 810 KeV gamma from ^{58}Co. The spectrum from each sample was analysed using the computer programme DIODE (Bullock and Large (1971)), which includes the measured efficiency of the detector, to produce the disintegration rate of the foils. Information on the branching ratios of each decay scheme is also input. A linear

fit is made to the background beneath each peak, which is a good assumption for the narrow peaks produced by the detector.

One complication which arises is due to the long irradiation time (c.24 hours) used in the irradiations. For both the monitors, but especially the ^{24}Na, a correction has to be applied for the decay of some of the nuclide during the irradiation itself. This was made in the following way.

If A_i is the number of atoms of the active nuclide (^{24}Na or ^{58}Co) present in the i^{th} time interval of the irradiation, and it is being produced at a rate of $n \Delta \Omega \; p_i t$ where n is the mean number of neutrons per steradian, Σ is the macroscopic cross-section, $\Delta\Omega$ the solid angle, t the thickness and p_i is a power factor to allow for the variation of the neutron source, then we have

$$A_{i+1} = A_i - \lambda A_i \Delta T + n \Delta \Omega \Sigma p_i \, t \Delta T$$

where λ is the decayconstant and ΔT is the length of the time interval. We can simplify this expression by choosing $B_i = A_i / n \Sigma \Delta\Omega \, t$, and then we obtain

$$B_{i+1} = B_i - \lambda B_i \Delta T + p_i \Delta T$$

If the irradiation is divided into M equal time intervals than we have

$$B_M = \frac{D}{\lambda n \Sigma \Delta\Omega \, t} \qquad 5.3.$$

where D is the disintegration rate at the end of the experiment from the definition of n as the mean number of the neutrons per steradian we have

$$n = \frac{N}{\sum_{i=1}^{M} p_i \Delta T} \qquad 5.4.$$

where N is the total number of neutrons per steradian in the

experiment. Using equations 5.3 and 5.4 and replacing the macroscopic cross-section with the product of the microscopic cross-section (σ) and the number density (N_A) we obtain

$$\sigma = \frac{D}{\lambda N_A \Delta\Omega t N} \left[\frac{\sum_1^M P_i \Delta T}{B_m} \right]$$

The term in brackets represents a correction factor to the rest of the expression, which would be valid if the active nuclide did not decay during the irradiation. The variation of neutron production - due to the machine fluctutions, stops for diffusion pump liquid nitrogen traps to be filled etc - was monitored using a chart recorder on the neutron count rate. This enabled the power factor, p_i, to be found for each interval. The accuracy of the correction factor depends on the size of the interval relative to the half-life of the radionuclide. For ^{24}Na ($T_{\frac{1}{2}}$ = 15 hours) a suitable interval was found to be 30 minutes. This interval was also used for ^{58}Co. For aluminium the correction factor was large, and in some cases approached a value of 2.

The measured activity, including the correction factor, was used together with the measured flux and solid angle to calculate the ^{27}Al(n, α)^{24}Na reaction cross-section. This cross-section was also measured at 14.0 MeV using the dD reaction. The correction for deuteron breakup in this case was only 5%. The break-up correction at other energies was negligible. The results are shown in figure 5.4, together with the ENDF/B-1V recommendation and previous measurements. The other data shown are weighted averages of data held by the NEA data bank (S a clay).

The uncertainty on the measurement is due to the uncertainty

on the neutron dose (section 5.1.2) and the counting statistics of the activity measurement (1%), which were added in quadrature .

The figure (5.4) shows that there is good agreement between the values obtained in the present experiment and previous determinations. This is a good indication of the accuracy of the flux and solid angle determination.

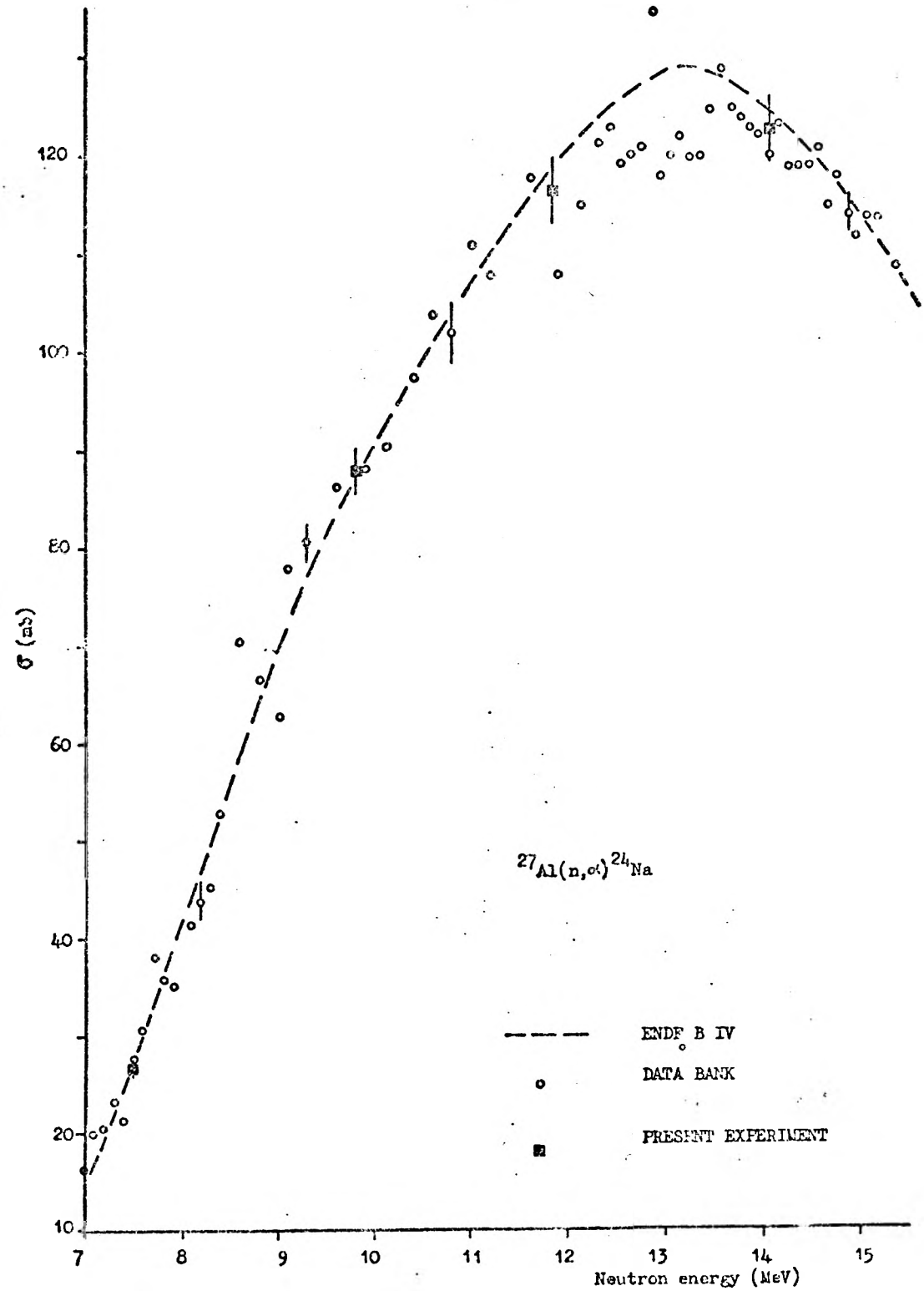

Figure 5.4 The $^{27}Al(n,\alpha)^{24}Na$ cross-section

5.1.5. The Tritium Production Cross-Section of Lithium-7

The tritium production cross-section of the lithium samples is calculated from:

$$\sigma = \frac{N_T}{n_n N_{Li}} \cdot f_{m.s} f_{l.f} \cdot f_{b.u} \qquad 5.5.$$

where N_T is the number of tritium atoms produced in the irradiation, n_n is the flux at the centre of the sample, which contained N_{Li} ^7Li atoms. The three factors, f_{ms}, f_{lf} and f_{bu} allows for multiple scattering (section 3.5), the labile fraction (section 3.3) and deuteron breakup (section 5.1.3.) respectively.

The mean flux at the centre of the sample is modified by scattering and absorption from the incident flux. This effect was determined by using aluminium foils at the front and the back of the sample pack, and assuming that the effect was linear. In some cases the flux at the centre of the sample was greater than would be expected from a $^1/_{d(d+1)}$ fall off and in other cases less. The size of the effect was approximately 1% although in one case it was 2%.

The number of tritium atoms is calculated from the measured count-rate in the liquid scintillation sample, together with the tritium counting efficiency (from the measured external standards channels ratio), the background, and the half-life of tritium. The background figure used was the mean of several measurements on unirradiated pellets. These were processed in the same way as the irradiated samples using the same chemicals. Some were processed at the same time as a batch of irradiated samples while others were processed alone. The background count rate was corrected for quenching (for the reasons put forward in section 3.2.3) before the mean value was found. The parameters

used in the calculation of the number of tritium atoms produced are shown in Table 5.5.

The results for the tritium production cross-sections, showing the values of the parameters used, are given in Table 5.6, and are plotted together with the ENDF/B-IV evaluation in figure 5.7. At 4.7 MeV incident neutron energy, nickel and titanium foils were used to monitor the flux, since the aluminium cross-section at this energy is too small. The calculated cross-sections for these foils were both low with respect to the literature values by a factor of 1.4, so the lithium cross-section at this energy was increased by this factor. (The uncertainity on this point is already large and the error due to this normalisation is small). This effect could be due to an error, (rather than an uncertainty) in the distance from the source to the sample pack.

Uncertainties

The number of tritium atoms, N_T, is deduced from

$$N_T = \frac{T_{\frac{1}{2}}}{1n2} \left(\frac{\text{count rate}}{\text{efficiency}} - \text{background} \right)$$

where $T_{\frac{1}{2}}$ is the half-life of tritium, which is 12.35 ± 0.1 years (Radiochemical Centre (Amersham) Data Sheet). The uncertainty on N_T has been calculated using the values given in Table 5.8. The counting statistics were ± 1%, the error on the efficiency calibration is 2.2% and the error on a single reading from the background determinations (rather than the error on the mean) was 6.8%.

The error on the mean flux of neutrons at the sample centre is a combination of the error on the number of incident neutrons (section 5.1.2) and the error on the correction for absorption and scattering (see above). The latter involves a

Neutron Energy	d	total counts per seconds	Channels ratio	Counting efficiency %	Net disintegrations per second	Number of tritium atoms produced
4.7	3.5	.48	.4532	24.4	0.52	2.92×10^{8}
5.64	6.7	.56	.4172	20.8	1.25	7.05×10^{8}
7.47	10.7	.59	.4020	19.3	1.62	9.12×10^{8}
9.77	10.7	.81	.4211	21.2	2.38	1.33×10^{9}
9.72	3.5	3.38	.4338	22.5	13.57	7.62×10^{9}
11.76	10.7	1.14	.4114	20.2	4.18	2.35×10^{9}

Figure 5.5. Calculation factors used in determining the number of tritium atoms produced (background = 1.45 cops and the tritium half life is 12.35 years.)

Neutron energy MeV	$N_{tritium}$	$N_{neutrons}$	$N_{Lithium}$	F_{ms}	f_{if}	f_{bu}	σ_{mb}
4.7	2.92×10^{8}	5.14×10^{11}	2.46×10^{22}	0.993	1.003	1.0	57.2 *
5.64	7.05×10^{8}	1.90×10^{11}	2.46×10^{22}	0.980	1.003	1.0	262
7.47	9.12×10^{8}	1.95×10^{11}	2.47×10^{22}	0.967	1.003	1.0	324
9.77	1.33×10^{9}	3.07×10^{11}	2.47×10^{22}	0.963	1.003	1.0	301
9.72	7.62×10^{9}	1.78×10^{12}	2.44×10^{22}	0.963	1.003	1.0	302
11.76	2.35×10^{9}	5.19×10^{11}	2.47×10^{22}	0.960	1.003	0.92	287

Figure 5.6 Calculational factors used to determine the tritum production cross section of ^{7}Li from the Tandom irradiations (see text.)

(*This measurement has been normalised, see text)

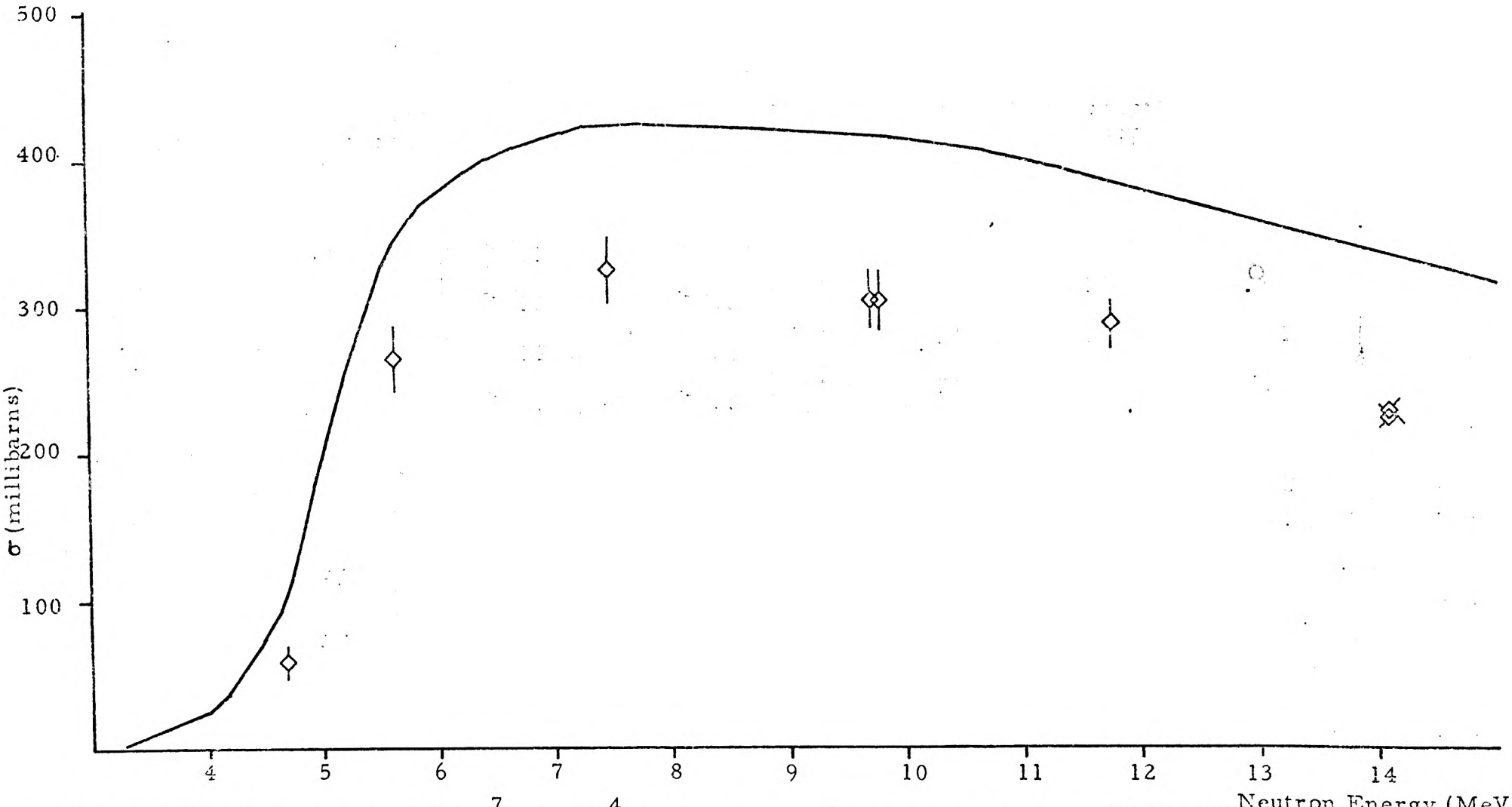

Figure 5.7 The cross section of the $^{7}Li(n, n't)^{4}He$ reaction. (points--present expt., solid line ENDF/B-IV)

En MeV	count rate (s^{-1})	$\frac{\sigma \text{ count}}{\text{count}}$ (%)	$\frac{\sigma \text{ efficiency}}{\text{efficiency}}$ (%)	$\frac{\sigma_{T_{1/2}}}{T_{1/2}}$ %	$\frac{\sigma \text{ background}}{\text{background}}$ %	Total %
4.7	.48	1	2.2	.8	6.8	1.9
5.64	.56	1	2.2	.8	6.8	8.2
7.47	.59	1	2.2	.8	6.8	6.4
9.77	.81	1	2.2	.8	6.8	4.6
9.72	3.38	1	2.2	.8	6.8	1.6
11.76	1.14	1	2.2	.8	6.8	2.9

Figure 5.8 Overall error and individual contributions (%) for the number of tritium atoms produced, in the Tandem irradiations.

correction of 2% at the most, and so contributes a negligible error compared to the error on the incident neutron flux. The error on the number of lithium atoms is due to an error in weighing the irradiated pellet (0.5%) and the uncertainty in the lithium content determination (0.2%) and is 0.54%.

The error on the remaining factors in equation 5.5 (labile fraction, multiple scattering and deuteron break-up) have been discussed in the appropriate sections. The overall error on the measured cross-section, together with the contribution from each term is given in Table 5.9.

En	$\frac{\sigma_{NT}}{N_T\%}$	$\frac{\sigma_n}{n\%}$	$\frac{\sigma_{Li}}{L_i\%}$	$\frac{\sigma_{L.f}}{l.F\ \%}$	$\frac{\sigma_{b.u}}{b.u\ \%}$	$\frac{\sigma_{m.s}}{m.s\ \%}$	overall %
4.7	1.9	5.1	.54	.3	0	.14	19.7
5.64	8.2	3.4	.54	.3	0	.41	8.9
7.47	6.4	2.9	.54	.3	0	.67	7.1
9.77	4.6	2.9	.54	.3	0	.74	5.5
9.72	1.6	5.2	.54	.3	0	.74	5.5
11.76	2.9	2.9	.54	.3	1.2	.81	4.4

Figure 5.9. Overall error and individual contributions (%) for the $^{7}Li(n,n't)^{4}He$ cross-section.

5.2. Cockcroft-Walton Irrdiations

5.2.1. The Neutron Source

The problem with using the $D(d,n)^3He$ neutron source reaction to produce 14 MeV neutrons on the Tandem, is that for 11 MeV incident deuteron energy, the 0^o yield of neutrons from D(d,np)d is greater than that of the main reaction. Also the maximum energy of neutrons from the break-up reaction is 7.5 MeV. Therefore, the activity induced in a sample by this secondary source of neutrons is frequently comparable with that from the 14 MeV neutrons. The contribution from break-up neutrons depends on the threshold and shape of the reaction cross-section being studied, and it is usual practice to use the dD reaction as a neutron source up to a neutron energy for which the contribution to the activity from break-up is 10%. This criterion applies, as indicated previously, to the measurement of the $^{27}Al(n,\alpha)$ cross-section at 14 MeV using dD, where the break-up correction is 5%. However, the correction for the $^7Li(n,n't)^4He$ would be approximately 80% which is unacceptably high considering the uncertainties in the break-up spectrum and in the $^7Li(n,n't)$ cross section at low neutron energies.

For these reasons the neutron source used for the 14.1 MeV irradiations was the $T(d,n)^4He$ reaction on the Cockcroft-Walton generator employing a solid titanium tritide target and an incident deuteron beam energy of 400 KeV. The target was 1.9 mg/cm^2 thick and the irradiations were carried out at 90^o to the incident beam. The thickness of the target is sufficient to ensure that most of the neutron output arises from the peak of the dT cross-section at 110 KeV. This means that the neutron energy variation with angle is very small. In order to produce

adequate tritium activity in the lithium samples over a period of 12 hours, a 100 μA beam current was used, and the samples were placed approximately 5 cms from the source. The target had a 0.5 mm copper backing and was cooled by pumping a 1mm thick layer of water across the outer surface.

The high current caused deadtime problems in the NE 213 detector because it could not be placed sufficiently far from the neutron source, and so the neutron ouput was monitored using the charged particles from the solid target. These two methods of flux measurement were compared at low count-rates and good agreement was found (section 4.3).

The water cooling assembly, although not containing much material, did make it difficult to determine precisely the distance between the neutron source and the lithium samples. This necessitated that the lithium cross-section measurement was a relative one, and aluminium monitor foils were used to measure the dose received by the lithium samples.

The lithium hydroxide samples used were contained as for the Tandem irradiations in a case of the same material, in an aluminium box and a cadmium case. After the irradiation, the samples were processed in the same way as previously.

The calculation of the $^{7}Li(n,n't)^{4}He$ cross-section proceded in the following way. Firstly the activity produced in the alumium foils was determined, (including the correction factor) as in the previous section. Then using a value for the 14.1 MeV cross-section of the $^{27}Al(n,\alpha)^{24}Na$ reaction of 123.6±2.3 millbarns (NEA data bank (Saclay)), which agrees with our measured value of 124±3 millibarns, the distance between the neutron source and the aluminium foil could be found. The flux was found from the number of silicon pulses and the detector solid

angle, and the solid angle of the alumium foil was taken as A/r^2.

From the construction of the sample pack the distance between the aluminium foil and the centre of the sample pack was known. This enabled the source to lithium pellet distance to be determined, which in turn allowed the calculation of the number of neutrons incident on the pellet.

The number of tritium atoms was calculated in the same way as in the previous section, and the results are given in Table 5.10.

The lithium cross-section was then calculated as outlined above, and the factors involved are given in Table 5.11, and plotted in Figure 5.7.

Uncertainties

The uncertainty on the number of tritium atoms produced, the number of lithium atoms, the labile fraction and the multiple scattering correction are the same in this case as for the Tandem irradiations.

The error on the number of neutrons incident on the sample is obtained from the error on the solid angle subtended by the alpha detector (1%), the statistical error on the ^{24}Na activity (1%), and the uncertainty on the $^{24}Al(n,\alpha)$ cross-section (1.9%) which gives an overall error of 2.4%. The overall error is given in Table 5.1.2.

The Cockcroft-Walton irradiations were carried out inside a concrete blockhouse of side and height 3m. In order to investigate the effect of neutrons scattered from the walls, two experiments were carried out. Firstly a 100% ^{6}Li pellet was irradiated in the same cadmium can as was used to shield ^{7}Li

samples. The produced tritium activity was less than one third of the activity produced in a ^{7}Li sample, and so when the correction is made for the relative ^{6}Li content in the normal samples the contribution to the tritium production from ^{6}Li can be seen to be negligible.

Secondly a nickel foil was irradiated and the value obtained for the $^{58}Ni(n,p)^{58}Co$ cross-section was 383±22 millibarns which is in agreement with the weighted mean value of 399±14 millibarns from the NEA data bank (Saclay). This indicates that the room return background in the blockhouse is very small for irradiations close to the target (approx. 5 cms) since the Q-value for this reaction is + 0.4 MeV.

	Neutrons/sr at 90°	aluminium activity dps	correction factor	aluminium mass mg	r_{Al}	mass of lithium hydroxide g	multiple scattering correction	cross section (mb)
RUN 1	2.45×10^{13}	1760	1.282	95.40	6.047	1.014	.956	221
RUN 2	2.57×10^{13}	1752	1.254	86.77	5.988	1.017	.956	226

Table 5.11 Calculation of the $^{7}Li(n,n't)^{4}He$ cross-section for the Cockcroft-Walton irradiations.

	Total counts per second	Channels ratio	counting efficiency %	net distintegrations per second	number of tritium atoms produced
RUN 1	1.60	.4300	22.1	5.81	3.27×10^9
RUN 2	1.76	.4348	22.5	6.37	3.58×10^9

Figure 5.10. Tritium Activity and the number of tritium atoms produced for the Cockcroft-Walton irradiations.

	$\frac{\sigma_{N_T}}{N_T}$ (%)	$\frac{\sigma_n}{n}$ (%)	$\frac{\sigma_{Li}}{Li}$ (%)	$\frac{\sigma_{l.F}}{l.F}$ (%)	$\frac{\sigma_{m.s}}{m.s}$ (%)	overall (%)
RUN 1	2.3	2.4	.54	.3	.9	3.5
RUN 2	2.2	2.4	.54	.3	.9	3.4

Table 5.12. Uncertainty contributions to the overall uncertainty on the $^{7}Li(n.n't)^{4}He$ cross-section at 14.1 MeV.

CHAPTER SIX

DISCUSSION AND CONCLUSION

6.1. Discussion of the present measurement.

In view of the large difference between the recommended cross-section of the $^{7}Li(n,n't)^{4}He$ reaction and the present measurement, it is perhaps useful to summarize the principal factors, on which the result depends, and how they were obtained. The cross-section of ^{7}Li is calculated as follows:

$$\sigma = \frac{N_T}{N_{Li}\ \Delta\Omega\ N_n}$$

where N_T is the number of tritium atoms produced, N_{Li} the number of ^{7}Li atoms in the sample of solid angle $\Delta\Omega$ and N_n the mean number of neutrons per steradian.

Firstly, the dose received by the sample is calculated in the same way for the ^{7}Li samples as for the Al foils used in the experiment. The cross-section results for aluminium agree well with the published data (figure 5.4) which gives confidence in the dose calculations.

Secondly, the number of lithium atoms in the sample was determined chemically in several different ways, all of which gave the same fraction of lithium (by weight) in the samples. No significant weight change was observed when the samples were weighed over an interval of several weeks, and so the amount of lithium in the samples is well known. The isotopic content of the material as obtained was stated to be 99.99% ^{7}Li. The samples used for the reactor irradiation ($\sim$ 0.5% ^{6}Li) had their isotopic ratio measured by mass-spectrometry, and this agreed with the weights of 99.99% $^{7}LiOH$ and 95% $^{6}LiOH$ which were used to make the samples, thus giving an extra check on the ^{7}Li fraction

of the original material.

Finally, the relevant question is are all the tritium atoms produced by the irradiation measured? Loss of energetic tritons is reduced to a negligible level by covering the pellets with a case of the same material. Loss, by diffusion, of tritium from the lattice is improbable by considering the chemical state in which it is bound, and also has been shown to be negligible over a period of several months. (Herzing et.al (1976). The liquid scintillation counting method is checked to the extent that two measurements at approximately the same incident neutron energy of widely different induced activites, give the same value for the $^{7}Li(n,n't)^{4}He$ cross section. This is a check on both the background and the variation of efficiency with quench. By far the most important evidence in favour of the tritium measurement system is the result for the $^{6}Li(n,t)^{4}He$ cross-section. The fact that this result is within one standard deviation of the accepted value (which is accurately known) gives a great deal of confidence in the conversion of recoil tritons to tritiated water without loss, and in the calibration of the liquid scintillation counting process.

6.2 Comparison with differential data

In figure 6.1. the results of this experiment, and other existing data are shown. Also shown are the points derived from the elastic scattering cross-section measurements of Purser et al.. Their experiment was a measurement of the elastic scattering cross-section of ^{7}Li using a time-of-flight technique between 7 and 14 MeV. The resolution of such an experiment is not sufficient to separate the elastic scattered neutrons from those inelastically scattered via the first excited state (.478 MeV) and so the elastic scattering cross-section was obtained by subtracting the (n,n'γ) cross-section measured by Dickens et al. (1974), from their results. For the present purpose, to produce data on the $^{7}Li(n,n't)^{4}He$ reaction, it is necessary to subtract the sum of elastic and inelastic scattering from the total cross-section, and so the data of Dickens et al. were added on to the elastic cross-section results of Purser et al. As the primary neutron energy increases it is necessary to subtract the cross-sections for other processes which become possible, (such as (n,2n)) and these data were obtained from Conlon (1972) as were the total cross-section values.

Also shown is a curve, the same shape as the ENDF/B/IV evaluation, but normalised to the measurements from the present experiment, by a reduction of 28%. It is agreement between existing differential data and this curve which will now be discussed.

Below 14 MeV the data has been obtained by the following authors: Rosen and Stewart, Batchelor and Towle, Wyman and Thorpe, Hopkins et al., Brown et al., Cookson et al., and Purser et al..

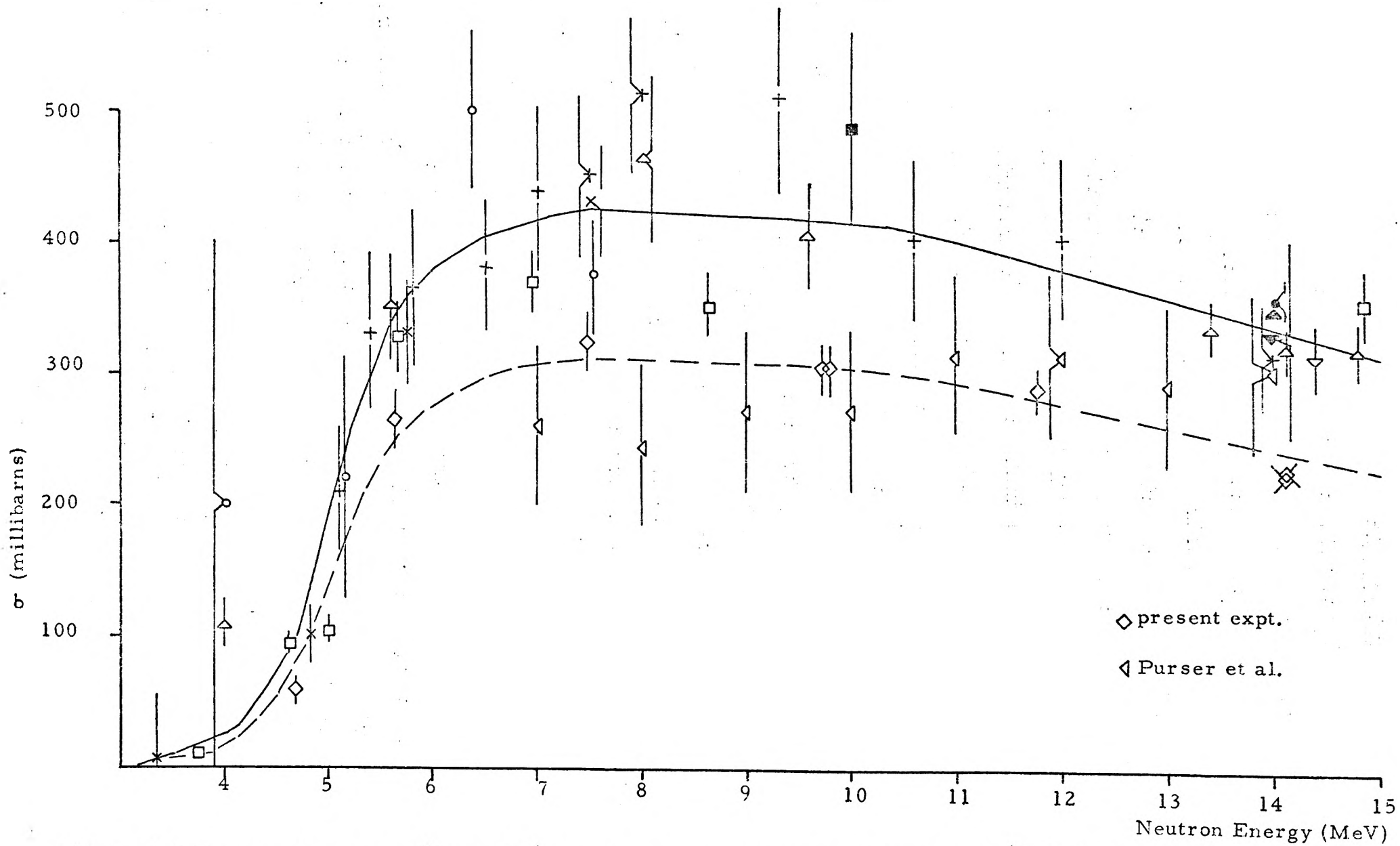

figure 6.1 Existing data on the $^{7}Li(n,n't)^{4}He$ cross-section (solid line ENDF/B-IV, broken line (ENDF/B-IV)*.725))

The data of Rosen, Batchelor, Wyman, Hopkins and Cookson , are approximately 2 standard deviations higher than the normalised curve, according to their quoted uncertainties. A smooth curve, of a different shape to the ENDF/B-1V evaluation could be drawn through the data of Brown and that of the present experiment, if the 14.8 MeV point of Brown in excluded. The data of Purser et al., although of considerable uncertainty, does agree with the normalised curve, and is 2 standard deviations below the evaluated curve.

A new evaluation is necessary to represent the cross-section, and although the data from the present experiment follows the shape of the existing evaluation, it is likely that this may not give the best fit to all the measurements. The present evaluation shape has no particular merit in that it is not the result of any theoretical model, but was the result of fitting to the data existing in 1964.

At 14 MeV the descrepancy between the data from the present experiment and the existing data is large in comparison with the standard deviations, and so in order to obtain a value for the cross-section with small uncertainty, more experiments with low uncertainities, will be necessary, preferably using as many different methods as possible.

6.3. Integral Measurements

Several integral experiments have been carried out over the interval 1954-1978. The two most recent have been carried out in West Germany at Julich (Herzing et al. (1976)) and at Karlsruhe (Bachmann et al. (1978)).

Both of these experiments used the tritium measurement system due to Dierckx (1976) and so their results might be expected to be similar. However, Herzing et al. say that the agreement between calculation and experiment is satisfactory within the accepted errors of the nuclear data whilst Bachmann et al. obtain serious discrepancies between both the neutron spectra and tritium production when the calculation is compared with the experiment. The latter even go so far as to recommend that the ENDF/B-IV evaluation of the $^{7}Li(n,n't)^{4}He$ reaction cross-section should be reduced by 15-20%. This observation agrees moderately well with the conclusion of the present experiment, and the disagreement of these two blanket experiments does show that the techniques of integral experiments still need further refinements.

6.4. Theoretical Implications

Theoretical studies on ^{7}Li have been carried out by Oastler (1977). These use R-matrix analysis to fit various observable properties of the ^{7}Li nucleus. Although a complete analysis has not yet been carried out taking into account the results of the present experiment, it is thought that a 28% reduction in the $^{7}Li(n,n't)^{4}He$ reaction cross-section would improve the fitting to other observables of the nucleus.

6.5. Conclusions and Comments.

The results of the present experiment indicate that the $^{7}Li(n,n't)^{4}He$ reaction cross-section would be better represented if the ENDF/B-1V evaluation was uniformly reduced by 28%. This has important consequences for the design of controlled thermonuclear reactors. Alsmiller et al. (1975) say that a 20% reduction in this cross-section would cause a 6% reduction in the tritium breeding ratio in a CTR with a metal blanket. Although in such a system the breeding ratio is already high, in other systems with tritium breeding ratios nearer unity, the reduction could cause these reactors to fall below the necessary tritium production rate.

A new evaluation of the $^{7}Li\ (n,n't)^{4}He$ reaction is needed to make the updated cross-section available for reactor designers and more measurements are necessary to reduce the uncertainty on the cross-section, especially at 14 MeV.

REFERENCES

ADAMS, J.M. and WHITE, G. AERE-R-8924 (1977)

AJZENBERG-SELOVE, F. and LAURITSEN, T., Nuc. Phys. A.227 (1974) 1

ALSMILLER, R.G., SANTORO, R.T., BARISH, J., and GABRIEL, T.A. Nuc. Sci. and Eng. 57 (1975) 122

ANTOLKOVIC, B., Nuc. Phys. A 219 (1974) 332

AXTON, E.J. Reactor Science and Technology. (J.N.E A/B) 17 (1963) 125

BACHMANN, H., FRITSCHER, U., KAPPLER, F.W. RUSCH, D., WERLE, H., and WIESE, H.W. Nuc. Sci. and Eng. 67 (1978) 74

BAILLIE, L.A., Int. J. Appl. Rad. and Iso. 8 (1960) 1

BATCHELOR, R. and TOWLE, J.M. Nuc. Phys. 47 (1963) 385

BENJAMIN, P.W., KEMSHALL, C.D., SMITH, C.D.E., AWRE NR/A-2/62 1962

BEYNON, T.D. Private Communication (1978)

BIRKS, J.B. The Theory and Practice of Scintillation Counting (1964). Pergammon Press

BOTHE, W., Z. Physik 120 (1943) 437

BROWN, F., JAMES, R.H., PERKIN, J.L., and BARRY J., J.Nuc. Energy A/B 17 (1963) 137

BUSH E.T., Anal. Chem. 35 (1963) 1024

CONLON, T.W. AERE-R07166 (1972)

COOKSON, J.A., DANCY, D. and HOPKINS, J.C., Nuc. Phys. A.91 (1967) 273

COOKSON J.A., HUSSEIN M., UTTLEY, C.A., FOWLER J.C., and SCHWARTZ, R.B. p.66 BSD SP 425 Nuclear cross-sections and technology. Proc. conf. Washington D.C. March 1975. Ed. Schrack and Bowman.

COOKSON J.A. Private Communication (1978)

COTRELL, A. 'Energy and the Environment - A review of the main features' in Energy and the Environment (1975) ed. J.Walker ISBN 0 70440204 1

CROCKER V.S., BLOW, S., and WATSON, C.J.H. Culham Laboratory Report CLM-P240 (1970)

CROOKES, Sir William Proc. Roy. Soc., 71 (1903) 405

CURRAN, S.C., ANGUS, J., and COCKCROFT, A.L. Phil. Mag. 40 (1949) 53

DIERCKX, R., Nucl. Instr. Meth. 107 (1973) 397

EVANS, E.A. Tritium and its compounds (1974) Butterworth, London.

GEIGER, H., Proc. Roy. Soc. A81 (1908) 174

GLASSTONE, S., and LOVBERG, R.H., 'Controlled Thermonuclear Reactions' (1960) Van Nostrand (Princeton)

GRAVES. E.F., LA 1688 (1943)

HANNA, G.C. Nuc. Sci. and Eng. 15 (1963) 325

HERMANN, F., Metalborse 24 (1934) 535

HERSING, R., KUIJPERS, L., CLOTH, P., FILGES, D., HECKER, R., and KIRCH, N., Nuc. Sci. and Eng. 60 (1976) 169

HOLBOROUGH, D.W., and LIPSCOMBE, B.A. AERE-R 6622 (1971)

HOPKINS, J.C., DRAKE, D.M., and CONDE, H. Nuc. Phys A.107 (1968) 139

HOPKINS, J.C. and BREIT, G., Nuc. Data Tables A9 (1972) 137

HUBBERT, M.K. IAEA-SM-146/1 (1971)

KUDO, H., TANAKA, K., and AMANO, J., J. Inorg. Nuc. Chem. 40 (1978) 363

LAWSON, D.J. Proc. Phys. Soc. B.70 (1957) 6

LEFEVRE, H.W., BORCHERS, R.R., and POPPE, C.H., Phys. Rev. 128 No.3 (1962) 1328

LINDNER, L., Private Communication (1977)

LISKIEN, H., and PAULSEN, A., Nuclear Data Tables 11 (1973) 569

LONG, G. 'Solar Energy: its potential contribution within the U.K.' Department of Energy Paper No.16. E.T.S.U. (Harwell) 1975

MACKLIN, R.L., and BANTA, H.E., Science 119 (1954) 350

McNAUGHTON, N.W. KING, N.S.P., BRADY, F.B. and ULLMANN, J.L. Nuclear Instr. Meth 129 (1976) 241

MEADOWS, J.W., and WHALEN, J.F., Nuc. Sci, and Eng. 40 (1970)12

MEISTER, H., Z.Naturforsh 11a (1956) 579

NORTHCLIFFE, L.C., and SCHILLING, R.F. Nuclear Data Tables 7 (1970) 233

OASTLER, A.J. Ph.D Thesis, Birmingham University (1977)

OSBORN, A.R., and WILSON, H.W. AWRE NR/C-1/61 (1961)

PENDLEBURY, E.D, AWRE-0-61/64 (1964)

PURSER, F.O., GOULD, C.R., SEAGONDOLLAR, L.W. NELSON, C.E. HOGUE, J.J., GLENDINNING, S.G., BEYERLE, SADIG EL KADI, BILPUCH, E.G. and NEWSON, H.W. 'Neutron and Fission Physics' in Triangle Unviersities. Nuclear Laboratory Annual Report (1977). TUNL XVI North Carolina 27706

RIBE, F.L. LA 1589 (1953)

RITCHIE, R.H., and ELDBRIDGE, H.B. Nuc. Sci. and Eng. 8 (1960) 300

ROBERTS, L.E.J. 'The General Energy Scene with a Brief Look at the future' in Energy and the Environment (1975) ed H.Walker ISBN o 7044 0204 1

ROSEN L., STEWART L., LA 2643 (1956) distributed 1961.

SMITH, D.L., and MEADOWS, J.W., ANL/NDM-9 (1974)

STANTON, N.R. COO-1545-92 (1971)

STEINER, D., and TOBIAS, M., Nuclear Fusion 14 (1974) 153

STEWART, L., in USNDC-CTR-1 (1974) ed. D. Steiner

TEXTOR, R.E. and VERBINSKI, V.V. ORNL-4160 (1968)

THOMAS, R.G., LA 1697 (1954)

TITTLE, C.W. Nucleonics 9 (No.1) (1951) 60

USAEC Washington 1239 (1973)

VALKOVIC. V., SLAUS, I., TOMAS, P., and CERINEO, M., Nucl. Phys. A.98 (1967) 305

Van URK, P., Ph.D. Thesis (1970) I.K.O Amsterdam

WESTCOTT, C.H., J. Nucl. Energy Part A: Reactor Science. 12 (1960) 113

WILLIAMS, M.M.R., Proc. Phys. Soc. 85 (1965) 413

WYMAN, M.E., and THORPE, M.M LA 2235 (1958)